Universitat Politècnica de Catalunya
Electrical Engineering Department

Institut de Recerca en Energia de Catalunya
Catalonia Institute for Energy Research

PhD Thesis

Analysis of the contribution of wind power plants to damp power system oscillations

Author: **José Luis Domínguez-García**

Advisors: **Dr. Oriol Gomis-Bellmunt**
Dr. Fernando D. Bianchi

Barcelona, April 2013

Catalonia Institute for Energy Research (IREC)
Electrical Engineering Research Area
Jardins de les Dones de Negre 1 2nd floor,
08930 Sant Adrià de Besòs, Barcelona, Spain

Printed in Barcelona by CPET, S.L.
First Print, April 2013

UNIVERSITAT POLITÈCNICA DE CATALUNYA
BARCELONATECH
Escola de Doctorat

Curs acadèmic:

Acta de qualificació de tesi doctoral

Nom i cognoms

DNI / NIE / Passaport

Programa de doctorat

Unitat estructural responsable del programa

Resolució del Tribunal

Reunit el Tribunal designat a l'efecte, el doctorand / la doctoranda exposa el tema de la seva tesi doctoral titulada

_____

_____.

Acabada la lectura i després de donar resposta a les qüestions formulades pels membres titulars del tribunal, aquest atorga la qualificació:

☐ APTA/E ☐ NO APTA/E

(Nom, cognoms i signatura) President/a		(Nom, cognoms i signatura) Secretari/ària
(Nom, cognoms i signatura) Vocal	(Nom, cognoms i signatura) Vocal	(Nom, cognoms i signatura) Vocal

_____, _____ d'/de _____ de _____

El resultat de l'escrutini dels vots emesos pels membres titulars del tribunal, efectuat per l'Escola de Doctorat, a instància de la Comissió de Doctorat de la UPC, atorga la MENCIÓ CUM LAUDE:

☐ SÍ ☐ NO

(Nom, cognoms i signatura) Presidenta de la Comissió de Doctorat	(Nom, cognoms i signatura) Secretària de la Comissió de Doctorat

Barcelona, _____ d'/de _____ de _____

$$2B^2$$

Abstract

Wind power has emerged as one of the most promising renewable energy sources. The very penetration levels of wind energy in power systems have altered several aspects of power system operation, such as system stability. Owing to the large penetration of wind power, transmission system operators (TSOs) have established special grid codes for wind farms connection. These grid codes require wind farms to provide ancillary services to the grid such as frequency and voltage regulation. In the near future, the capability of damping power system oscillations will be required. As a result of the development of such requirements, the concept of wind power plant (WPP) arises being defined as a wind farm which is expected to behave similarly to a conventional power plant in terms of power generation, control and ancillary services.

As future grid codes will require power oscillation damping contribution from wind power, the thesis is mainly focused on the analysis of the power system stabilizer (PSS) capability of wind power plants. The change produced by wind power plants based on different wind turbine technologies on power system small signal dynamics is analysed to determine their possible contribution to damp oscillations. The effect of the distance from the tie line to the wind power plant on the controller response and the influence of wind power plants proximity to synchronous generators are demonstrated to be critical factors. At this point several questions are raised as: What are the most critical factors? How can be ensure a proper contribution, at least the best possible response? Can it be ensured to be independent to the power system and the controller selected?

To answer these questions, this thesis conducts research on proper selection of input-output signal pairs to damp out electromechanical oscillations using wind power plants without drawing attention to a particular control design. This is necessary conclusions about the power system independently of a particular controller. The capability to damp is an intrinsic characteristic of the system and should not be affected by a particular controller (PSS). Firstly, different analysis techniques are compared, considering both controllability and observability measures and input-output interactions. This enables recommendations to be drawn so as to the selection of the the best signal pairs to damp power system oscillations considering different approaches, such as single-input single-output (SISO) and multivariable control (MIMO). Second, a new criterion to select the best input-output signals used by a PSS based on WPPs is presented, considering explicitly local and remote signals in the analysis. Taking into account fundamental design limitations and using controllability and observability concepts, the criterion is able to identify the most suitable pair of input-output local signals without consider any particular controller.

Finally, due to the increase of wind power generation - including offshore locations - and the concept of an interconnected Pan-European network, a new offshore wind power plant AC network similar in design to the European SuperGrid "SuperNode", is analyzed. The cost effect of choosing a non-standard operating frequency on the offshore AC network is investigated. As the offshore AC network is isolated from onshore networks through the use of HVDC links, it may be operated in an asynchronous fashion and at a suitable frequency. The cost associated with operating the network at a fixed frequency in the range 20 to 120 Hz is investigated, focusing on the frequency-cost-scalings of electrical devices (such as cables, transformers and reactive compensation) and the related offshore infrastructures.

Resum

L'energia eòlica s'ha convertit en una de les fonts d'energia renovable més prometedores. Actualment, l'elevat nivell de penetració de l'energia eòlica a la xarxa elèctrica ha conduït a la modificació del comportament de diversos aspectes d'aquesta, com per exemple, l'estabilitat. Degut a aquesta gran penetració, els operadors de xarxes de transmissió (TSOs) han establert procediments d'operació especials per a la connexió de grans parcs eòlics. Aquests codis requereixen als parcs elics que realitzin serveis auxiliars al sistema elèctric com, per exemple, la regulació de freqüència i la regulació de la poténcia reactiva. En un futur proper, la capacitat dels parcs eòlics per esmorteir les oscil·lacions del sistema de potència es requerirà (en l'actualitat ja existeixen esborranys de nous procediments d'operació que ho inclouen). A causa d'aquest requeriments, el concepte de central de generació d'energia eòlica es defineix com un parc eòlic que s'espera que es comporti de manera similar a una central de generació elèctrica convencional en termes de poder realitzar tasques tals com generació, control i serveis auxiliars.

Ja que un futur requeriment dels operadors de xarxa serà la contribució de l'energia eòlica en l'esmorteiment de les oscil·lacions de potència, en aquesta tesi s'estudia la capacitat de les centrals eòliques per actuar com estabilitzador dels sistemes elèctrics de potència. A més a més, s'analitza l'efecte de les centrals d'energia eòlica al comportament dinàmic del sistema elèctric considerant l'estabilitat de petita senyal, per a determinar quina podría ser la possible contribució proporcionada per aquestes tecnologies. S'ha estudiat que l'efecte de la distància des d'el punt de connexió amb la central d'energia eòlica a la resposta del control estabilitzant i la influència de la proximitat

de les centrals eòliques als generadors síncrons són factors crítics. D'aquest fet surgeixen algunes preguntes com: És aquest el factor més crític? Com es pot assegurar una contribució adequada, si més no la millor resposta possible, per ajudar a estabilitzar el sistema elèctric? Es poden asegurar quina serà la contribució a l'estabilitat del sistema elèctric independentment de la xarxa i l'esquema de control escollit?

Per respondre a aquestes preguntes, aquesta tesi ha realitzat investigacions sobre l'adequada selecció de parells de senyals d'entrada-sortida per esmorteir les oscil·lacions electromecàniques amb centrals eòliques evitant dissenyar el controlador i proposant metòdes fàcilment adaptables a qualsevol sistema elèctric. En primer lloc, s'han comparat diferents tècniques d'anàlisi tenint en compte tant les mesures de controlabilitat i observabilitat com les interaccions entre les senyals d'entrada i sortida. D'aquesta comparació, certes recomanacions es donen a l'hora de seleccionar els millors parells de senyals per esmorteir les oscil·lacions del sistema elèctric de potència considerant diferents esquemes de control com ara entrada única sortida única (SISO) i control multivariable (MIMO). En segon lloc, s'ha proposat un nou criteri per seleccionar les senyals d'entrada i sortida utilitzades per un control estabilitzador per centrals d'energia eòlica. On, a diferència amb anteriors metòdes de selecció proposats, el criteri presentat considera explícitament tant senyals locals com senyals remotes dins el seu anàlisi. Aquest criteri és capaç d'identificar la parella de senyals locals d'entrada i sortida més adequada sense realitzar el disseny del controlador, considerant tant les limitacions fonamentals del disseny del controlador imposades per el sistema com els conceptes de controlabilitat i observabilitat.

Finalment, a causa del augment de la generació d'energia eòlica, principalment en localitzacions marines, i al concepte d'una xarxa elèctrica comuna Pan-Europea, s'ha realitzat l'anàlisi d'un nou concepte de xarxa en corrent altern (AC) dins de les centrals d'energia eòlica marina, amb un disseny similar al concepte investigat a la Super-Xarxa Europea "Supernode". En aquest treball s'ha investigat l'efecte que té en els costos la tria una freqüència nominal d'operació no estàndard en dita xarxa en corrent altern. La xarxa en AC que es forma entre les turbines eòliques i el convertidor de transmissió és aïllada tant de les xarxes terrestres per l'ús d'enllaços en corrent continu (HVDC) com de la pròpia de les turbines per el convertidor que porten incorporat. Aquest fet implica que aquesta xarxa pot ser operada sense sincronitzar a qualsevol freqüència. En aquesta tesi, s'ha estudiat quin és el cost associat amb l'operació de la xarxa a una freqüència fixa dins del rang de 20-120 Hz, focalitzant principalment en l'escalat del costos dels diferents elements elèctrics (com ara cables, transformadors i compensació reactiva) i

infraestructures necessaris en instal·lacions marines respecte la freqüència.

Acknowledgements

This work has been carried out at the Electrical Engineering Research Area (EERA) of Catalonia Institute for Energy Research (IREC). This thesis has been financially supported by IREC through the 01–10_WIND_ENERGY grant.

First of all, I would like to express my sincere gratitude to my supervisors Dr. Oriol Gomis-Bellmunt and Dr. Fernando D. Bianchi for their supervision, their guidance and encouragement. I would like to thank them also their kind advices which keep me inside the real and applied engineering boundaries, even when my thoughts and ideas tried to runaway.

I am also extremely grateful to all my EERA–IREC colleagues (Lázaro, Jordi, Lucía, Cristina, Miguel, David, Albert, Gerard, Oscar, Joaquim, Ignasi Andi and Manel) for the interesting discussions during all this time. I would like to thank specially to Mikel and Francisco for their helping and friendship.

I sincerely thank all the Institute of Energy at Cardiff University for make me feel like at home during my stay there. Special mention to Dr. Carlos Ugalde-Loo who also contributes in this thesis, Dr. John Licari and Dr. Luke Livermore for all their help and friendship.

Finally, I would like to thank my family for their continuous support and encouragement during the development of this thesis. Specially, thank to my wife Begoña and my daughter Blanca, for their love, affection and patience; since they provide me the strength necessary to do not give up and to be able to finish this work.

Contents

List of Tables

List of Figures

Acronyms

AVR	Automatic Voltage Regulator
BR	Breaking Resistor
CCP	Common Coupling Point
CRHP	Closed Right Hand Plane
CSC	Current Source Converter
DDSG	Direct Drive Synchronous Generator
DDR	Dynamic Rotor Resistance
DFIG	Doubly Fed Induction Generator
EMF	ElectroMagnetic Field
EPSO	Evolutionary Particle Swarm Optimization
FACTS	Flexible AC Transmission System
FMAC	Flux Magnitude and Angle Controller
FRCIG	Full Rate Converter Induction Generator
FRCWT	Full Rate Converter Wind Turbine
FSWT	Fixed Speed Wind Turbine
FSWT-PMSG	Fixed Speed Wind Turbine - Permanent Magnet Synchronous Generator
FSWT-SCIG	Fixed Speed Wind Turbine - Squirrel Cage Induction Generator

HSV	Hankel Singular Value
HV	High Voltage
HVDC	High Voltage Direct Current
ICAD	Individual Channel Analysis and Design
LFO	Low Frequency Oscillation
MIMO	Multiple-Input Multiple-Output
MPPT	Maximal Power Point Tracking
MSF	Multivariable Structure Function
MT-HVDC	Multi-terminal HVDC
MV	Medium Voltage
NMP	Nom-Minimum Phase
PBH	Popov-Belevitch-Hautus
PLL	Phase Locked Loop
PMSG	Permanent Magnet Synchronous Generator
PSO	Particle Swarm Optimization
PSS	Power System Stabilizer
RGA	Relative Gain Array
RHPP	Right-Hand Plane Pole
RHPZ	Right-Hand Plane Zero
SCIG	Squirrel Cage Induction Generator
SCIG-WT	Squirrel Cage Induction Generator - Wind Turbine
SISO	Single-Input Single-Output
SMES	Super-conducting Magnetic Energy Storage
STATCOM	Static Synchronous Compensation
SVC	Static Var Compensator
TSO	Transmission System Operator
VSC-HVDC	Voltage Source Converter - High Voltage Direct Current
VSWT	Variable Speed Wind Turbine
VSWT-DDSG	Variable Speed Wind Turbine - Direct Drive Synchronous Generator
VSWT-DFIG	Variable Speed Wind Turbine - Doubly Fed Induction Generator
VSWT-FRCIG	Variable Speed Wind Turbine - Full Rate Converter Induction Generator
WPP	Wind Power Plant

WRIG	Wound Rotor Induction Generator
WT	Wind Turbine
XLPE	Cross-Linked Polyethylene

1 Introduction

As a result of worldwide environmental concern, reducing greenhouse gas emissions has become one of the most important targets agreed under the Kyoto protocol [1]. Moreover, the European Union promotes the so-called 20-20-20 Target Plan which aims to reach 20% energy efficiency improvement, to reduce 20% greenhouse gas emissions and to obtain, at least, 20% of its energy consumption from renewable sources by 2020 [2].

Wind power is rapidly increasing its presence in the power generation mix as one of the most promising renewable power source [3]. For many countries wind power has already become an important electricity source, e.g, Denmark, Portugal, Spain and Germany. The percentage levels of power provided by wind sources (the penetration levels) are 21%, 18%, 16% and 11%, respectively [4]. Moreover, installation of offshore wind power is growing fast during last few years, since there is more constant wind and less space limitation. According to [5, 6, 7], Figures 1.1, 1.2 and 1.3 show global wind power evolution all over the world.

Due to such increase in wind power generation's share, power systems stability and reliability may be adversely affected. The characteristics of wind farms are substantially different from conventional power plants, such as hydraulic, nuclear or thermal [8, 9]. These facts have led to the establishment of grid codes regarding wind farm connection, and their integration in the grid [10, 11, 12]. According to these codes, wind farms must comply with requirements including voltage sag ride through capability [13, 14], frequency regulation [15, 16], and active and reactive power regulation [17, 18]. In the future more wind farm contribution will be required by the system operators. The capability to damp power system oscillations will play an

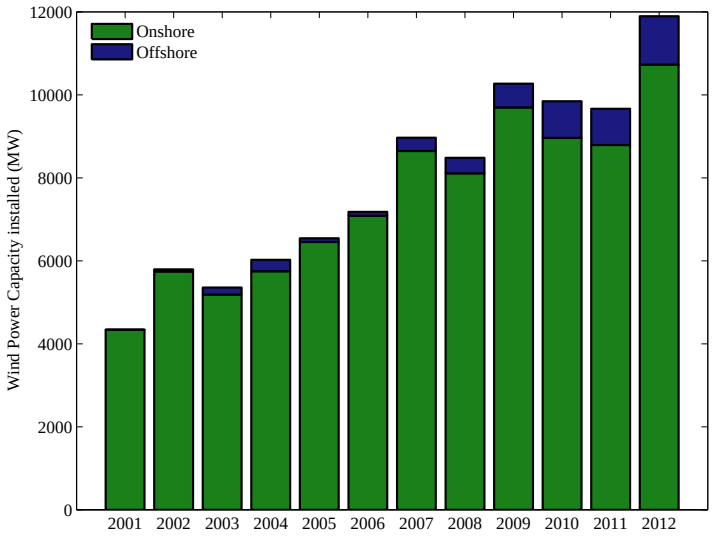

Figure 1.1: Wind power capability installed in EU

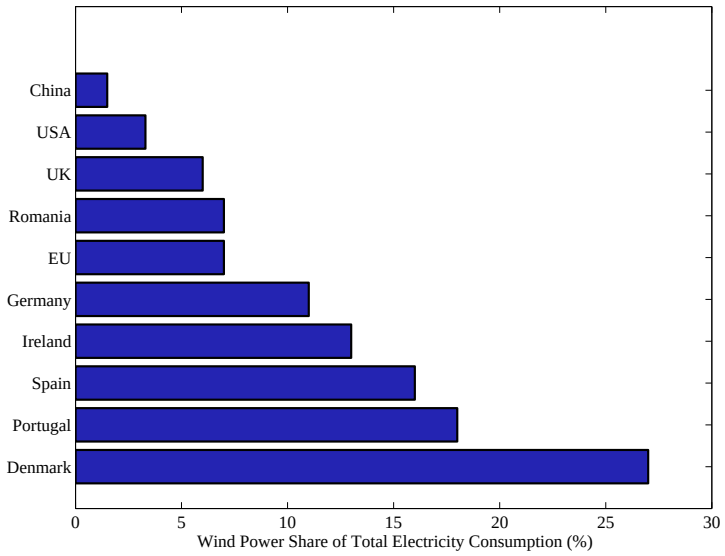

Figure 1.2: Wind power share of total electricity consumption

important role. Since 2008, there is a draft of the new Spanish grid code for wind power in which reference has already been made to inertia emulation and power oscillation damping [19]; moreover, ENTSO-E includes,

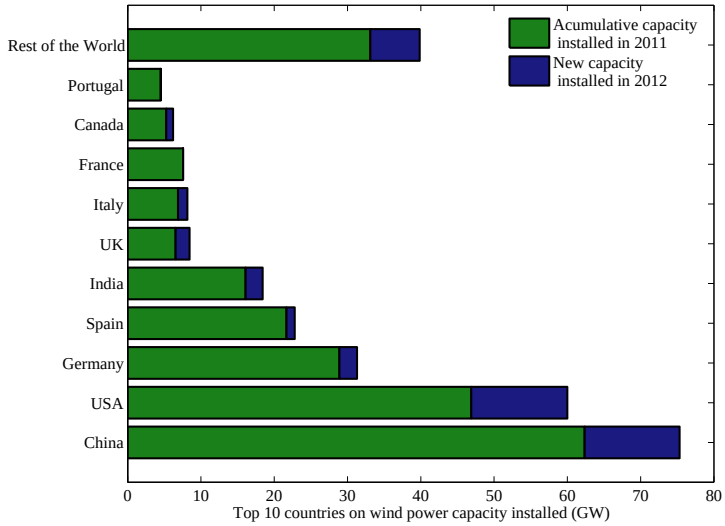

Figure 1.3: Accumulative wind power capacity per country installed in GW

in the final version of the "ENTSO-E Network Code for Requirements for Grid Connection Applicable to all Generators", the power system stabilizer capability as a requirement for any generation units (including wind farms) larger than 10 MW (in the case of UK, Baltic countries and Nordic Area) and 50 MW for Continental Europe Area [20].

The stability of power systems is related to the electromechanical interactions and the behavior of the generators connected to the grid. Therefore, the influence of wind power penetration on the power system is an important issue to be studied [21]. It is important to analyze wind power behaviour under different wind power technologies and controls, as they present different dynamic characteristics causing different effects on the grid [22, 23]. The contributions to power system oscillations damping have been studied considering different technologies, e.g., HVDC links and their controllers [24, 25, 26, 27, 28, 29], by means of flexible AC transmission systems (FACTS) [30, 31, 32] and using wind farms [17].

1.1 Research motivations and objectives

Power oscillations appear in power system because of the inner dynamics of the system when it responds to disturbances. The increase of wind power generation (or distributed generation, in a more general manner) af-

fects power systems behavior since wind technologies, including both asynchronous generators and converter-based wind turbines , are reducing power system global inertia [33]; hence, power system dynamics is changing. The dynamic characteristics of wind farms are substantially different from conventional power plants. For that reason, TSOs have defined some grid codes regarding wind farm connection, and how wind farms must interact with the electrical network [10, 11, 12]. Nowadays, power system oscillation damping is not a mandatory TSO requirement but there is a draft of the new Spanish grid code for wind power that considers this necessity [19];a requirement that has also been taken into account by ENTSO-E for the European common Grid Code, depending on the power generator unit size (including wind power) [20]. Such new challenge for wind power generation has motivated the core of the work carried out throughout this thesis. The main goals of the present thesis are summarized as follows.

- To understand the impact of each wind turbine technology on the power system small signal stability; since, they modify the power system behavior.
- To investigate the possible contribution of wind power plant focusing in variable–speed converter wind turbines (FRCWTs) to damp out power system oscillations.
- To evaluate the influence of different factors related to wind power plants (such as cable length connection) on the contribution provided to power system oscillation damping.
- To compare different controllability/observability and signal interaction analyses for power system oscillation damping using wind power plants to select the best signal pair.
- To study control design limitations imposed by the impossibility of carrying out direct measurements of the signals selected for control.
- To develop the tools to select effectively the wind power plant local signals to properly damp power system oscillations without the requirement of designing the controller.
- To study technical and economic issues related to offshore wind power plants considering current technologies. Allowing fast implementation of the European SuperGrid which, at its first stage, is focused on an offshore HVDC grid connection different European countries.

1.2 Thesis contributions

The main contributions of the thesis are summarized below along with their associated publications:

- To investigate what is the impact of wind turbine technologies on power system stability **[J2]**.
- To implement a power system stabilizer for variable speed wind turbines **[J3, J5, C2, C5]**.
- To study and compare the effect of different factors such as reference signals controlled, cable length and wind power plant location, on power oscillation damping contribution from wind power plants **[J5, C5]**.
- To provide a recommendation guideline to select the best input-output signal pairs for different control schemes to damp power system oscillations by means of wind power plants signals, either through single-input single-output (SISO) or multivariable (MIMO) control **[J7]**.
- To put forward input-output signal selection criteria in order to achieve the best possible control response considering the fundamental limitations imposed by the use of wind power plant local signals to damp out oscillations at synchronous generators; this criteria is completely independent of the controller **[J6]**.
- To analyze both technical and economic aspects regarding the use of non-standard operating frequency at offshore AC networks **[J4]**.
- To develop frequency dependent cost functions of the electrical components required for SuperNode concept installation **[J4]**.

The publications indicated above are fully detailed in Appendix A.

1.3 Thesis outline

This thesis has been divided into eight chapters. The main core of the thesis is to study the capability of wind power plants to contribute to power system stability, focusing in power system oscillation damping. This has been organized as follows.

In Chapter 2, a brief overview of some power system background required for small signal stability analysis is introduced.

Chapter 3 reviews the influence of wind power generation on small signal stability and provides a review of the different control methods for wind turbines (WT) proposed in literature to damp both inner and power system oscillation modes.

In Chapter 4, a comparison of different PSS controllers from WPPs to damp inter-area oscillation modes with local signals is done; moreover, the influence of the distance from WPP to the main network on the controller and the effect of the WPP location are analyzed.

In the first three chapters, the effect several factors as the controller included, the signals used as input and outputs of such controller and the power system model, can be observed on the capability of damping oscillations. As a consequence, it is difficult to draw a clear conclusion or recommendation. To circumvent this issue, power oscillation damping is analyzed using tools which are independent from the controller.

In Chapter 5, different input-output selection methods for SISO and frequency domain methods for MIMO systems are compared, assuming the possible contribution of WPPs to damp such oscillations in the point of WPP connection.

Chapter 6 proposes a criterion to determine the best input-output local signals of WPP to damp power system oscillations at synchronous generators by considering the fundamental control limitations of the systems.

Chapter 7 differs slightly from the main study objective, since it deals with the analysis of a new offshore wind power plant design considering the economic effect of operate the offshore AC network at non-standard frequencies.

Finally, some conclusions and future research lines arising from the thesis are drawn in Chapter 8.

2 Power systems background

An electrical power system can be defined as a set of various individual interconnected electrical elements creating a large, complex and dynamic system which is capable of generating, transmitting and distributing electricity within a large geographical area, required to satisfy electricity demand [34]. Such elements interconnection could lead to a large variety of dynamic interactions. Some of those interactions only affect to a few number of the elements, others to a large part of the power system and, also, others could involve the whole system.

This chapter aims to give a general overview of the main concepts and background required to better understanding of the analysis presented throughout this thesis.

This chapter is organized as follows. In Section 2.1, a brief description of the concepts related to power system stability and small signal stability is done. In Section 2.2, a short description of the main elements present in a power system (such as lines, transformers, synchronous generators and wind power plants) is given. Moreover, some modelling assumptions for power system stability analysis are presented. Finally, in Section 2.3, an introduction to the mathematical basis required for small signal stability analysis is presented.

2.1 Power system stability

Power system stability can be defined as the ability to maintain equilibrium during normal conditions and to recover an acceptable equilibrium after a

disturbance [35, 36].

Power system stability can be classified according to the response of the system to a fault [37] (Figure 2.1).

- Rotor angle stability is concerned with the ability of the interconnected synchronous machines of a power system to maintain or restore equilibrium between electromagnetic torque and mechanical torque, and also to keep the synchronization between them.
- Frequency stability can be defined as the capability of a power system to recover the balance between the system generation and the load, with minimum loss of load.
- Voltage stability refers to the capability of a power system to maintain the steady state of all bus voltages both under normal operating conditions and after a disturbance.

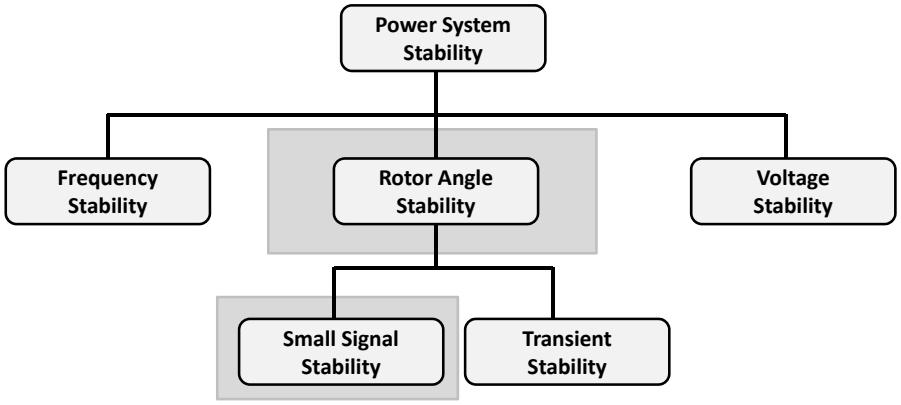

Figure 2.1: Classification of the power system stability concepts

Depending on the particular fault, rotor angle stability can be classified in two different groups [35]:

- Transient stability or large-disturbance stability is related to the ability of the power system to maintain synchronism when it is subjected to a severe disturbance, such as a short circuit on a transmission line. Disturbance severity and initial operating point are key factors to this analysis. In this case, the phase angle of the synchronous machine rotors suffer large deviations affecting the power-angle relation.

- Small signal stability or small-disturbance stability considers the ability of the power system to maintain synchronism during small disturbances. The effect of small disturbances on the variables of the system is considered in small signal stability analysis, and these disturbances are considered small enough to make acceptable the linearization of the non-linear equations of the power system. Small disturbances can be, for example, minor changes in the load or in the generation of the power system.

The study of small signal stability may result in two different response modes

- Non-oscillatory or aperiodic mode due to lack of synchronizing torque. The synchronizing torque is the component of torque change in phase with the rotor angle perturbation. The aperiodic problem has been largely solved by the use of automatic voltage regulators (AVR) in the generators.

- Oscillatory mode due to lack of damping torque. The component of torque in phase with the speed deviation is the damping torque. Oscillation modes are usually cancelled by means of Power System Stabilizers (PSS).

The small-signal modes of oscillation can be classified as [38, 39].

- Power system oscillations
  - **Inter-area modes.** They are oscillation modes occurring between groups of generators that are far among them. Generators that belong to one area oscillate against other group of generators from other areas. This sort of oscillation appear usually when there is a power transfer between areas that are connected through a tie-line. The frequency range of these oscillation modes are approximately between 0.1 to 0.7 Hz.
  - **Local modes or Intra-area modes.** This kind of oscillation mode are related with the rotor angle oscillation of a single synchronous generator against the rest of power system or the rest of the local area where the generator belongs. The frequencies of such modes are usually in the range of 0.7 to 2 Hz.

- Machine oscillations $>$ 2 Hz.

- **Torsional modes.** They are related to the interaction among the mechanical system of the synchronous generators and some power system elements such as reactive power compensators.
- **Control modes.** These oscillation modes consider the effect of various controllers within the power system including excitation control, power converters, etc.

This classification permits to identify the causes of the oscillations and to propose damping control strategies.

The thesis is mainly focused on small signal stability analysis. For that reason, some background material about small signal stability is introduced to ease understanding of the rest of the thesis.

2.2 Power system representation

As previously defined, a power system is understood as a group of different electrical components interconnected among them as shown in Figure 2.2.

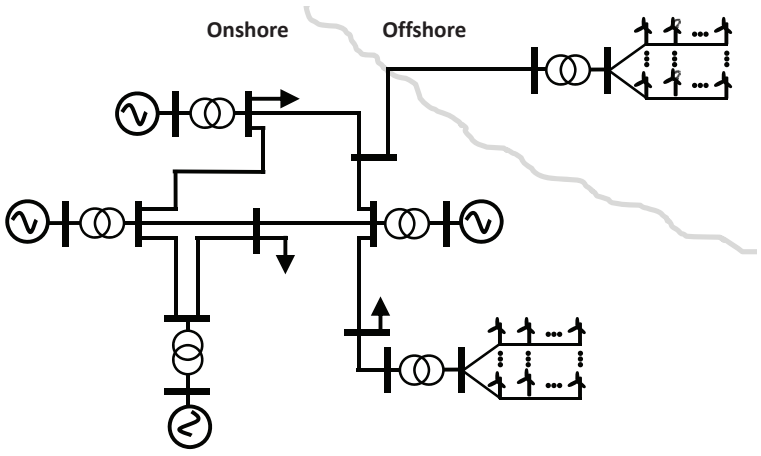

Figure 2.2: Representation of a meshed power system with wind power generation

For power system analysis including stability, models of all the main elements which encompass a power system such as lines, transformers, power generators (synchronous and wind in this case) must be developed. In this section, a brief description of each component of a power system including WPP is presented. Moreover, in the next subsections, a brief introduction

to the modelling of such components and some simplification assumptions made for the present thesis are given. The combination of these elements provides the power system set of differential and algebraic equations required to develop power system analysis including both dynamic and static.

2.2.1 Lines and cables modelling

Cables and lines are the elements used to transmit and distribute electrical power through various areas. Transmission lines and cables are commonly represented by their π-equivalent circuit with lumped parameters, shown in Figure 2.3. Such equivalent provides an approximation of the line (or cable) performance from its terminals [40].

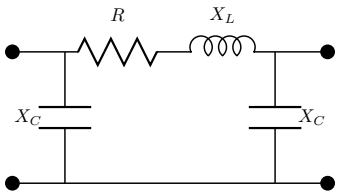

Figure 2.3: Representation of the transmission line π-equivalent

For power system stability analysis, this model may be simplified in a different manner if it is modelling a cable or a line. For the case of lines, they can be only modelled lossless by inductances, neglecting both the resistive and the capacitive effect. Conversely, cables can be modelled as a shunt capacitor [40, 36].

2.2.2 Transformer modelling

Transformers are important component of the power system since they provide the capability of linking different network parts operating at different voltage levels. Moreover, they are capable to control voltage by means of the tap changer. Transformers can be ideally represented by the equivalent circuit shown in Figure 2.4. This circuit can be approximated to an equivalent π-circuit (similar to the scheme shown in Figure 2.3) after some assumptions are made [34].

For the analysis of power system stability, transformers models may be simplified as an inductance due to their significant inductive nature [41].

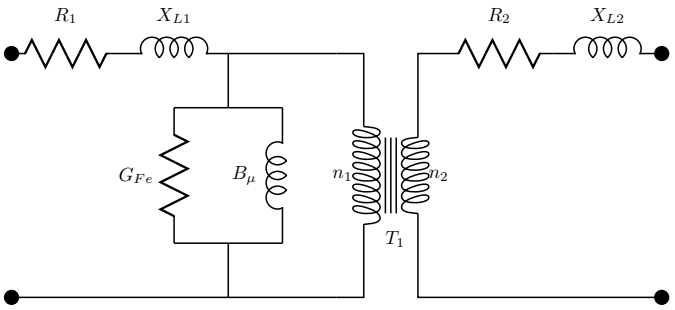

Figure 2.4: Representation of the equivalent circuit of a two-winding transformer

2.2.3 Synchronous generator modelling

Synchronous machines are one of the most important elements in a power system, and they have large effect in power system stability [41], even more in electromechanical oscillations. There exist various levels of complexity of synchronous machines dynamic models; but, with exception of very small power systems, complex models of the synchronous machines cannot be used for stability studies [42]. It is worth to remark that high order models used to add only little extra information into power system stability analysis [33].

The simplest synchronous machine representation is the so-called classical model which is used to explain some of power system stability fundamentals. It is described by the swing equation (Newton's second law for rotating masses),

$$M\frac{d^2\delta}{dt} = P_m - P_e - D\omega \tag{2.1}$$

where δ, ω, P_m, P_e and $D\omega$ represent the rotor angle, the rotating speed of the rotor, the mechanical power, the electrical active power generated and the damping power of the synchronous generator, respectively.

This equation can be rewritten into a set of differential equations such as,

$$\begin{aligned}\frac{d\delta}{dt} &= \omega - \omega_s \\ \frac{d\omega}{dt} &= \frac{1}{M}\left(P_m - P_e - D\omega\right)\end{aligned} \tag{2.2}$$

where $P_e = \dfrac{E'V}{X'}\sin\left(\delta - \theta\right)$ assuming the generator as a voltage source, E' behind a transient inductance, X' without losses.

Another simplified model used within the thesis for theoretical studies, neglects the effect of the damper windings. This is a third order model of the synchronous machine considering the swing equation and the d-axis electromagnetic field (EMF) transient dynamics. This model represents the synchronous generator as a voltage source behind a transient inductance as shown in Figure 2.5.

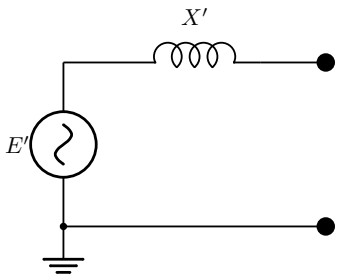

Figure 2.5: Representation of a synchronous generator as a voltage source behind a transient inductance

In order to reach such model, some assumptions for the synchronous machine must be taken into account:

- The resistor resistance R_s and stator transients $\frac{1}{\omega_s}\frac{d\psi}{dt}$ are neglected.
- The d and q axes donot contain damper windings.

The third order synchronous machine model is given by

$$\begin{aligned}
\dot{\delta} &= \omega - \omega_s, \\
\dot{\omega} &= \frac{\omega_s}{2H}\left(P_m - \frac{E'V_1}{X'}\sin(\delta-\theta) - D\omega\right), \\
\dot{E}' &= \frac{1}{T_0}\left(E_f - \frac{X}{X'}E' + \frac{X-X'}{X'}V\cos(\delta-\theta-D\omega)\right).
\end{aligned} \tag{2.3}$$

The derivation of the equations can be found in literature, e.g., [42, 33].

2.2.4 Wind power plant

A wind power plant can be defined as a wind farm which, owing to its large power generation capacity, is required to behave similarly to conventional

synchronous generators. It means that wind power plants are required to accomplish with TSOs demands, in terms of power generation, control and ancillary services. These requirements can be found in the grid codes developed by national TSOs, e.g., [11, 10]; although at this time, a common European grid code is being prepared by the ENTSO-E [20].

For that reason and the rapid technology development, it is important to know if the sort of wind turbines that are installed would be able to act as a wind power plant. Some of the most common wind turbine generator systems are briefly described in the following. Afterwards, how the wind power plant modelling assumptions for power system stability analysis are introduced.

Common wind turbine technologies

Wind power generation systems is evolving fast; for that reason, different concepts of wind turbine technologies are currently installed all over the world. These wind turbine technologies are usually classified as type A, B, C and D (in United States named type I, II, III, IV, respectively), depending on the capability of frequency regulation of each wind turbine configuration [8, 43, 44, 17]. It is worth to remark that the concepts known as variable speed are (C and D), at the moment, the most popular [45].

Fixed speed wind turbine - Type A Figure 2.6 shows a fixed speed wind turbine. This wind turbine topology is implemented with a squirrel-cage induction generator (SCIG), and is directly connected to the power system through a step-up transformer. A capacitor bank is used to compensate the reactive power requirement of the SCIG. Moreover, induction generators have a critical transient response of the currents during their connection and disconnection, a smoother grid connection is achieved by using a soft-starter. The turbine speed of this type of wind turbine is fixed or nearly fixed ($\approx \pm$ 1%) to the electrical frequency of the grid.

Partial variable speed wind turbine - Type B A schematic of Type B wind turbine representing the partial variable speed wind turbine is presented in Figure 2.7. This wind turbine topology encompasses a wound rotor induction generator (WRIG) equipped with a dynamic rotor resistance (DRR). The wind turbine is builded by connecting an external rotor resistance R_{ext} to the rotor circuit of an induction generator (IG), while the stator is connected directly to a step-up transformer similarly as previous Type A wind turbine. Also, as occurs with the fixed speed wind turbine, there is the requirement

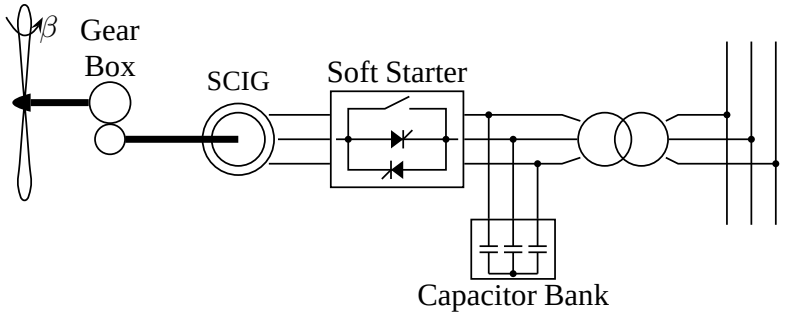

Figure 2.6: Fixed speed wind turbine with squirrel cage induction generator

of reactive power compensation and soft-starter. This type of wind turbines are known as partial variable speed due to they are capable to regulate the rotor resistance increasing the turbine speed range in a moderate manner with a slip range from 2% to 10% (always above rated turbine speed). The excess of power is dumped as heat loss. The regulation of DRR control can help to improve power quality, reduce flicker emission from wind turbines to the power grid, among others [46].

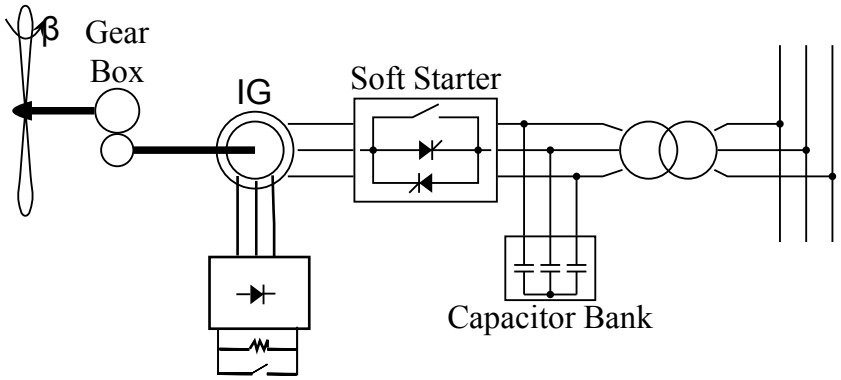

Figure 2.7: Partial variable speed wind turbine equipped with wound rotor induction generator with dynamic rotor resistance

Variable speed wind turbine with a partial rated converter - Type C Type C wind turbine which is commonly named as doubly-fed induction generators (DFIG) is represented in Figure 2.8. This wind turbine configuration uses a WRIG and a partial rated power converter (approximately 30% of

the nominal power of the generator) which is connected to the rotor circuit. In this wind turbine technology, the generator stator windings are connected directly to the grid through a step-up transformer and the rotor is connected through the power converter which controls the rotor currents and decouple rotor speed from the electrical frequency of the grid. Moreover, this configuration does not require neither reactive power compensation nor soft-starter, since such operations are performed by the partial rated converter. Although Type C corresponds to a limited variable speed wind turbine, it is accepted as variable speed since it can be operated in a wider range of dynamic speed which is ± 30% approximately.

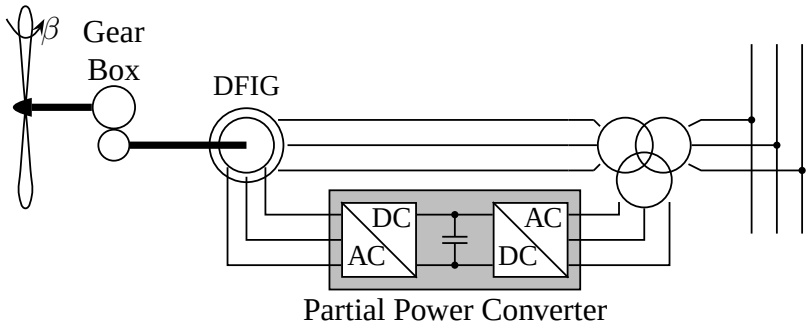

Figure 2.8: Variable speed wind turbine driving a doubly-fed induction generator

Variable speed wind turbine with a full rate converter - Type D In Figures 2.9(a) and 2.9(b), two different configurations of full rate converter wind turbines (FRCWT), also known as type D, are drawn. These wind turbine topologies connect the generator to the network by means of a full rate power converter. The power converter performs, as occurs in Type C wind turbines, the reactive power compensation and the smoother grid integration. The generator can be excited either electrically or by permanent magnets. These wind turbine technologies can have gearbox (see Figure 2.9(a)) or avoid its usage called direct drive (see Figure 2.9(b)). In the case of direct drive, its implementation is possible since the full rate power converter completely decouples the generator from the grid; thus, it can be controlled at any turbine speed.

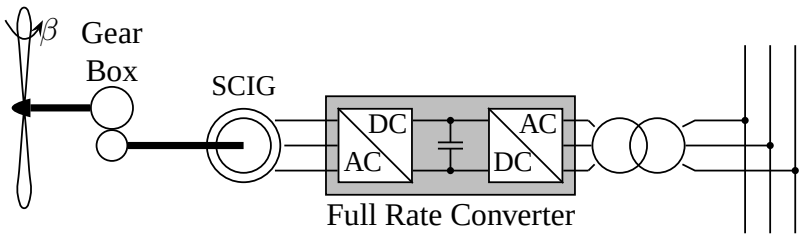

(a) Variable speed wind turbine with full rate converter induction generator

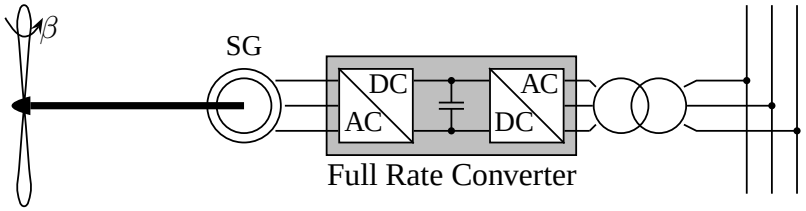

(b) Variable speed wind turbine with direct drive synchronous generator

2.2.5 Wind power plant modelling

A wind power plant encompasses a large number of wind turbines. Due to this fact, the complete model of these power generation systems are complex and it can not be easily used for power system stability analysis. To overcome this problem, equivalent models of the wind power plants are used to emulate all wind farm behavior considering just one big wind turbine connected to the power system [47]. Also, aggregate models (an intermediate way between equivalent and complete models) would be modelled by implementing a part of each wind turbine individually (for instance, mechanical part or wind) and other as a just one big element (e.g., power converter or generator) [48]. For power system stability analysis, FRCWT can be more simplified. It can be modelled as a negative load, since their dynamics are decoupled from the network by the power converter. Moreover, power converter dynamics would be neglected since they are much faster than power system electromechanical modes [49]. This is the approach used within the thesis to describe WPPs.

2.3 Mathematical basis of small signal stability

As previously stated, power systems are usually described by a set of nonlinear differential equations together with a set of algebraic equations, i.e.,

$$\begin{aligned} \dot{x} &= f(x,u), \\ y &= g(x,u), \end{aligned} \tag{2.4}$$

where

$$x = \begin{bmatrix} x_1 \\ x_2 \\ \vdots \\ x_n \end{bmatrix} u = \begin{bmatrix} u_1 \\ u_2 \\ \vdots \\ u_m \end{bmatrix}, \quad y = \begin{bmatrix} y_1 \\ y_2 \\ \vdots \\ y_r \end{bmatrix}, f = \begin{bmatrix} f_1(x,u) \\ f_2(x,u) \\ \cdots \\ f_n(x,u) \end{bmatrix}, \quad g = \begin{bmatrix} g_1(x,u) \\ g_2(x,u) \\ \vdots \\ g_r(x,u) \end{bmatrix}$$

where x is the vector of the state variables, u is the vector of the system inputs, y is the vector of the system outputs, and f and g are the vectors of nonlinear functions. Moreover, n is the order of the system, m is the number of inputs considered in the system, and r is the number of outputs.

For a small signal stability analysis, the system (2.4) is linearized around an operating point [34]. Linearization is reasonable because, as previously stated, the disturbances are assumed to be small. Then, the power system can be written as a linear system of the form

$$\begin{aligned} \Delta\dot{x} &= A\Delta x + B\Delta u, \\ \Delta y &= C\Delta x + D\Delta u, \end{aligned} \tag{2.5}$$

where

$$A = \begin{bmatrix} \frac{\partial f_1}{\partial x_1} & \cdots & \frac{\partial f_1}{\partial x_n} \\ \vdots & \ddots & \vdots \\ \frac{\partial f_n}{\partial x_1} & \cdots & \frac{\partial f_n}{\partial x_n} \end{bmatrix}, B = \begin{bmatrix} \frac{\partial f_1}{\partial u_1} & \cdots & \frac{\partial f_1}{\partial u_m} \\ \vdots & \ddots & \vdots \\ \frac{\partial f_n}{\partial u_1} & \cdots & \frac{\partial f_n}{\partial u_m} \end{bmatrix},$$

$$C = \begin{bmatrix} \frac{\partial g_1}{\partial x_1} & \cdots & \frac{\partial g_1}{\partial x_n} \\ \vdots & \ddots & \vdots \\ \frac{\partial g_r}{\partial x_1} & \cdots & \frac{\partial g_r}{\partial x_n} \end{bmatrix}, D = \begin{bmatrix} \frac{\partial g_1}{\partial u_1} & \cdots & \frac{\partial g_1}{\partial u_m} \\ \vdots & \ddots & \vdots \\ \frac{\partial g_r}{\partial u_1} & \cdots & \frac{\partial g_r}{\partial u_m} \end{bmatrix}$$

and Δ denotes a small variation with respect to the operating point, A is the state matrix, B the input matrix, C the output matrix and D is a matrix describing the direct connection between the input and the output.

The linear system presented in (2.5) is represented by the scheme shown in Figure 2.9.

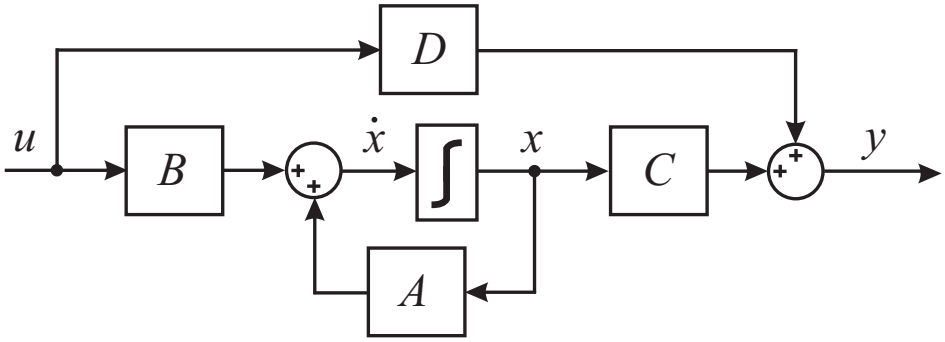

Figure 2.9: State space block diagram representation

2.3.1 Eigenvalues

The stability of the system (2.5) can be analyzed by computing the eigenvalues of the state matrix A. The eigenvalues are the roots of the system characteristic equation

$$\det(\lambda I - A) = 0 \tag{2.6}$$

where det is the determinant. The solutions of the equation (2.6) λ_i may be real or complex. The eigenvalues provide dynamic characteristics of the system to small disturbances. Since it can be proved that the response of (2.5) is given by

$$y = \sum_{i=1}^{n} R_i e^{\lambda_i t}. \tag{2.7}$$

Moreover, according to Lyapunov's first method, the small signal stability of a nonlinear dynamic system is determined by the location of the roots of the characteristic equation [41]. Each eigenvalue can be expressed as

$$\lambda_i = \sigma_i \pm j \cdot \omega_i, \tag{2.8}$$

where σ_i and ω_i determine the response of the system as follows.

- When $\sigma_i < 0$ for all i, the system is asymptotically stable.
- When at least in one of the eigenvalues, $\sigma_i > 0$, the system is unstable.

- When exist one eigenvalue with $\sigma_i = 0$, the system is marginally stable.

- When at least in one of the eigenvalues, $\omega_i \neq 0$, the system has a oscillatory response.

- When $\omega_i = 0$ for all i, the system has a non oscillatory response.

Therefore from the evaluation of the eigenvalues, system stability can be determined and also if the power system may present any type of oscillation, as shown in Figure 2.10. Moreover, the real part σ_i of the eigenvalue λ_i provides the damping of the amplitude of the oscillations; meanwhile, the imaginary part ω_i indicates the oscillation mode frequency.

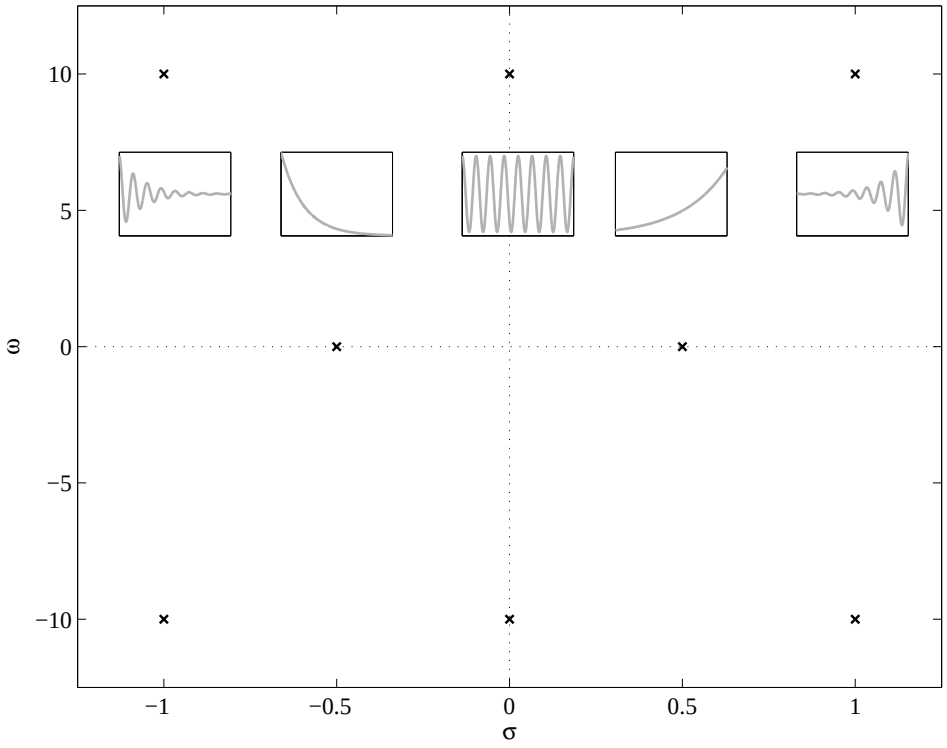

Figure 2.10: Representation of the dynamical response depending on eigenvalue location

The damping ratio ξ_i permits to state how damped are the oscillation modes, and it is calculated as follows

$$\xi_i = \frac{-\sigma_i}{\sqrt{\sigma_i^2 + \omega_i^2}} = \frac{-\sigma_i}{\omega_{ni}}, \tag{2.9}$$

where $\omega_{ni} = \sqrt{\sigma_i^2 + \omega_i^2}$ represents the undamped frequency of the mode.

Therefore, eigenvalues with real part close to the right hand plane and smaller damping ratio will be the most important in stability analysis, since they would became unstable easily.

2.3.2 Eigenvectors and participation factor

An eigenvector can be easily understood as a non-null state vector which after being multiplied by the state matrix A, returns a proportional of such vector. The ratio between both vectors is the eigenvalue related to the eigenvector [50]. There is an eigenvector associated to each the eigenvalues. The right eigenvector Φ_i of the eigenvalue λ_i must satisfy the following equation

$$A\Phi_i = \lambda_i \Phi_i; \tag{2.10}$$

otherwise, the left eigenvector Ψ_i of the eigenvalue λ_i must satisfy

$$\Psi_i A = \lambda_i \Psi i. \tag{2.11}$$

Right and left eigenvectors are orthogonal between them. Therefore, they can be normalized in order to ease their understanding, such practice is usual in power system.

$$\Psi_i \Phi_i = I; \tag{2.12}$$

thus, the left eigenvector could be calculated as

$$\Psi_i = \Phi_i^{-1}. \tag{2.13}$$

The participation factor reveals what state variables are affecting to the desired mode to be damped. The participation factor permits to determine the contribution of each state to a particular eigenvalue. Moreover, the participation factor helps to determine exactly the sort of oscillation mode appearing.

The participation matrix is defined from right and left eigenvectors as follows,

$$P = \Phi_i \Psi_i^T \tag{2.14}$$

where

$$P = \begin{bmatrix} p_{11} & \cdots & p_{1n} \\ \vdots & \ddots & \vdots \\ p_{in} & \cdots & p_{nn} \end{bmatrix}, \tag{2.15}$$

with $p_{1i} = \Phi_{1i}\Psi_{i1}$ [51]. The participation matrix values are generally complex; however, only the magnitude of the value is considered due to the angle does not give useful information. In order to ease it understanding and individual mode analysis, a column scaling of the participation matrix is done. This scaling ensures that the total sum of the column is equal to 1, then the contribution on the mode of each state variable is represented in per unit.

3

Literature review of power oscillation damping supported by wind power

3.1 Introduction

Power system small signal stability is mainly related to electromechanical interactions between synchronous generators and the electrical network. This effect arise commonly after a system disturbance, and shows the existing inner dynamics of the power system. It is worth to remark that with the introduction of converter-based generation technologies the power system is reducing its global inertia implying lower natural damping. It is important to analyze the effect of different wind power technologies and controls into the power systems, as they present different dynamic characteristics.

This chapter aims to discuss wind power impact on small signal stability and to provide a review of the different control methods for wind turbines (WT) to damp both inner and power system oscillation modes. It is important in order to understand what can be done from wind turbines.

This chapter is organized as follows. The impact of different wind turbine technologies in power system oscillations is analyzed in Section 2. In Section 3, the methods proposed to damp out inner oscillations of the wind turbine are presented. The capability of wind farms to provide an extra power delivery to damp power system oscillation is discussed in Section 4. Finally, in Section 5, the conclusions are outlined.

3.2 The impact of wind farms in power system oscillations

In this section, the influence of wind farms on the oscillation damping of power systems is analyzed. In recent years, several researchers have analyzed the effects of oscillatory modes from two different points of view: oscillation modes of wind farms against power systems and inner oscillation modes of wind turbines. Most of the research in the literature considers equivalent models of the wind farms to emulate an aggregated behavior in just one big wind turbine connected to the power system [47]. However, in some cases, this approach is not the most appropriate to reduce the wind farm to one-equivalent machine [48]. For example, to determine the oscillatory behavior of the wind turbine components, it is usually necessary to analyze a single wind turbine against an infinite grid.

3.2.1 Oscillations in power system with wind farms

Wind turbines are generally not synchronously connected to the grid; hence they do not participate in electromechanical oscillations. Wind power itself does not induce new low frequency oscillation modes into power systems because their generator technologies do not engage in power system oscillations [52, 53, 54].

Due to the rapid increment of wind power penetration in power systems, it is important to analyze how this fact could affect the dynamic behavior of the power systems. Several researchers divide this analysis not only by the penetration level, but also by changes in the system, such as the substitution of conventional generators by wind farms or the location of wind farms in different power system buses [17, 55, 56].

Here, in order to study the dynamic effect of main wind turbine technologies on the grid, the study is divided into fixed speed and variable speed wind turbines.

Power system with fixed speed wind turbines

According to [17, 21, 52], fixed speed wind turbines (FSWT), understood as wind turbine driving squirrel cage induction generators (SCIG-WT) (Figure 2.6), improve the damping of power system oscillation modes. Moreover, due to their asynchronous nature they do not engage in power system oscillations nor do they induce new oscillatory modes [52]. It is agreed that SCIGs show

better damping contribution on inter-area modes than on local oscillation modes [52, 55, 49, 57, 58, 59].

However, some studies reveal that there are special situations where the impact of FSWT could have a detrimental effect on the oscillatory behavior of the power system, e.g., the full load condition of the wind turbines in a weak grid [55, 57], the penetration level in the power systems [21], the connection strength of the tie lines [60] or the location of the wind farm [59].

Although SCIG is the most common generator in FSWT, there are others, like permanent magnet synchronous generators (PMSG) which may engage in power system oscillations since they are synchronous generators directly connected to the grid like conventional power generators. FSWT-PMSG could have stability problems when a disturbance occurs in the power system [61].

Power system with variable speed wind turbines

Variable speed wind turbines (VSWT) are partially or totally decoupled from the grid by a power converter regulating the power delivered by the WT. As a result, power system oscillations do not affect the wind turbine [21, 62].

Unlike FSWT, the influence of VSWT on power system oscillations does not draw a clear answer. In order to analyze the impact of VSWT on electromechanical oscillations, there are some important factors to be considered including wind turbine technology used, control mode of the VSWT and wind power penetration [63].

VSWT technologies can be divided on doubly fed induction generators (DFIG) and full rate converter wind turbines (FRCWT) as shown in Figure 2.8 to 2.9(b). This classification is used in order to analyze the impact of VSWT technologies on low frequency oscillations.

DFIG is the most analyzed VSWT because it is the most common technology. Researchers study the influence of the general DFIG-scheme without considering the possible impact of the control on power systems have come to divergent conclusions. Some authors have concluded that DFIGs can enhance power system damping [17, 52, 56, 64], regardless of the wind farm location [59, 65] or that DFIGs have even been able to provide good damping performance into a weak area of the grid [66, 67]. However, in other studies it is shown that DFIGs can decrease the damping of the inter-area oscillation mode [49], or reduce the damping in special cases such as when the increment of wind power contributes to an increase in the power system stress [68, 69] or when its increase reduces the damping because it can

collapse weak interconnection lines [70].

Some results reveal that VSWT-DFIGs are able to interact with the PSS of synchronous machines. These WT can damp initial oscillations of the power systems for small disturbances but may decrease voltage stability under large disturbances, in comparison with other synchronous machines [71].

When comparing control methods in the analysis of the interaction between the VSWT-DFIG and the power system, the conclusions are quite different. WT with power factor control, the oscillation modes could be slightly better damped [53, 72] or have a detrimental effect on the damping [67, 73]. On the other hand, WTs with frequency control help to enhance damping of the oscillatory modes [53, 72]. This is because the rotor oscillations are observable from the grid frequency signal. It should be noted that all previous control methods mentioned do not regulate reactive power.

The effect of an additional voltage control loop to regulate reactive power could be detrimental depending on the particular choice of the control parameter and also on the location on the measurement point [67, 74]. The interaction of the voltage control with the frequency control may achieve a slight improvement according to [72]. In Table 3.1, a summary of the influence of VSWT-DFIG is classified by the control used.

Within FRCWT technologies are Direct Drive Synchronous Generators (DDSG) (Figure 2.9(a)) which is the most common, and Full Rate Converter Induction Generators (FRCIG) (Figure 2.9(b)). DDSGs have been categorized by some authors in the same group as DFIGs [21, 55], therefore, they concluded that the impact in power systems oscillations of DDSG is similar to DFIG. Again, conclusions are divergent, for instance, a damping enhancement of the power system oscillations is reported in [58, 76]. On the contrary, the damping could be decreased if a power factor control mode is used [49, 43] or if a voltage control is introduced to regulate the reactive power [77].

In contrast, with FRCIGs, the damping of the inter-area oscillation is increased either by power factor control [78] or by voltage control [79].

There is alternatively variable speed wind turbine technology connecting a synchronous generator directly to the grid with a hydro-dynamically controlled gearbox [80]. In this technology, wind power penetration could be relevant, since it is a synchronous machine connected to the grid and thus is able to engage with power system oscillations.

Convergent results on the influence of wind power on power system stability are summarized in Table 3.2.

Control	Influence
Power Factor	- Small enhancement of the power system damping [53, 72]
	- Some negative effects on the damping of power system oscillations are reported in [67, 73]
Voltage control	- Optimization of voltage control constants with power oscillation constraints improves the damping [75]
	- Sensibility to the control parameters, incorrect values may be detrimental to the damping [67, 74]
Frequency control	- Enhance the damping of the power system oscillations [53, 72]

Table 3.1: Summary of results on the impact of the DFIG controls on power system oscillations

3.2.2 Inherent oscillations of wind turbines

In WTs there are several rotating elements and electrical devices interacting. Hence, it is interesting to investigate the oscillations that could appear in the machine or in the wind farm. A wind turbine has many inner oscillation modes, e.g., for-after tower movements. From an electrical point of view, only the torsional modes are important since they are the only ones that may affect the power system. Again, this study is divided in FSWT and VSWT.

Fixed speed wind turbines

In FSWT, the main oscillation modes are associated to the drive-train. Notice that the mechanical dynamics of the wind turbines must be described with at least a two-mass [81], or three-mass model [82], since a single-mass

Technology	Influence
FSWT-SCIG	- Can improve damping of the power system [52, 55, 49, 58, 59]
	- Can deteriorate oscillatory behavior under special conditions [52, 57, 59, 60]
FSWT-PMSG	- Has problems in stability [61]
VSWT-DFIG	- Can enhance power system damping [17, 52, 53, 56, 59, 64, 65, 66, 67, 72, 75]
	- Can decrease the damping of inter-area oscillations modes [49, 67, 68, 69, 70, 73, 74]
VSWT-DDSG	- Can improve oscillatory behavior of the power system [58, 76]
	- Can affect negatively in oscillations [49, 43, 77]
VSWT-FRCIG	- Can affect positively in power system oscillations [78, 79]

Table 3.2: Summary of results on the influence of wind power technology on power system oscillations

shaft models cannot properly represent mechanical oscillations.

Mechanical oscillations are critical since they induce fatigue stresses on the drive-train components, increasing the risk of damage to the mechanical system. Drive-train oscillation modes are dynamically dominant in the WT. These oscillation modes depend on the shaft stiffness, the network reactance, the rotor resistance and the operating slip.

Under normal operation, torsional oscillations are well damped since the slip curve of the induction generator acts as an effective damper [17, 83]. However, the system can be lead to oscillate by different disturbances. For instance, the wind speed variations may excite these modes causing reso-

nance phenomena at special gear ratios [84]. Moreover, an electrical disturbance close to the common coupling point (CCP) may provoke mechanical stresses [85, 86]. Also, the torsional oscillations can be excited by the aerodynamics of the wind turbine [87]. Even, wind fluctuation in an specific speeds can cause drive-train oscillations to the wind turbine [88].

Variable speed wind turbines

In VSWT, besides of the shaft, the power converter can also affect the inner oscillations. However, it can be noticed that the inherent oscillations of the machines does not dependent on VSWT technologies. These oscillations are mainly associated with the drive-train and with the converter [67, 76, 89].

In VSWT operating at constant generator torque, there is a slight damping provided by the induction generator in comparison with FSWT since the torque does not vary with the generator speed [17, 83]. This fact implies that torsional oscillation modes in VSWT are less damped than in FSWT.

The interaction between these inner oscillations and different converter controls is interesting to analyze. Voltage control could present a poorly damped shaft oscillation mode for certain parameter setting [90]. Incorrect controller constants may cause an amplification of the oscillations during a fault in the CCP. Analyzing this control configuration in more detail, a range of controllability and stability can be determined [91]. In [92, 93], a study of the sensibility of the oscillation modes to different parameters is presented, e.g., wind speed and mechanical torque input, and the critical stability points, known as Hopf Bifurcation, are determined.

In [94], the behavior of different power control strategies, as in maximal power point tracking (MPPT) and power smoothing have been analyzed. The first control has a positive effect on the oscillation damping of the generator, whereas power smoothing control has no damping effect.

A scheme giving an overview of the key points of the impact of wind farms on power system oscillations is shown in Figure 3.1.

3.3 Damping control for wind turbine inner oscillations

In this section, the controllers designed to enhance the damping of torsional oscillations are analyzed. This section is organized by the type of control that is used, such as mechanical and converter-based regulation.

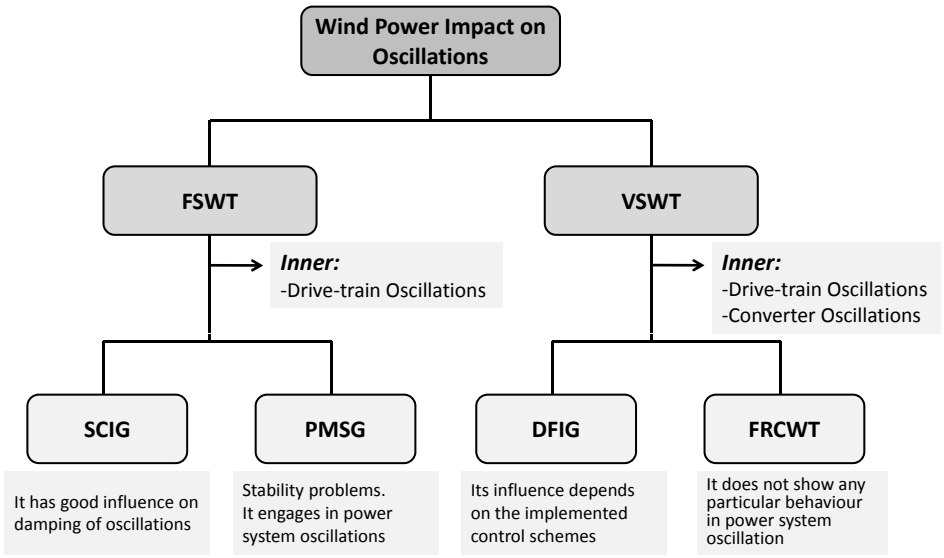

Figure 3.1: Brief summary of the impact of Wind Farms on oscillations

3.3.1 Mechanical regulation

Inner oscillation modes of the wind turbine can be mechanically damped by regulation of the blades using the pitch control, by the inclusion of mechanical dampers in the wind turbine drive-train or by the inclusion of some external devices such as FACTS.

Generally, the mechanical stress suffered by the wind turbine (for instance torsional oscillation) is generated by a difference between the turbine and the generator torque. This difference could be produced by several causes, such as an electrical fault close to the wind turbine or wind gusts. This torsional oscillation could be smoothed by pitch angle control which reduces the torque in the turbine [95, 96, 97].

Direct-drive wind generators which directly couple the generator to the wind turbine, eliminate the requirement of a gearbox. However, they make the conventional generator design of the windings ineffective to damp oscillations, requiring a damper in the wind turbine [98]. In this paper, a spring and a mechanical damper are included to enhance the damping of the mechanical oscillations.

Since mechanical regulation is slow and limited in FSWT, the use of external devices is necessary to obtain a faster response to faults. In [99, 100] is stated that the torsional oscillations can be further damped by including

a STATCOM device rather than using only pitch angle control. In addition, a STATCOM controlled to mitigate SSR and to damp torsional oscillations simultaneously is presented in [101].

3.3.2 Converter-based regulation

There are some research developments regarding inner oscillations of the wind turbine and their damping using a control of the converter. A PID controller for drive-train oscillation damping included on the generator torque regulation is presented in [17, 83, 102]. From these documents, it can be concluded that a PID torque controller could effectively help to enhance torsional oscillation damping of the wind turbine on the desired frequencies. This controller can be seen as a band-pass filter of the form

$$G\frac{2\xi\omega s(1+s\tau)}{s^2+2\xi\omega s+\omega^2}, \tag{3.1}$$

where G is the gain, ω is the frequency that must be close to the frequency to be damped, ξ is the damping of the controller and τ is used to compensate the time delays in the system. The parameters can be properly tuned using a root locus plot [83].

In [103] a conventional PSS scheme has been introduced to regulate the DC link using the machine speed as input. Also, a minor control loop composed of a high-pass filter and a second-order controller has been proposed for VSWT [104]. This proposal is cheap, requires less parameters identification and is easy to implement on the actual controls. A comparison of pitch control with gain scheduling and a drive train damper has been demonstrated in [105]. This study shows that the controller is able to achieve a significant reduction of the oscillations in the drive-train and to reduce the possibility of fatigue damage. In order to reduce the mechanical loads in the drive train, a self-tuning control scheme acting on the pitch actuator and on the power converter has been proposed in [106]. This adaptive controller varies the parameters of the torque controller to minimize the torque variation of the drive train. In [107] a sliding mode control is proposed to optimize the power efficiency and the torsional dynamics. This paper presents a controller that provides a compromize between power extraction efficiency and torque oscillation smoothing.

Wind turbine inner oscillations are an important issue, not only due to the delivered power quality but also because of the stress suffered by the mechanical system of the wind turbine, mainly the drive-train. Some methods to damp drive-train oscillations have been patented, for example, a vibra-

tion damper designed to damp drive-train oscillations with a peak detector in order to reduce the tower oscillation effect [108] and a moment corrector by means of the rotational speed error [109]. In [110], an implementation of a new controller is proposed to avoid the use of Fourier Transform that results inaccurate during frequency variations. Also a method to improve the quality of the power delivered to the grid by means of DC-link voltage regulation is presented in [111].

Figure 3.2 provides a summary of the regulation proposals of the torsional oscillations following the section structure.

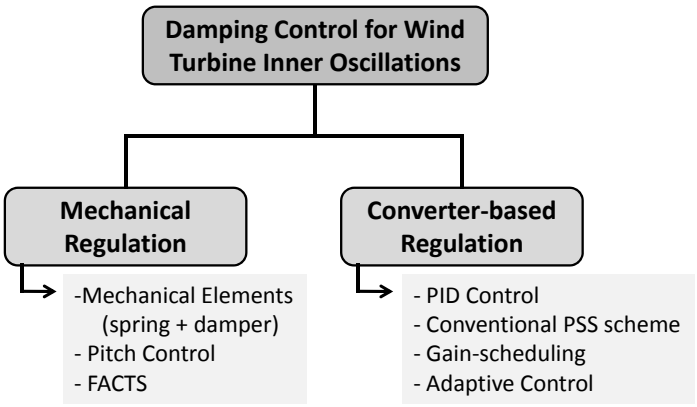

Figure 3.2: Summary of control proposals to damp wind turbine inner oscillations

3.4 Control of wind farms for enhancing the damping of power system oscillations

In this section, the active contribution of wind farms to damp the oscillations suffered by the power system using FSWT and VSWT is analyzed. VSWT can regulate the power delivered to the grid by means of power converters, which can independently control active and reactive power using vector control [112] or flux magnitude and angle controller (FMAC) [113], and using properly a pitch angle control, whereas in FSWT, only the pitch angle control can provide power regulation [95].

This section has been organized by the type of extra-regulated power delivered to the grid, such as active, reactive or active-reactive power regulation.

3.4.1 Active power regulation

The regulation of active power is the logical and direct approach to damp power system oscillations because the oscillations are produced by active power differences between generation and consumption. Therefore, these oscillations can be reduced by controlling active power delivery.

Active power can be regulated by means of mechanical systems or by using power converters.

Mechanical regulation

It is well known that mechanical regulation of wind turbines is slower than the control of electrical variables [17, 95]. Hence, its effect can be noticed with some delay. Mechanical regulation to counteract power system oscillations is mainly focused on pitch angle control and is more common in FSWT [114].

The most simple control alternative to damp out power oscillation consists of a PID controller acting on the pitch angle, where the controller input is the frequency error [115]. This scheme can be seen in Figure 3.3, where F_{meas} and F_{ref} are the measured frequency from the grid and the reference frequency, respectively, ΔP is the power deviation calculated by a droop controller from the frequency deviation, P_{meas} is the measured power from the WT and P_{ref} is the reference power. β is the pitch angle, and P_m is the mechanical power of the WT. Another more complex solution is the fuzzy logic controller also acting on the pitch angle which is shown in Figure 3.4. This controller can deal with the nonlinearities and the non-accurate knowledge of the system [116].

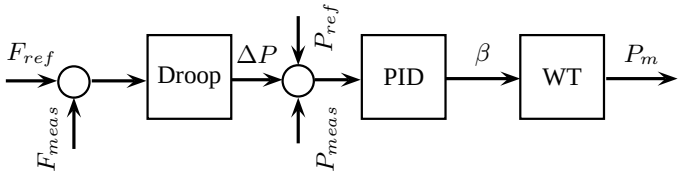

Figure 3.3: PID pitch angle controller scheme

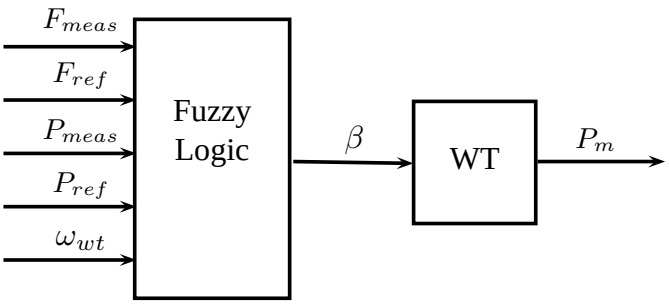

Figure 3.4: Fuzzy Logic pitch angle controller scheme

Pitch angle control proposals for other kinds of grid support may be implemented with the purpose of damping power system oscillations. For example, a pitch angle regulation for frequency control, which uses the frequency error as input and delivers a pitch angle variation, could be suitable to reduce these oscillations [117, 118, 119].

Mechanical and external regulation

Although pitch control systems are capable of improving wind farm stability, they may act too slowly to compensate some of the oscillations. Thus, as in FSWT there is only the possibility of power regulation (pitch angle control), the use of external equipment (FACTS) is required to increase its damping contribution. Such equipment could include dynamic breaking resistors (BR) which only regulate active power, a static synchronous compensator (STATCOM) which can control reactive power and super-conducting magnetic energy storage (SMES) which is able to regulate both active and reactive power at the same time [120]. In [121] external regulations are shown to be more effective in the wind farm stabilization than pitch angle control. In [122] is presented that the system is better damped by using simultaneously STATCOM and pitch angle control, than by using uniquely a STATCOM.

Power converter regulation

In contrast with mechanical regulation, active power regulation by means of power converter is a fast acting control. Currently, the majority of the controller proposals to damp power system oscillations are of active power modulation in the converter.

As in frequency control [123], the first steps in additional power oscillation damping controller for wind power is to copy the power system stabilizer from the synchronous generators [124], and to introduce it into the wind turbine controller.

The main function of a power system stabilizer is to damp low frequency oscillations. Commonly, a PSS consists of three blocks as Figure 3.5 shows. The washout block, a proportional controller and the lead/lag block. The PSS input can be any signal affected by the oscillations of the synchronous machines. However, machine speed, terminal frequency or power is normally used. The output signal is usually a voltage variation in the excitation system. The washout filter is a high pass filter that rejects the low frequencies and steady states of the input

$$T_w(s) = \frac{s\tau_{wh}}{1 + s\tau_{wh}}. \tag{3.2}$$

The PSS is expected to respond only to transient changes. The selection of the washout time constant value (τ_{wh}) depends on the type of modes under study. The proportional controller K determines the amount of damping introduced by the PSS. Finally, the lead/lag block consists of a phase compensator. It provides the desired lead or lag phase in order to reduce rotor oscillations. This dynamic compensator is usually made up of two lead-lag stages as shown below

$$T_{ph}(s) = \frac{(1 + s\tau_1)(1 + s\tau_3)}{(1 + s\tau_2)(1 + s\tau_4)}. \tag{3.3}$$

The time constants (τ_1, τ_2, τ_3 and τ_4) are selected in order to provide a phase lead in the frequencies of interest.

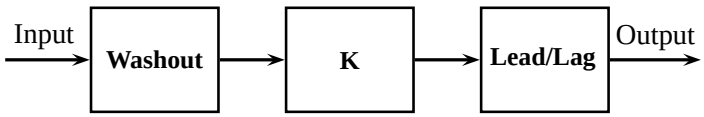

Figure 3.5: Conventional PSS scheme

Most of the schemes used in the converter control are based on vector control, whereas a few are based on flux magnitude and angle control (FMAC). Considering this fact, the extra active power loop is divided according to their control scheme.

For a FMAC control scheme in a DFIG wind turbine, in [113, 125] the use of conventional power system stabilizer controls with the angle variation

as output and use the slip of the DFIG as input has been proposed. Similarly, other alternatives include the use of conventional PSS but with the introduction of the electrical stator power as input instead of the slip [126], or even choosing a terminal voltage signal, which has good visibility of the inter-area oscillation of the power system as input and generating an active power variation signal [127]. All input and output signals presented above in the conventional PSS scheme present proper behavior enhancing power system stability. However, some authors have expressed some doubts about the influence of tower shadow and wind variation on the performance of a conventional PSS controller for DFIG wind turbines with various inputs, such as electrical generating power, rotor speed and grid frequency [128]. The DFIG wind turbine presents a good damping response with all the inputs, although the rotor speed was adversely influenced by the torque variations due to the tower shadow which amplifies the PSS response and consequently the turbine torque, whereas wind variation effect is almost filtered.

Optimal control options have also been proposed. The idea is to tune the controller parameter to minimize some criteria. Among these alternatives, in [129] a genetic algorithm (in particular, a bacteria foraging algorithm) is used to adjust the parameter control of DFIG. Implemented in a DFIG connected to an infinite bus, [130] gives promising results when the optimal tuning is done for any sub-synchronous speed. However, if the parameters are optimized for any super-synchronous speed, the controller response is poorer than for the other speed cases [130]. A mixed control of eigenstructure assignment and a multi-objective nonlinear optimization method for the conventional PSS have been developed in [131]. This controller with multi-input signal, speed and stator power can serve to mitigate the inner oscillations of the DFIG and to damp out the power system oscillations.

Also, an FMAC control scheme in a full power converter with a conventional PSS scheme is included in the grid-side converter controller, where the grid frequency is the input and the voltage angle variation is the output in [132]. It is shown that the oscillations are better damped when the power oscillation damping controller is added in the wind turbine controls.

Conventional PSS has also been implemented for vector control schemes. The oscillation damping achieved by these schemes have been studied for several input-output pairs and optimizing controller parameters. Taking the voltage variation as output in the active power loop, as is usual in the control of the excitation in synchronous machines, the performance of the scheme has been evaluated using different inputs including the speed of voltage angle, the active power in one of the lines and the difference in rotor speed of the synchronous generators [133, 134]. These studies reveal that

although all of the proposals are able to improve the damping, the use of power in one of the lines presents much better results. Other authors, who also use the conventional PSS, have proposed a simple tuning procedure to adjust the PSS parameters selecting the bandwidth of the controller [135]. In this scheme, the voltage of the wind farm terminal is chosen as input and a variation of the power reference as output.

Some researchers have proposed a reduced version of the conventional PSS, comprising a filter and a proportional controller with the grid frequency as input and the power reference as output [136]. The proposed scheme has exhibited an effective damped behavior of the inter-area oscillations.

Other authors have used root locus methods to design the controllers. Here, the idea is to add pole-zero pairs in order to attract the root locus toward more damped locations in the left-hand side of the complex plane, ensuring stability. These methods permit the controller to improve just one oscillation mode with a simple control scheme [137]. In order to affect more oscillatory modes, a more complex controller is required [138, 139]. These methods are effective to damp desired oscillation modes. However, a good knowledge of the global system is necessary.

Optimization algorithms have been introduced to overcome the tuning problem of WT controllers. Particle swarm optimization (PSO) and the evolutionary particle swarm optimization (EPSO) method attempt this [75, 140].

A vector control scheme in a PMSG wind turbine with classical PSS has been analyzed in [94] under different active damping controls such as power regulation, DC-Link regulation, torque regulation and an improved torque regulation, where the outputs are active power reference variation, DC link voltage reference variation and torque variation, respectively. All of the active damping schemes have generator frequency as input. All the schemes present a good damping performance, but some of them need a phase compensator to damp out some power oscillations, except for power regulation where the input and the output are directly in phase.

A grid frequency based PSS for variable speed wind turbines has been proposed [141, 142, 143, 144]. It is shown in Figure 3.6 where ω_{wt} is the speed of the wind turbine, Δf_{grid} is the grid frequency deviation, P_{wpss} is the output of the PSS controller, P_{wind} is the power calculated by the speed controller and P_{mech} is the mechanical power from the WT. It can be implemented under different control schemes such as FMAC or vector control, and its output is added to the speed regulation output. Thus this control also is able to affect the turbine regulations. It is important to note that this control is simpler than conventional PSS. Moreover, it can be

implemented in wind turbines without additional costs and it only requires local variables, obviating the use of wide-area communication systems.

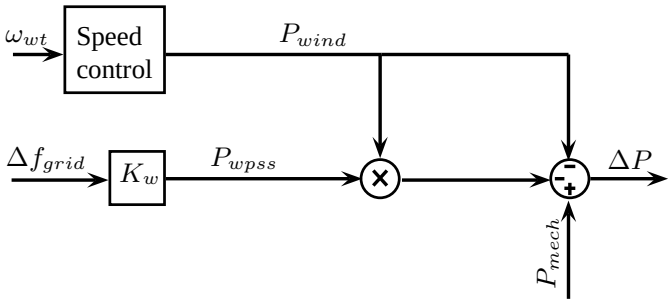

Figure 3.6: Simple power damping controller scheme

Although, active power regulation is a good approach to damping out the power system oscillations, it can negatively affect drive-train oscillations [145, 146, 139].

A classification of the different input-output pairs proposals for the conventional PSS controller can be seen in Table 3.3. The inputs are the electrical power P_e, the voltage in the WT terminal V_{WT}, the frequency of the grid f_{grid}, the electrical power in one of the lines of the power system P_{line} and the difference of the angle between two synchronous machines $\delta_i - \delta_j$. The outputs are a voltage angle variation for the FMAC control scheme $\Delta\delta$, a power reference variation ΔP_{ref} and a d-component voltage variation for the vector control scheme ΔV_d.

3.4.2 Reactive power regulation

There are only a few results reporting the use of reactive power regulation to damp the oscillations in power systems. Most of them are applied in DFIG wind turbine technology using vector control.

As in the active power regulation case, the implementation of a conventional PSS scheme in the reactive power loop has been studied. The conventional PSS scheme has been evaluated by using a voltage variation as output and different inputs such as local signals (e.g., speed of voltage angle) and remote signals (e.g., power in one of the lines and the difference in rotor speed of the synchronous generators) [133, 134]. From these studies, it is possible to conclude that wind farms with an additional controller are capable of damping oscillations. All proposed alternatives achieve a good

Input \ Output	$\Delta\delta$	ΔP_{ref}	ΔV_d
Rotor speed /Slip	[113, 125, 126, 128]		[133, 134]
P_e	[126, 128]		
V_{WT}	[127]	[135]	
f_{grid}	[128, 132]	[136]	[133, 134]
P_{line}			[133, 134]
$\delta_i - \delta_j$			[133, 134]

Table 3.3: Classification of conventional PSS proposals depending on inputs and outputs

damping of power system oscillations, but the use of local signals as input presents the best performance.

Some researchers agree that active power modulation affects electromechanical torque of the wind turbine, whereas reactive power modulation does not since the converter acts similarly to a static var compensation (SVC) [138, 139]. The controller uses the angle difference between two groups of synchronous generators and a increment in reactive power reference as output. It is designed by root locus methods in order to place the zeros and the poles of the system in the desired location of the complex plane. The results presented in [147] indicate that this alternative is effective to damp the oscillations.

3.4.3 Active and reactive power regulation

Active and reactive power regulation can be achieved by a VSWT converter control which allows modulation of the quantity of active and reactive power delivered by the wind farm.

Power converter regulation

As mentioned above, the power converter can modulate active and reactive power independently in order to damp oscillation. Hence, it is possible to propose schemes based on simple control tools with two power loops independently designed but acting simultaneously.

Similar to cases previously discussed, there are results using conventional PSS controllers in both active and reactive loops [148]. In this work, different inputs are analyzed including the deviation of generator rotor speed (a remote signal) and the frequency deviation of the DFIG terminal voltage (a local signal). In all cases, these alternatives are effective to damp the network oscillations without affecting the DFIG shaft oscillation mode, although its impact is much more noticeable in cases where the remote signals are considered as input.

Another power damping controller design is based on FACTS and VSC-HVDC control methods to damp rotor oscillation of the conventional plants which are designed as a simplified conventional PSS scheme [149].

Finally, a method to find a mixed active and reactive control strategy is the energy function approach which is based on the second Lyapunov method. This control strategy is represented in Figure 3.7, where V_{wt} is voltage of the wind turbine terminal and f is the frequency calculated by the phase locked loop (PLL) from the V_{wt}. The energy function (E) is given by

$$\begin{aligned} E &= E_K + E_P, \\ \tfrac{d}{dt}E &= \tfrac{d}{dt}E_K + \tfrac{d}{dt}E_P < 0, \end{aligned} \tag{3.4}$$

where E_K is the kinetic energy and E_P the potential energy.

The energy function can be determined by the classical model of the synchronous generators. The incremental active and reactive powers are computed from the derivative of this energy function. Notice that the derivative of the energy function must be negative to keep the system stable.

The active power law is usually determined by a kind of kinetic response emulation; whereas the reactive power law is commonly defined considering that the wind farm emulates the behavior of a SVC. Classical droop control is used for active power regulation with different local signal inputs, for instance, the wind farm terminal voltage derivative [72] and the wind farm terminal frequency variation [149], whereas a nonlinear kinetic equation is performed using wind farm terminal angle speed and the wind farm terminal angle acceleration [150].

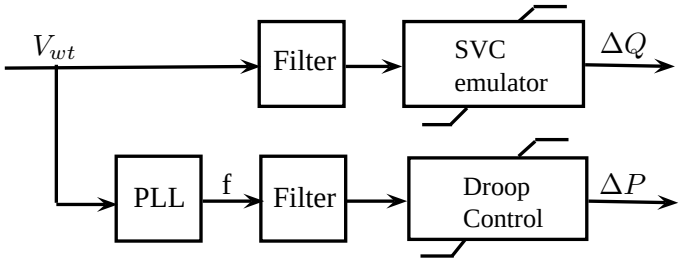

Figure 3.7: Energy Function Approach controller scheme

According to some studies, energy function control does not need coordination with other network controllers and its response does not depend on the location of the wind farm since the controllers are obtained from the equations which are independent of power systems [72]. Some authors conclude however that by using the same control approach the active power loop is most efficient when the wind farm is connected close to a synchronous power plant and the reactive power modulation is best when is located away from conventional generators [149]. Depending on the wind farm location the stabilizing control is able to damp either inter-area oscillations or intra-area oscillations [150].

A classification of the control proposals relating to both the control schemes and the regulated power is shown in Table 3.4. In Figure 3.8 a scheme has been drawn giving a summary of the proposals of power oscillation controllers following the section structure.

3.5 Conclusions of the chapter

In this chapter, a review of the current research on the effect of wind farms on power system stability, showing both their influence on the oscillations such as in the power system and their inner oscillations. Their contributions to the improvement of the stability are evaluated and presented.

It is commonly accepted that wind farms cannot engage with power system oscillations since they usually include asynchronous generators and power converters. It is also accepted that FSWTs produce beneficial effects on the damping of the power system oscillations. On the contrary, the results for VSWT do not draw clear conclusions about their effects on power system stability. The results in case of VSWT depend on the control included in

Power \ Control	Conventional	Root Locus	Lyapunov	Pitch Angle	Pitch + Ext. Equipment	Optimization Algorithm
Active	[113, 125, 126, 127, 128, 132, 133, 134, 135, 145]	[137, 138, 139]		[114, 115, 116, 120, 121]		[129, 130, 131, 140]
Reactive	[133, 134]	[138, 139, 147]				
Active & Reactive	[148, 149]		[72, 149, 150]		[99, 100, 120, 121, 122]	

Table 3.4: Classification of controller scheme proposals by affected power

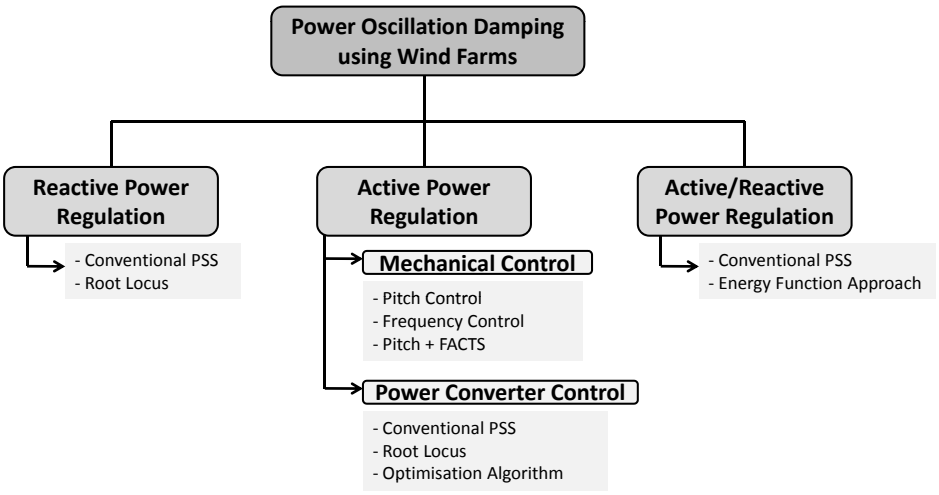

Figure 3.8: Summary of Power Oscillation Damping control proposals

the wind farm. The power factor or voltage controls may have in general a detrimental effect on the damping, whereas frequency control can enhance power system stability.

Wind farms have their own oscillation modes. The modes associated with the converter and the drive-train modes mainly arise in the mechanical part of the wind turbine and may be amplified during a voltage fault. These oscillations can be damped by means of power converter control or by means of mechanical regulation with pitch control or mechanical elements.

A number of works have proposed the use of additional control loops in order to help to damp the power system oscillations. These controllers are based on three different principles: to vary the active power delivered to the grid, to modulate the reactive power delivered and to regulate the active and reactive power simultaneously. The reactive power control can only be done by acting on the power converter, whereas the active power control can be implemented using the power converter or pitch control system.

According to the work reviewed in this chapter, a clear trend toward the use of active power control to improve the stability of power systems can be observed. Nevertheless, the results on reactive power control are promising and they should be studied carefully. The effect of reactive power regulation could be important for power systems due to its capacity to change the power flow of the busses having lower effect in drive-train oscillations.

4

Comparative analysis of power system stabilizer capability of wind power plants

4.1 Introduction

As previously stated, wind power generation (using any electrical concepts) does not induce new oscillatory modes into power system, because the generator concepts used in wind turbines do not engage in power system oscillations [52]. For example, fixed speed wind turbines (FSWT) has intrinsically more damped oscillation modes [151], and generators of variable speed wind turbines (VSWT) are decoupled from the grid by a power converter [151].

The extra contribution of FSWTs to the stability is limited [116], therefore it is not very effective as a PSS. On the other hand, VSWTs are capable of enhance power system oscillation damping since they have a power converter delivering the desired active and reactive power to the grid [49]. Thus, the use of VSWT has been suggested to actively contribute the grid to damp rotor oscillations [125, 149]. This power regulation is done by the addition of a PSS scheme to the converter control, which demands to the wind turbine a variation on the power delivery [126, 138, 152, 153]. This power variation modifies the power flow of the whole power system in order to damp the desired oscillation modes.

WPPs can be far away from the main network, a clear example are offshore installations. Oscillatory modes may be not observable on WPP local signals thus reducing the effectiveness of the PSS. In this case, the use of communications may be required; however they have some drawbacks such as signal delay and reliability issues. Moreover, the remote location implies that the system is away from synchronous generation areas, therefore WPP only can act against inter-area oscillation modes which are, as previously stated, in frequency range of 0.1 to 0.7 Hz [57, 132, 74].

The aim of this chapter is to clarify if the wind power plants are capable to damp inter-area oscillation modes by using local signals and to analyze if there are several factors which could influence on the PSS controller response.

This chapter is organized as follows. PSS design for WPP is presented in Section 2. PSS capability of a WPP is simulated; the influence of its distance from WPP to shore and the effect of the WPP location are discussed in Section 3. Finally, in Section 4, the conclusions are summarized.

4.2 Power system stabilizers for wind turbines

PSS input can be any signal affected by the oscillation to be damped. Thus, to avoid the use of wide-area communications in the control, local signals are selected as inputs to the PSS. The WPP connection point is selected as measurement point in order to avoid the filtering effect introduced by the transformer connected between the grid and the WPPs. Moreover, it is important to take into account that WPPs are usually connected into the grid far from generation areas, as shown in Figure 4.1. Since the proximity of WPP to synchronous generators is an important factor, it is not possible to increase the damping of the local (or intra-area) oscillation modes with the PSS capability of WPP. Therefore, the design of the PSSs can only be focused on the damping of the inter-area oscillation modes.

The PSS control is based on the design of a conventional PSS for a synchronous generators [124]. However, in wind turbines the phase compensation is not required to produce damping torque; therefore lead/lag compensator is not necessary. According to [145, 149, 153], the PSS control can be composed of a proportional controller, a limiter and a band pass filter (or washout filter) to limit the frequency range where the controller is acting (Figure 4.2). The inputs and the outputs used in PSSs for wind turbines can be different from the conventional PSS. The controller input can be any variable affected by the power system oscillation, for example, grid frequency,

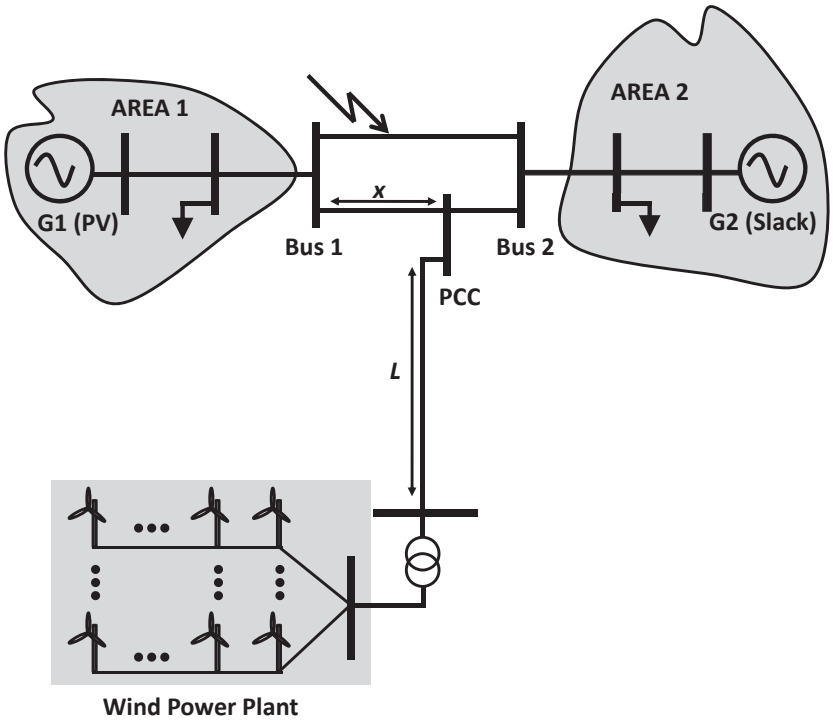

Figure 4.1: Representation of the power system utilized in this study

voltage of the bus and generator speed. The output can be any variable capable of varying the power delivered to the grid including active or reactive power, generator slip or excitation voltage. Actually, the PSS introduces small variations referred to the reference values of the output signals. This PSS control can be individually included in each wind turbine of the WPP.

4.3 Case studies

The power system under study is a simplified version of the original well-known two area network described in [154], with a WPP connected to the tie-line between the two areas. These areas are simulated to simplify the study as a large synchronous generator each, with the governor and the excitation systems but without the PSS controller included on them. The WPP is assumed as an aggregate model for simulation, therefore the PSS

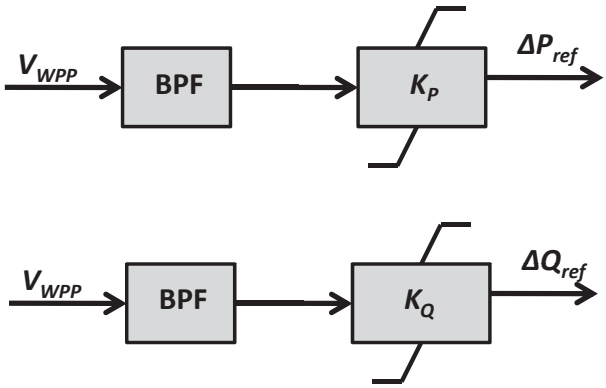

Figure 4.2: Block representation of the active and reactive power PSS controller

control is also assumed as an aggregate controller. The system appears represented in the Figure 4.1. The power system parameters considered in this study are prensented in Tables 4.1 and 4.2. A three-phase fault of 0.133s is considered in the middle of the tie-line in order to excite power system oscillations. In this study a WPP of 50MW is assumed which is less than 5% of wind power penetration on the system. This value is chosen to get a conservative situation and to avoid that the WPP was dominant in the power system dynamics.

For the present study, the WPP connection point voltage is selected as input signal and active and/or reactive power reference as the output for the PSS controllers. The band pass frequency of the filter is between 0.08 Hz and 1.5 Hz, since the inter-area modes are in the range from 0.1 Hz to 0.7 Hz. The active (Kp) and reactive (Kq) gains have been set in 10^4 and -10^5, respectively. The values of these gains are important since they can affect the stability of the system. The output saturations have been also included to limit the controller outputs between -0.15 and 0.15 in p.u., in both cases [145]. The parameters considered within this study regarding the PSS controller of the wind turbine are remembered in Table 4.3.

P_n	V_n	f_n	R_s	X_d	X_q
900 MVA	20 kV	60 Hz	0.0025 pu	1.8 pu	1.7 pu

X'_d	X'_q	X''_d	X''_q	X_l
0.3 pu	0.55 pu	0.25 pu	0.25 pu	0.2 pu

T'_{d0}	T'_{q0}	T''_{d0}	T''_{q0}	H_1	H_2
8 pu	0.4 pu	0.03 pu	0.05 pu	6.5 pu	6.175 pu

Table 4.1: Parameters of the synchronous generators 1 and 2 used in the power system under study

V_n	f_n	P_{L1}	Q_{lL1}
230 KV	60 Hz	483.5 MW	50 Mvar

Q_{cL1}	P_{L2}	Q_{lL2}	Q_{cL2}
50 Mvar	883.5 MW	50 Mvar	175 Mvar

Table 4.2: Parameters of the constant loads 1 and 2 used in the power system under study

P_{wt0}	Q_{wt0}	K_p	K_q	T_w	T_h
50 MW	0 Mvar	10^4	-10^5	2 s	0.1 s

Table 4.3: Parameters of the PSS controller of WPP used in the power system under study

4.3.1 PSS controller of WPP

The analysis is divided in three study cases. First, the PSS capability of the WPP is studied by the use of different PSS control schemes. Second, the influence of the length of the cable which links the WPP and the main network, in the PSS control response is analyzed. Third, the influence of the WPP location at the tie-line in the PSS contribution is studied. The

different cases are simulated by using the SimPowerSystem toolbox from MATLAB/SIMULINK.

4.3.2 Case 1: Comparison of different PSS schemes

In this case a comparison between different control schemes was carried out to evaluate the PSS capability of the WPP. The system under study is simulated in four scenarios:

- no PSS installed in the WPP controllers (used as base case),
- WPP with an extra active power loop to damp oscillations (P-PSS),
- WPP with an extra reactive power loop to damp oscillations (Q-PSS),
- WPP with both additional control loops (active and reactive power, PQ-PSS) with the same aim.

In Figure 4.3, the active power flowing through Bus 1 which connects Area 1 with the rest of the system is shown. Since Area 2 has larger loads than generation systems, the active power flows from Area 1 to Area 2. In this figure, it can be observed that the system without WPP PSS compensation (no PSS) presents an almost critically stable dynamic behavior. The inclusion of an extra reactive power loop into the system shows slight damping improvement. On the other hand, the addition of an extra active power loop into WPP presents an important improvement on damping oscillation modes. Finally, it can be observed that the simultaneous use of active and reactive power shows even a better damping capability. The better response obtained with P-PSS than Q-PSS is an expected result since active power affects directly mechanical dynamics, whereas reactive power affects indirectly rotor dynamics.

Figure 4.4 presents the active power delivery response of the WPP. It can be seen that for the No-PSS and Q-PSS cases, the WPP is delivering a constant value of active power. On the other hand, in P-PSS and PQ-PSS cases, the WPP is delivering a compensating signal to damp the oscillations. Moreover, it can be observed that this response reaches the saturation limits for both cases. Although in the PQ-PSS case, the active power delivered enters into the linear zone sooner than the power delivered by the P-PSS. This is a consequence of the interaction with the reactive power loop.

In Figure 4.5, the reactive power delivered by the WPP is plotted. As occurs with the active power, in the No-PSS and P-PSS cases, the WPP

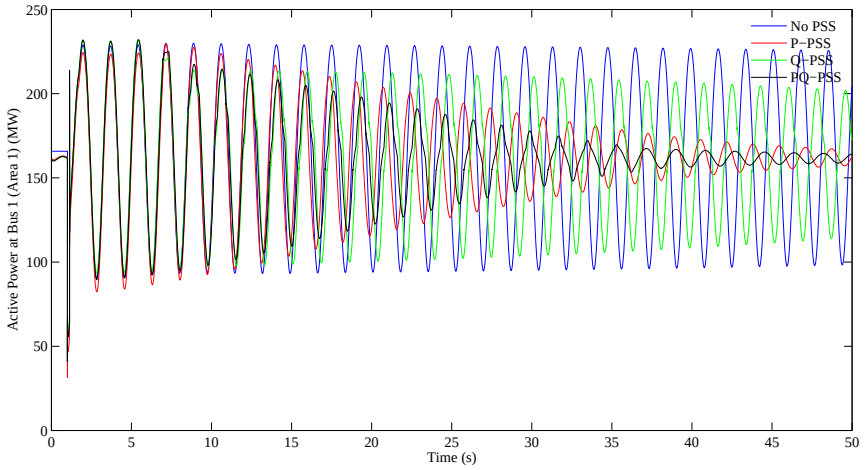

Figure 4.3: Active power flowing through Bus 1, which connects Area 1 with the tie-line for different PSS schemes (Case 1)

remains at their reference value (0 Mvar). The Q-PSS and PQ-PSS react against the oscillation. In both cases the reactive power reaches the saturation limits. However, the Q-PSS does not leave the saturation during all the simulation time because of its lower effect on the oscillatory mode which requires more reactive power feeding from the WPP.

Figures 4.6(a) and 4.6(b) show the voltage magnitude and a zoom of it at Bus 1, respectively. As happens with the active power at the same bus, PQ-PSS provides better damping capability on the voltage than other controllers. However, P-PSS loop also obtains promising results.

The magnitude and the corresponding zoom of the voltage at point of connection of the WPP with the grid are presented in Figures 4.7(a) and 4.7(b), respectively. In this case, it can be observed that as it happens in the voltage magnitude at Bus 1, the PQ-PSS and P-PSS rapidly damp the oscillation. The voltage at the WPP bus is the input signal for the PSS controllers, therefore rapid damping of this signal implies less actuation time of these controllers.

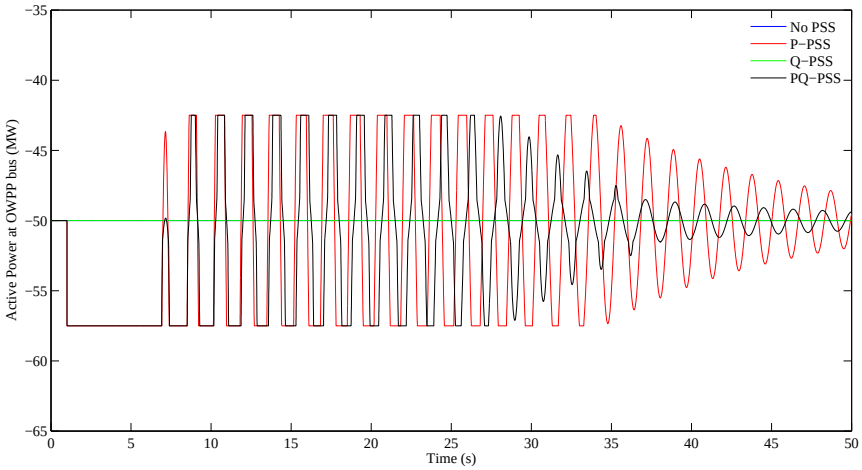

Figure 4.4: Active power delivered by the WPP for different PSS schemes (Case 1)

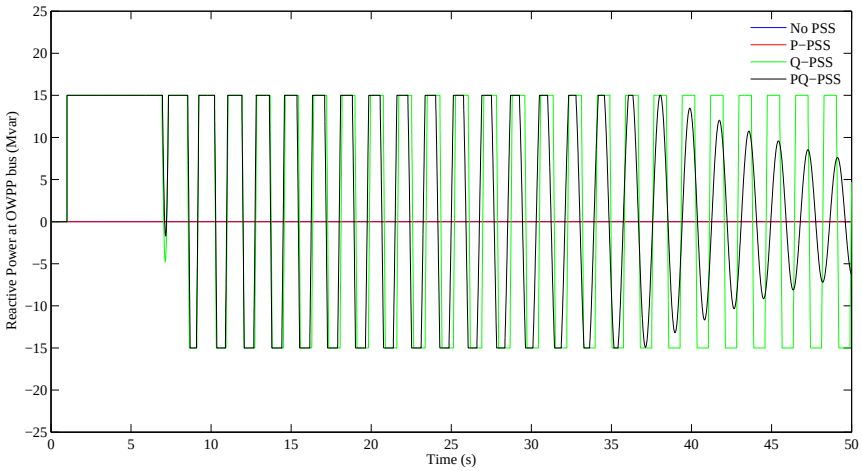

Figure 4.5: Reactive power delivered by the WPP for different PSS schemes (Case 1)

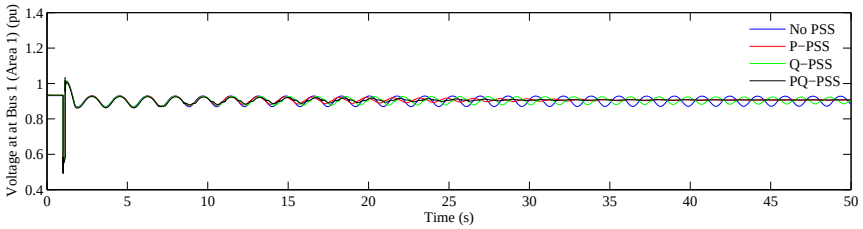

(a) Voltage Magnitude at Bus 1

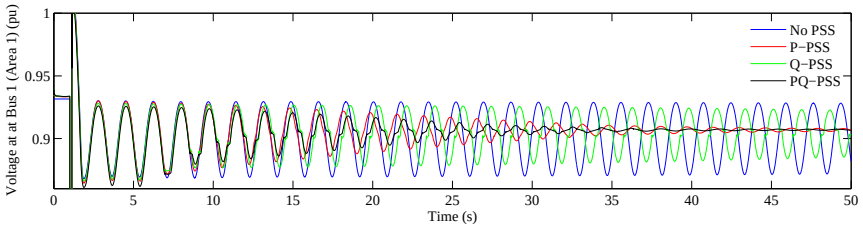

(b) Zoom of Voltage Magnitude at Bus 1

Figure 4.6: Voltage Magnitude at Bus 1 for different PSS schemes (Case 1)

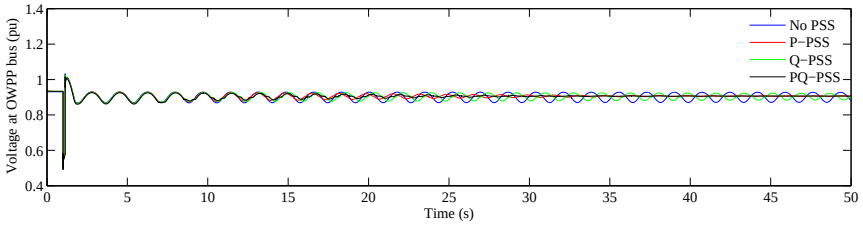

(a) Voltage Magnitude at WPP connection Bus

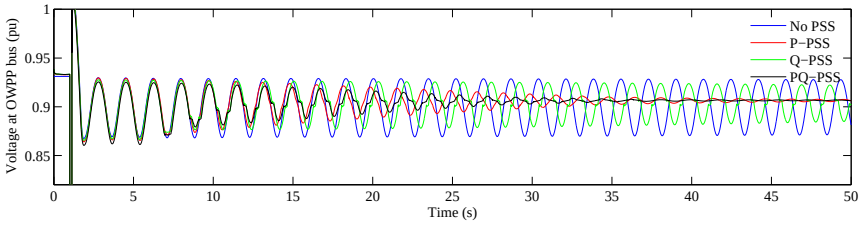

(b) Zoom of Voltage Magnitude at WPP connection Bus

Figure 4.7: Voltage Magnitude at WPP connection Bus for different PSS schemes (Case 1)

4.3.3 Case 2: Effect of cable length on PSS capability

In this case, the effect of the cable length on the PSS capability is analyzed. Since only local variables are used in the PSS, the length of the cable may have marked effect on its damping capability. To this end, the system is simulated under four different cable lengths: 10, 30, 50 and 70 km, respectively. In order to evaluate all the lengths under the same case, the PQ-PSS controller is connected for all the simulations. PQ-PSS was selected since it presented the best damping behavior in the previous subsection.

Figure 4.8 presents the active power flowing through Bus 1. A reduction in the PSS damping capability for longer cable length can be observed. This is an expected result because the visibility of the oscillation is lower when the cable length increases. However, the oscillation damping achieved by the PSS controller is still quite important. The system is still better damped at 70 km with PQ-PSS controller than the same system with shorter line using only the Q-PSS controller shown in Figure 4.3.

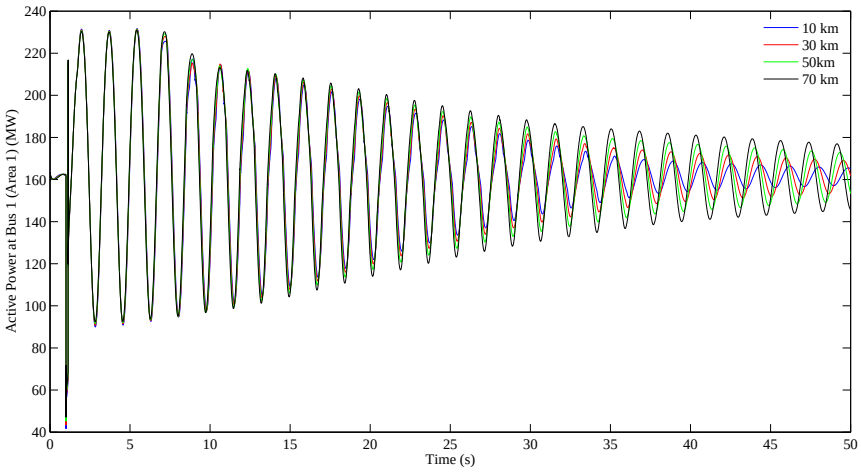

Figure 4.8: Active Power flowing through Bus 1 which connects Area 1 with the tie-line for different cable length (Case 2)

In Figures 4.9 and 4.10, the active and reactive power delivered by the WPP is presented. It can be observed that for long cables the amplitude of the compensation signals is smaller. This is a consequence of the visibility of the oscillation in the measurement point and of the parameters of the controller are the same for all the cases. Clearly, the PSS must deliver large active and reactive power to achieve the same damping. However, in Figures

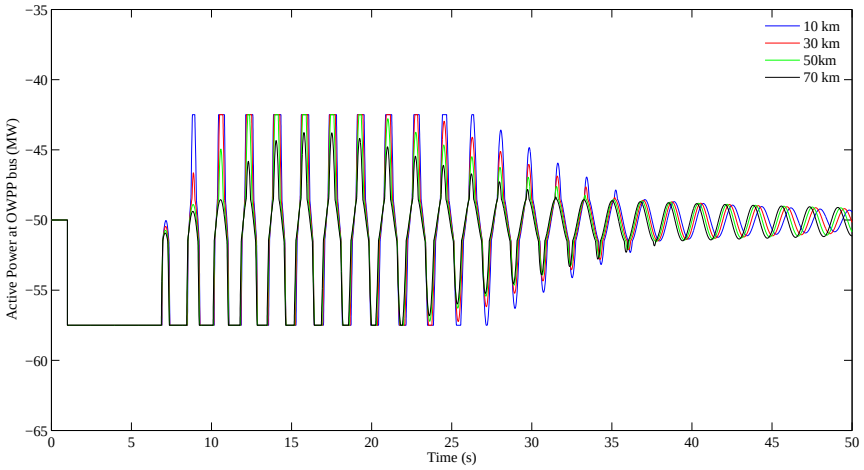

Figure 4.9: Active power delivered by the WPP for different cable length (Case 2)

4.9 and 4.10, the compensation signals are smaller for long cables because of the PSS parameters were not optimized for each length. Figures 4.11(a) and 4.11(b) show the voltage magnitude and a zoom of it at Bus 1, respectively. Again, the damping contribution is greater for short cable lengths.

The voltage magnitude and a zoom of it at the connection point of the WPP with the grid are presented in Figures 4.12(a) and 4.12(b), respectively. In this case, it can be observed that longer cable lengths imply larger voltage decays. This is a consequence of the WPP controls, which has been designed to deliver a fixed active and reactive power values without voltage regulation.

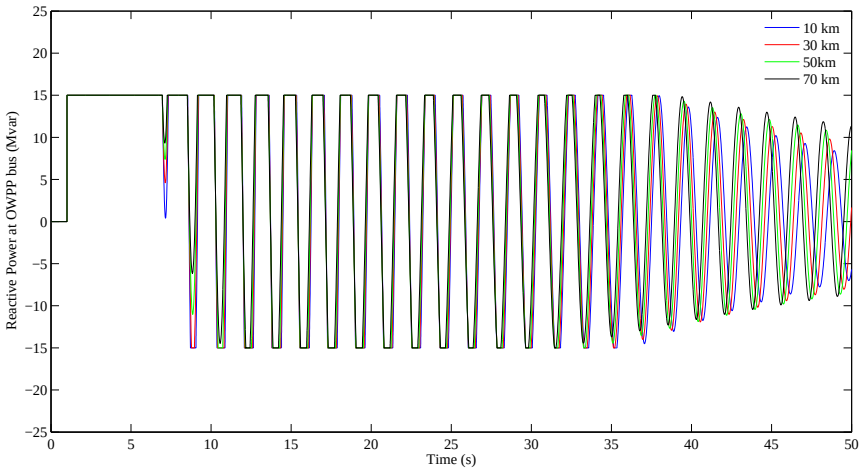

Figure 4.10: Reactive power delivered by the WPP for different cable length (Case 2)

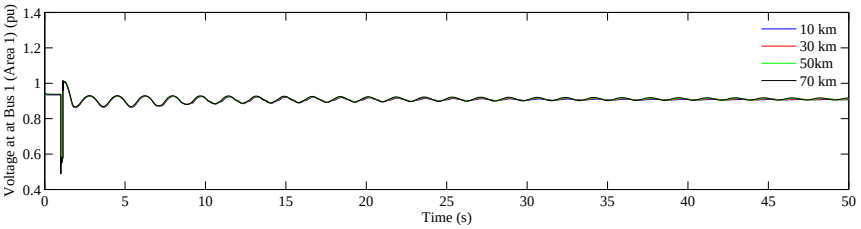

(a) Voltage Magnitude at Bus 1

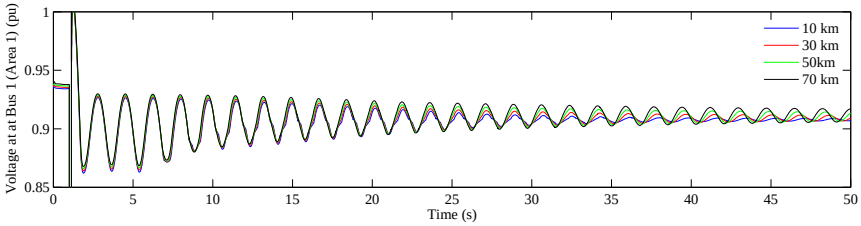

(b) Zoom of Voltage Magnitude at Bus 1

Figure 4.11: Voltage Magnitude at Bus 1 for different cable length (Case 2)

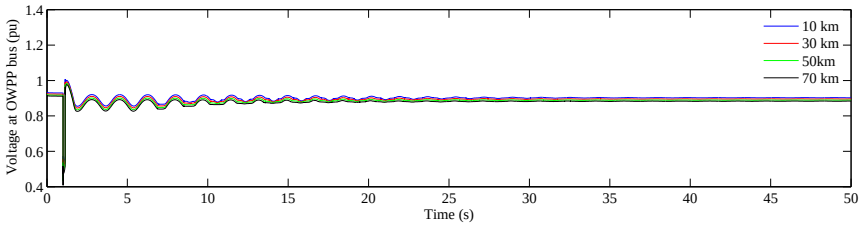

(a) Voltage Magnitude at WPP connection Bus

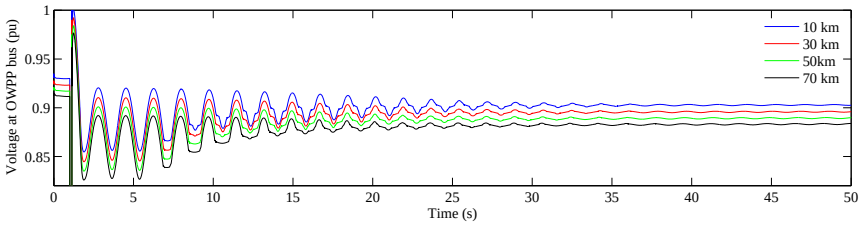

(b) Zoom of Voltage Magnitude at WPP connection Bus

Figure 4.12: Voltage Magnitude at WPP connection Bus for different cable length (Case 2)

4.3.4 Case 3: Effect of WPP location on PSS capability

In this case, the effect of the WPP location on the PSS capability is analyzed. Since only local variables are used in the PSS, the location of the WPP may have marked effect on its damping capability. To this end, the system is simulated under four different positions on the tie-line from Area 1: 0, 55, 110 and 165 km, respectively. This increasing distance to Area 1 is selected since the slack generator is located at Area 2; therefore the synchronous generator of Area 1 is the one who oscillates. In order to evaluate all the locations under the same case, the PQ-PSS controller is connected for all the simulations. PQ-PSS is used since it presented the best damping behavior in the first study case and a cable length of 1 km is selected, to have good visibility of the system oscillation.

Figure 4.13 presents the active power flowing through Bus 1. It can be observed that the power transferred is better damped for the WPP locations close to the area 1. Even, for the 165 km case, it became unstable meaning that the damping controller had no effect.

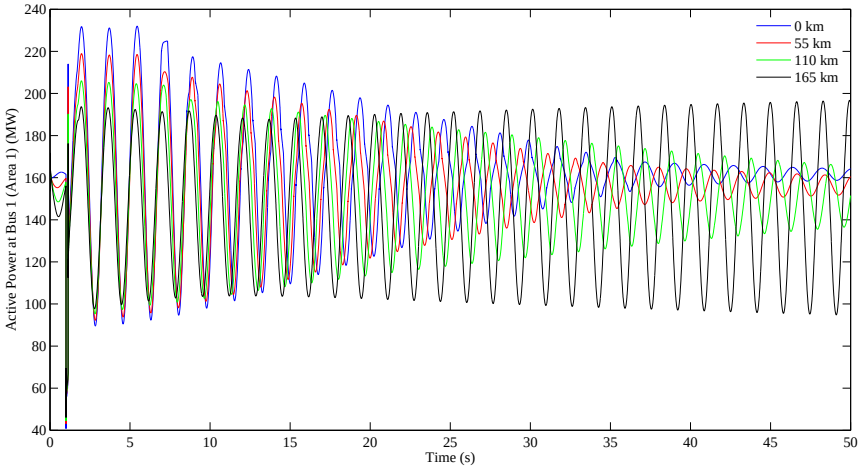

Figure 4.13: Active Power flowing through Bus 1 which connects Area 1 with the tie-line for different WPP locations (Case 3)

In Figures 4.14 and 4.15, the active and reactive power delivered by the WPP is presented. It can be seen that the faster PSS responses are obtained by the closest locations. The faster PSS response is obtained by the 55 km case, since the 0 km case makes the fault effect less severe than the other cases. It can be observed that in the 165 km case the system became

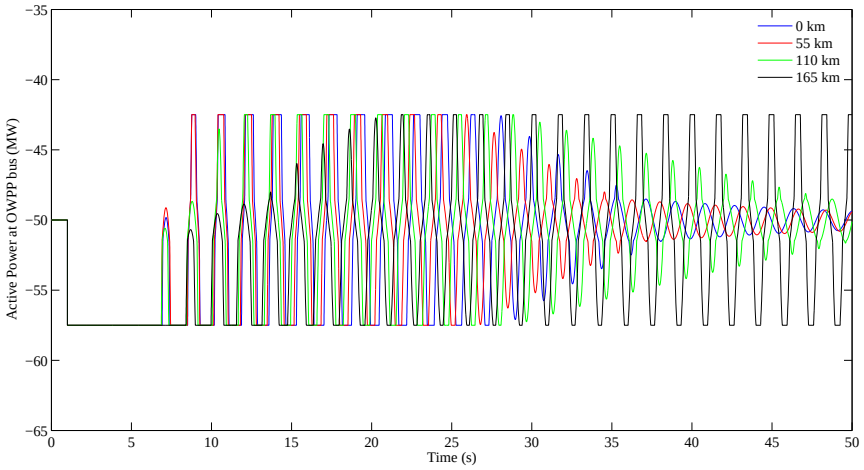

Figure 4.14: Active power delivered by the WPP for different WPP locations (Case 3)

unstable. This may be a consequence that the input of the PSS now is more influenced by Area 2. In Figure 4.14 can be observed that the reference active power run out from saturation for all the cases, except for the last one, which means that the power system oscillation is being damped. The same occurs in Figure 4.15, although the control response remains more time in saturation. Figure 4.16(a) and 4.16(b) show the voltage magnitude and a zoom of it at Bus 1, respectively. Again, the damping contribution is greater for close WPP locations. It can be seen that the voltage level in Bus 1 is different because of the WPP effect on it.

The voltage magnitude and a zoom of it at the connection point of the WPP with the grid are presented in Figure 4.17(a) and 4.17(b), respectively. In this case, it can be observed that the 55 km and 110 km WPP locations cases present lower voltage level. This is a consequence of the WPP controls, which has been designed to deliver a fixed active and reactive power values without voltage regulation, and that they are far from the synchronous generators. On the other hand, the 165 km has higher average voltage level since it is the closest case to the slack generator.

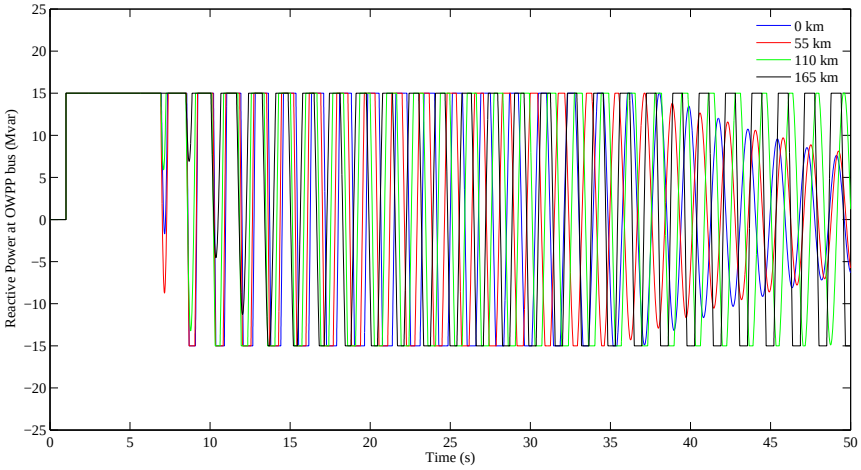

Figure 4.15: Reactive power delivered by the WPP for different WPP locations (Case 3)

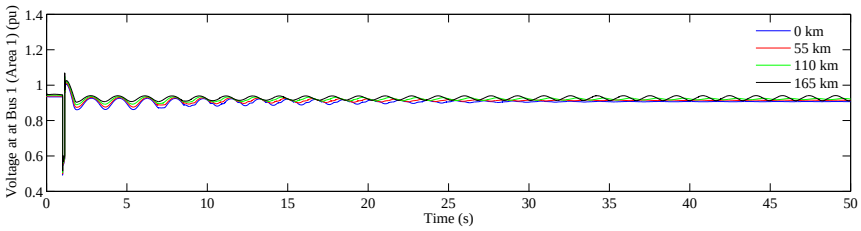

(a) Voltage Magnitude at Bus 1

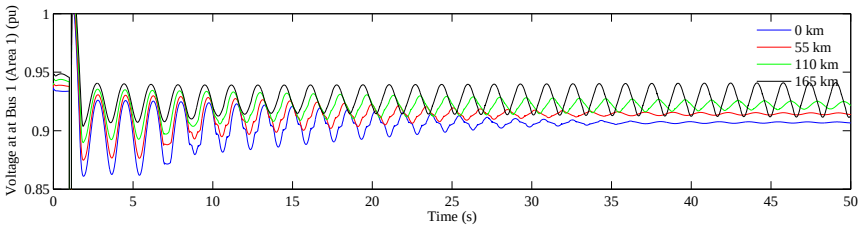

(b) Zoom of Voltage Magnitude at Bus 1

Figure 4.16: Voltage Magnitude at Bus 1 for different WPP locations (Case 3)

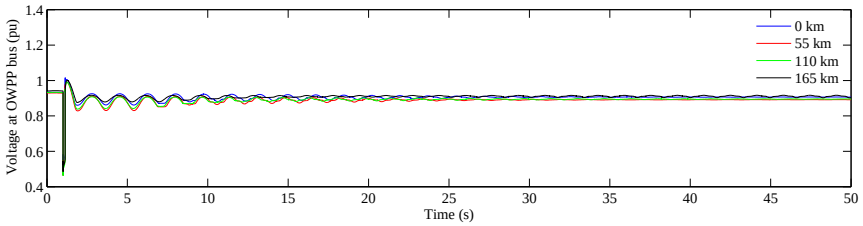

(a) Voltage Magnitude at WPP connection Bus

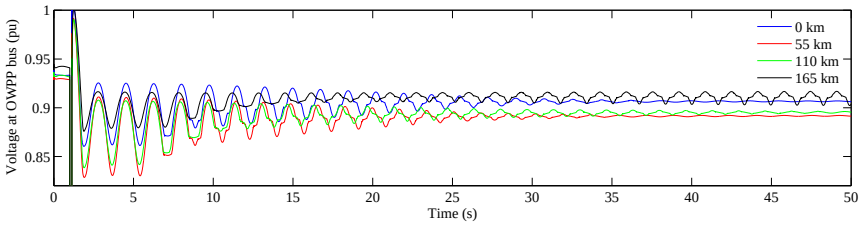

(b) Zoom of Voltage Magnitude at WPP connection Bus

Figure 4.17: Voltage Magnitude at WPP connection Bus for different WPP locations (Case 3)

4.4 Discussion and conclusions of the chapter

The PSS capability of WPP has been analyzed in three different scenarios. First, a comparison of several PSS schemes including the use of only active power as a compensation signal (P-PSS), the use of only reactive power (Q-PSS) and the use of active and reactive power simultaneously (PQ-PSS). In all cases, the PSSs have been designed as a simplified conventional PSS for synchronous generators considering the WPP voltage (local signal) as input. The responses obtained from the three PSS schemes have been compared to a WPP connected to the power system without any PSS. PSS controllers for wind turbines have shown promising damping properties. The best damping behavior has been observed in the case of a controller with active and reactive power PSS. A controller acting only on the active power has also shown good performance on damping inter-area oscillations.

The influence of the cable length connecting the WPP to the power system on the damping capability has also been analyzed. Since only local signals can be used to compute the compensation signals in PSS without communications, the distance between the WPP and the point of common coupling (PCC) has a strong effect on the damping capability. The presence of the oscillations is lower for long distances. Nevertheless, simulation results have shown that for significant distances the WPP still provides a satisfactory damping capability. Therefore, PSS schemes without communications are capable of damping oscillations even when located far away from the PCC.

The effect of the WPP location on the tie-line on the damping capability has been also studied. It is seen that if the WPP is located far from the synchronous generator affected by the power system oscillation, the WPP cannot help to damp it out. It can be concluded that WPP could contribute efficiently to enhance power system stability by regulating both active and/or reactive power. However, a critical issue is the PCC location of the WPP: if the PCC is located far from the oscillating synchronous generator, the WPP will not be able to help to damp power system oscillations.

5

Input-output signal selection for damping of power system oscillations using wind power plants

5.1 Introduction

As seen in previous chapters, either wind power impact and stabilizing response obtained by the use of wind power plants into power system are largely dependant on various aspects including wind turbine controls implemented, the signals used as input and outputs of such controller, the power system model, among others. Hereinafter, the development of tools, that are independent from the control implemented, to analyze the damping contribution from wind power plants to power system stability is carried out.

Different methods to select the best feedback signal to damp power oscillations have been discussed in [155, 156, 157, 158, 159, 160, 161], but the case for WPPs has not been yet well covered. Recent research focuses in the best input-output signal pairs employing controllability/observability analyzes such as residues analyzes, geometric measures, among others [155, 159, 161]. Other works study the interaction between different controllers for a MIMO case and try to determine if a decentralized controller is possible by using, for example, the relative gain array (RGA) [162, 161]. In [163], fundamental

limitations of control design by using local signals to damp remote oscillations are analyzed, where the interaction of local and remote signals have an important influence.

The aim of this chapter is to compare and analyze different controllability and observability and signal interaction analyzes for power system oscillation damping employing local signals from WPPs. The main advantages and drawbacks of each alternative are examined. Frequency domain tools such as the RGA and the multivariable structure function (MSF) [164, 165, 166] are employed to assess the interaction between signal pairs. Using the frequency domain approach, the arising control design and performance limitations under the presence of right hand plane zeros (RHPZs) are clearly defined [167]. The use of some of these methods is recommended to select the best input-output pairs which ensure a good controllability and observability of the desired oscillation mode, while providing a clear insight of the potential and limitations of the damping controller. These suggestions provide a guideline to select the best input-output signal pairs for different control schemes to damp power system oscillations by means of WPPs signals, either through single-input single-output (SISO) or multivariable (MIMO) control.

This chapter is organized as follows. In Section 2, a problem statement is introduced. A brief overview of different techniques for controllability and observability analysis and frequency domain analysis to determine input-output interaction are presented in Section 3. In Section 4, a simple case study to compare these different analysis tools is done. Finally, in Section 5, the conclusions and some tool selection guidelines are summarized.

5.2 Power system oscillation damping contribution using wind power plants

WPPs considering only converter-based wind turbines dynamics are considerably faster that operational frequency and electromechanical dynamics within the power systems. Also, it is worth to remark that WPPs are completely decoupled from network dynamics, in terms of electromechanical stability; this issue only deals with the behavior of the synchronous machines [151]. For that reasons, WPP model can be simplified for small signal analysis of the power systems.

WPPs are commonly regulating the active and reactive power delivered to the grid. The former is obtained by controlling the machine-side converter to transfer the maximum active power from the generator, and the later by controlling the grid-side converter [18]. Thus, these signals are an appro-

priate selection to be used as damping control signals. As input signals of the PSS to be included in the WPP, both local and remote signal measurements could be selected. From these, the electrical signals can be obtained in phasor variables (magnitude and phase angle).

At this point, it is important to highlight that the selection of the proper input-output pair (or pairs), to design the PSS either SISO or MIMO, presents large influence in the control response, and it is even more important for WPPs since they could be located far away from the synchronous generators where electromechanical oscillations occurs.

To be more precise, as stated in Subsection 2.3, power systems can be described by a set of nonlinear differential and algebraic equations of the form

$$\begin{aligned} \dot{\hat{x}} &= f(\hat{x}, \hat{u}) \\ \hat{y} &= l(\hat{x}, \hat{u}) \end{aligned} \tag{5.1}$$

where $\hat{x} = [x_1, x_2, \ldots, x_n]^T$ is the state, $\hat{u} = [u_1, u_2, \ldots, u_m]^T$ is the input, $\hat{y} = [y_1, y_2, \ldots, y_r]^T$ is the output, and $f(\cdot) = [f_1(\cdot),\ f_2(\cdot), \ldots, f_n(\cdot)]^T$ and $l(\cdot) = [l_1(\cdot), l_2(\cdot), \ldots, l_n(\cdot)]^T$ are nonlinear functions [41].

For small signal analysis, system (5.1) is linearized around an operating point and can be written in state-space form as

$$\begin{aligned} \dot{\Delta x} &= A\Delta x + B\Delta u \\ \Delta y &= C\Delta x + D\Delta u \end{aligned} \tag{5.2}$$

where Δx, Δu and Δy are values with relation to the operating point, A, B, C, and D are matrices of adequate dimensions, and the corresponding transfer function is given by

$$G(s) = C(sI - A)^{-1}C + D. \tag{5.3}$$

Figure 5.1 shows a feedback loop using a controller K relating the inputs with the outputs of system.

As previously stated for the case of damping power system oscillation using wind power plants, the inputs to the system (or control signals) could be the active, P_{wt}, and the reactive power, Q_{wt}, delivered by the wind power plant, and the outputs (or measured signals) the voltage magnitude, V_{wt}, and the voltage phasor angle,θ_{wt} , at the connection point of the wind power plant. This provides several control alternatives to be considered including both SISO and MIMO control schemes. For the SISO case, there are various input-output pair options, for example, $u = P_{wt}$ with $y = V_{wt}$, $u = Q_{wt}$ with $y = V_{wt}$, among others. In the MIMO case, the input and output signals are

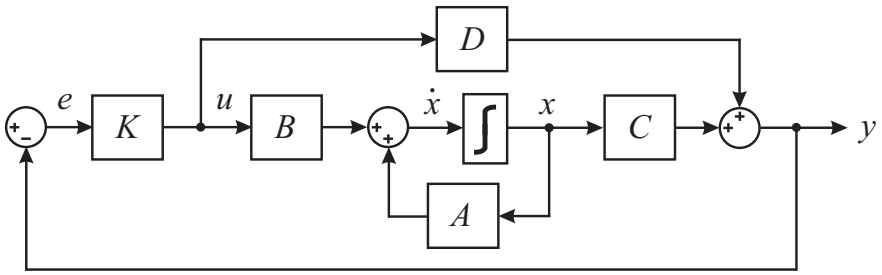

Figure 5.1: Block diagram of a plant with feedback

all the proposed at the same time ($u = [P_{wt}\, Q_{wt}]^T$ $y = [V_{wt}\, \theta_{wt}]^T$). The control scheme for MIMO can be centralized or decentralized; where, for the last scheme, the proper order input-output signal pair selection has importance in order to permit to design more effective controllers [167]. Commonly, the selection criteria for both SISO and MIMO control schemes are based on controllability and observability concepts and limitations associated with the frequency response of the open loop system.

5.3 Input–output selection methods

5.3.1 Controllability and observability measures

Controllability indicates how the state variables describing the behavior of a system can be affected by its inputs. Observability is associated with the possibility of determining the states from the outputs. More precisely, the system (6.1) is said to be controllable, if for any initial state $x(t_0)$, $t_1 > 0$ and final state x_1, there exists finite input u such that $x(t_1) = x_1$. The system (6.1) is observable if, for any $t_1 > 0$, the initial state $x(t_0)$ can be determined from $u(t_1)$ and $y(t_1)$ [167].

In damping of power oscillations, it is necessary to determine controllability and observability for specific eigenvalues. Next, a brief description of tests commonly used for this purpose is presented.

Popov-Belevitch-Hautus (PBH) test

The test consists in evaluating the rank of the matrices

$$\mathcal{C}(\lambda_k) = \begin{bmatrix} \lambda_k I - A & b_i \end{bmatrix}, \tag{5.4}$$

$$\tag{5.5}$$

$$\mathcal{O}(\lambda_k) = \begin{bmatrix} \lambda_k I - A \\ c_j \end{bmatrix}, \tag{5.6}$$

where λ_k is the k-th eigenvalue of the matrix A, I is the identity matrix, b_i is the column of B corresponding to i-th input u_i and c_j is the row of C corresponding to the j-th output y_j. The mode λ_k of linear system (6.1) is controllable if matrix $\mathcal{C}(\lambda_k)$ has full row rank. Similarly, the mode λ_k is observable if $\mathcal{O}(\lambda_k)$ is full column rank [167].

The rank of matrices $\mathcal{C}(\lambda_k)$ and $\mathcal{O}(\lambda_k)$ can be evaluated by their singular values. The singular values of a matrix M are defined as

$$\sigma_i = \sqrt{\lambda_k(M^T M)}(k = 1, \ldots, n) \tag{5.7}$$

with $\sigma_1 \geq \ldots \geq \sigma_n \geq 0$. The matrix rank is then given by the number of non-null singular values. In practice, due to numerical limitations, the rank is the number of singular values greater than a given tolerance. Therefore, the minimum singular values σ_n provides a measure of how close to singular is the matrix. In the case of matrices $\mathcal{C}(\lambda_k)$ and $\mathcal{O}(\lambda_k)$, σ_n indicates how far is the system of being uncontrollable or unobservable, respectively, with respect to the i-th input and j-th output.

The choice of input and output signals through the PBH test is done by selecting those with the larger minimum singular values σ_n of matrices $\mathcal{C}(\lambda_k)$ and $\mathcal{O}(\lambda_k)$ [156]. Although this is reasonable input-output selection criterion to determine the most controllable and most observable signals, it is not always clear which pair presents the better joint controllability and observability characteristics. From control point of view, the joint measure is one actually important.

Residue analysis

Given the transfer function $g_{ij}(s)$ from the input u_i to the output y_j, it is always possible to express it as a sum of partial fractions of the form

$$g_{ij}(s) = \frac{y_j(s)}{u_i(s)} = c_j(sI - A)^{-1}b_i + d_{ij} = \sum_{k=1}^{n} \frac{R_k}{s - \lambda_k} + d_{ij} \tag{5.8}$$

where R_k is the residue associated to the mode λ_k [168]. The residue R_k provides an idea of how the mode λ_k is affected by the input u_i and how visible is from the output y_j. Therefore, the residues are clear measures of joint controllability and observability of a particular oscillation mode that is commonly used in damping oscillation analysis [41, 169, 159].

The residues can be computed directly from the state space realization from the expression

$$R_k = c_j \phi_k \psi_k b_i \tag{5.9}$$

where ϕ_k and ψ_k are the right and left eigenvectors of the matrix A, respectively, corresponding to the eigenvalue λ_k. As in general the residues are complex numbers, the best input-output signal pair is given by the maximum value of the residue magnitude. The residues depend on the scale of the input and output signals and not always provide a clear comparison among transfer function associated to variables with different units.

Geometric measures

These controllability and observability measures, respectively, are defined as

$$m_{ci} = \cos(\theta(\psi_k, b_i)) = \frac{|b_i^T \psi_k|}{||\psi_k||\,||b_i||}, \tag{5.10}$$

$$\tag{5.11}$$

$$m_{oj} = \cos(\theta(\phi_k, c_j)) = \frac{|c_j \phi_k|}{||\phi_k||\,||c_j||}, \tag{5.12}$$

where $\theta(\psi_k, b_i)$ is the angle between b_i and ψ_k, and $\theta(\phi_k, c_j)$ is the angle between c_j and ϕ_k. The geometric measures provide an idea of how aligned are the columns of the matrix B, the rows of C with an eigenvector of A and superscript T stands for the transpose operation. If the $m_{ci} = 0$ the column of b_i is orthogonal to the eigenvector ψ_k and the control will not be effective to modified the state associated to eigenvalue λ_k. Similarly, if $m_{oj} = 0$, c_j and ϕ_k are orthogonal and the mode λ_k will not be observable from the output y_j [170].

A joint controllability and observability measure can be defined as

$$m_{coij} = m_{ci} m_{oj}. \tag{5.13}$$

A zero value of m_{coij} indicates that λ_k is non-controllable/non-observable from the i-th input and the j-th output. The geometric measures provide a similar information to the residues, with the advantage of being normalized

and independent of the scale of the signals. These measured have been used to determine the best input-output pair in power damping applications [170, 60].

Some authors have proposed the use of Hankel singular values (HSVs) for the selection of input output pairs [157]. However, it is not possible to connect the controllability and observability of a particular mode with the HSVs [167]. For this reason, the use of HSVs will not be considered in this study.

5.3.2 Limitations caused by right hand plane zeros (RHPZs)

It is well-known that non-minimum phase zeros (zeros in the right hand plane, RHPZ) impose limitations on the achievable performance [171, 172]. To ensure closed-loop stability, the controller cannot cancel RHPZs and the frequency response of the closed-loop transfers will have fixed points that cannot be altered by the controller. For instance, the sensitivity transfer $S(s)$ takes the value 1 at a RHPZ independently of the controller; that is, if ξ is a RHPZ, then

$$S(\xi) = (I + K(\xi)G(\xi))^{-1} = 1.$$

These constraints become serious limitations if the RHPZs are close to the mode to be damped, since the magnitude of the closed-loop transfer cannot be arbitrary reduced. If the controller set is reduced to proportional controls, the constraints are more serious. A simple root locus analysis reveals how strong are these limitations. Since the closed-loop poles tend to the open loop zeros, if an open loop poles is close to an RHPZ, a small increment of the gain may result in unstable system and thus it is not possible to affect the lightly damped mode. Therefore, any pair with RHPZs in the range of LFOs should be avoided.

The limitations imposed by RHPZs have been used to propose input-output selection procedures in [173, 172]. In the context of damping oscillations in power systems have been used in [163, 157, 158].

5.3.3 Input-output interactions

An alternative view of the problem of input-output paring can be obtained from the frequency domain. They allow to evaluate input-output interactions and thus determine if decentralized controllers will be able to achieve a reasonable closed-loop behavior.

RGA

It allows to evaluate interactions among different inputs and outputs [167]. In the context of input-output pair selection, it can help to determine the input-output with higher interaction and also to evaluate the advantage or not of using multivariable controllers.

The RGA matrix H is defined as

$$H(s) = [\eta_{ij}(s)] = G(s) \otimes G(s)^{-T} \tag{5.14}$$

where $[\eta_{ij}]$ denotes the element ij of the matrix H and the operator $\otimes$ denotes the Hadamard or Schur product (element by element product)[167].

For example, in case of systems with two inputs and two outputs (2×2 system),

$$G(s) = \begin{bmatrix} g_{11}(s) & g_{12}(s) \\ \\ g_{21}(s) & g_{22}(s) \end{bmatrix}, \tag{5.15}$$

the RGA is given by

$$H(s) = \begin{bmatrix} \eta_{11}(s) & 1 - \eta_{11}(s) \\ \\ 1 - \eta_{11}(s) & \eta_{11}(s) \end{bmatrix}, \tag{5.16}$$

with

$$\eta_{11}(s) = \frac{g_{11}(s)g_{22}(s)}{g_{11}(s)g_{22}(s) - g_{12}(s)g_{21}(s)} \tag{5.17}$$

The following conclusions can be drawn from the RGA (5.16) [167, 164].

- If η_{11} is close to 1, the pairs $u_1 - y_1$ and $u_2 - y_2$ are decoupled and can be controlled independently. In this case, a centralized multivariable controller will not achieve better performance than the decentralized one

  $$K(s) = \begin{bmatrix} k_{11}(s) & 0 \\ \\ 0 & k_{22}(s) \end{bmatrix}, \tag{5.18}$$

  in which k_{11} and k_{22} can be designed independently.

- If η_{11} is close to zero, the RGA indicates that the best pair to decentralized control should be $u_1 - y_2$ and $u_1 - y_2$ and the controllers can be designed independently if the input-output pairs are reordered.

- Otherwise, the input-output pairs are not decoupled and decentralized control should be designed carefully. For stable plants, input-output pair on negative steady state RGA elements should be avoided. Otherwise, if the sub-controllers are designed independently each with integral action, then the interactions will cause instability either when all the loops are closed or when the loop corresponding to the negative relative gain becomes inactive.

Notice that the RGA depends on the frequency. Therefore, the previous analysis should be done in the frequency range of interest; i.e. the range where LFOs arise.

MSF

It is the building block for Individual Channel Analysis and Design (ICAD) [174, 175]. An appropriate interpretation of the MSF at low and high frequency allows to determine: the existence and required structure of diagonal controllers, the dynamical structure of the closed-loop system, a reliable measurement of robustness, and the possibility to satisfy design specifications [164].

In ICAD, the dynamical structure of $G(s)$ is determined by individual channels $C_i(s)$ resulting from pairing each input to each output by means of diagonal controllers [174]. Consider the 2×2 system in (5.15) and the decentralized controller (5.18). Then the closed-loop system can be represented as two SISO individual channels $C_i(s)$, each including a feedback loop and its controller, as shown in Figure 5.2. The multivariable structure of the plant is encapsulated by the scalar transfer function $\gamma_a(s)$. This representation is equivalent to the original system with no loss of information [174].

In general, $C_i(s)$ has the open loop SISO transmittance [174]

$$C_i(s) = k_{ii}(s)g_{ii}(s)\left(1 - \gamma_a(s)h_j(s)\right) \tag{5.19}$$

where

$$\gamma_a(s) = \frac{g_{12}(s)g_{21}(s)}{g_{11}(s)g_{22}(s)} \tag{5.20}$$

is the MSF and

$$h_j(s) = \frac{k_{jj}(s)g_{jj}(s)}{1 + k_{jj}(s)g_{jj}(s)} \tag{5.21}$$

describes the impact of controller $k_{jj}(s)$ on the i-th control loop, subjected to the disturbances

$$d_i = \frac{g_{ij}(s)}{g_{jj}(s)}h_j(s)r_j(s), \tag{5.22}$$

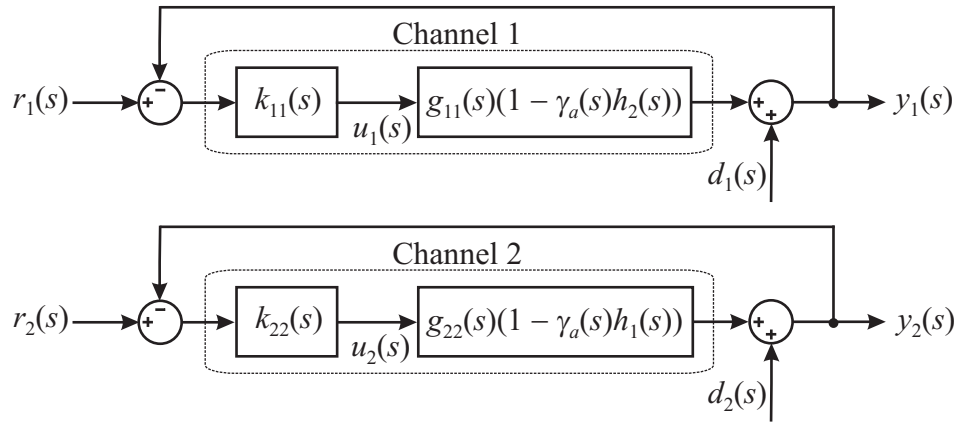

Figure 5.2: Individual channel representation of a 2×2 system

which represent the effect of reference $r_j(s)$ on channel $C_i(s)$. As it can be seen from Figure 5.2 and (5.19)-(5.22), the behavior of $C_i(s)$ is both affected by its controller $k_{ii}(s)$ and by channel $C_j(s)$ [174, 175]. Moreover, the MSF [164]:

- determines the dynamical characteristics of each input-output configurations and indicates the potential performance of a feedback control system,
- its adequate interpretation ensures an effective control system design,
- its magnitude quantifies the coupling between input-output channels in the frequency domain,
- is related to the plant transmission zeros (zeros of $1–\gamma_a(s)$, $|G(s)| = g_{11}(s)g_{22}(s) - g_{12}(s)g_{21} = 0$).
- $\gamma_a(s) = 1$ determines the non-minimum phase condition,
- its closeness to (1,0) in the Nyquist plot indicates to what extent the plant is sensitive to uncertainty in terms of gain and phase margins.

If the channels are defined by pair u_1-y_2 and u_2-y_1, then the MSF is given by

$$\gamma_b(s) = \frac{g_{11}(s) \cdot g_{22}(s)}{g_{12}(s) \cdot g_{21}(s)} = \gamma_a^{-1}(s) \tag{5.23}$$

and

$$C_i(s) = k_{ij}(s) g_{ji}(s) \left(1 - \gamma_b(s) h_j(s)\right). \tag{5.24}$$

Notice that H can be expressed in terms of MSF [164],

$$H = \begin{bmatrix} \dfrac{1}{1-\gamma_a(s)} & \dfrac{\gamma_a(s)}{\gamma_a(s)-1} \\ \dfrac{\gamma_a(s)}{\gamma_a(s)-1} & \dfrac{1}{1-\gamma_a(s)} \end{bmatrix} = \begin{bmatrix} \dfrac{\gamma_b(s)}{\gamma_b(s)-1} & \dfrac{1}{1-\gamma_b(s)} \\ \dfrac{1}{1-\gamma_b(s)} & \dfrac{\gamma_b(s)}{\gamma_b(s)-1} \end{bmatrix}. \tag{5.25}$$

5.4 Case of study

The different methods presented in Section 5.3 are assessed through the test system shown in Figure 5.3, which includes wind power generation. This system has been previously used to show the interaction between conventional generation and WPPs [133]. The WPP including converter-based wind turbines is considered as a negative load, since the converter dynamics are considerably faster than the electromechanical dynamics that this work is focused on. This approach has been previously used in [49]. The power system and synchronous machine parameters can be found in Tables 5.1 and 5.2 [71, 133].

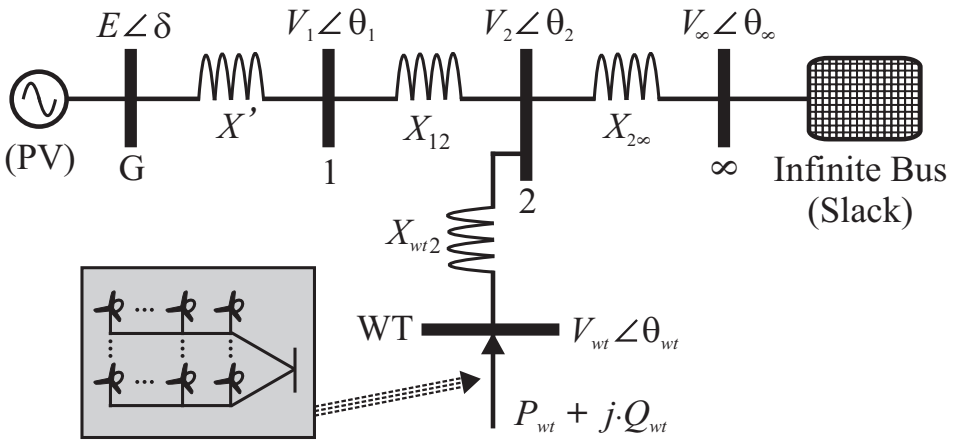

Figure 5.3: Electrical network representation of the power system under study

P_g	P_{wt}	Q_{wt}	E'	ω_s (rad/s)	X_{12}	X_{wt2}	$X_{2\infty}$
0.8	0.4	0	1	100π	0.1	0.1	0.2

Table 5.1: Power system parameters (in p.u. except indicated)

T_0	H (s)	X_{ta}	X'
6	4	1.1	$0.15 + X_{ta}$

Table 5.2: Synchronous machine parameters (in p.u. except indicated)

5.4.1 Linearization

The linearization procedure and the matrices that encompasses the linear system are clearly described in Appendix B. The linearized system is represented, as previously presented, in state-space form as (5.2)

$$\begin{aligned} [\dot{x}] &= [A]\,[x] + [B]\,[u]\,, \\ [y] &= [C]\,[x] + [D]\,[u]\,, \end{aligned} \tag{5.26}$$

where

$$\begin{aligned} x &= \begin{bmatrix} \delta \\ \omega \\ E' \end{bmatrix}; \\ u &= \begin{bmatrix} P_{wt} \\ Q_{wt} \end{bmatrix}; \\ y &= \begin{bmatrix} V_{wt} \\ \theta_{wt} \end{bmatrix}. \end{aligned} \tag{5.27}$$

The state variables represent the mechanical dynamics and the exciter control variable of the synchronous machine. The input and output variables represent local signals: the inputs are the aggregated active and reactive power, and the output signals are the voltage magnitude and phase angle of the WPP.

The operating point values used to linearize the power system used as study case are presented in Table 5.3. This operating point is obtained from the resolution of the power flow equations.

From the small signal analysis of the linear model of the power system, matrix A has a stable lightly damped oscillation mode at $\lambda_{12} = -0.0119 \pm$

E'_0 (p.u.)	δ_0 (rad)	V_{wt0} (p.u.)	θ_{wt0} (rad)	V_{20} (p.u.)
1	0.5283	0.9889	0.2858	0.9897

θ_{20} (rad)	V_{10} (p.u.)	θ_{10} (rad)	V_{ib0} (p.u.)	θ_{ib0} (rad)
0.2449	0.9961	0.3262	1	0

Table 5.3: Operating point values used to Taylor series development

$8.30375j$, with frequency 1.322 Hz and a damping coefficient, in p.u., of 0.00144. This oscillation mode is selected to be analyzed.

5.4.2 Controllability and observability measures comparison

The controllability and observability measures previously mentioned were compared in the system under study. According to the input and output defined in (5.26), four possible signal pairs can be analyzed:

- P_{wt}-V_{wt},
- Q_{wt}-V_{wt},
- P_{wt}-θ_{wt},
- Q_{wt}-θ_{wt}.

PBH test

The singular values corresponding to the $\mathcal{C}(\lambda_1)$ and $\mathcal{O}(\lambda_1)$ are listed in Tables 5.4 and 5.5. Notice that matrix $\mathcal{C}(\lambda_1)$ depends on matrices b_i and not on c_j. For this reason, Table 5.4 has only two columns. The same applies to $\mathcal{O}(\lambda_1)$, with results in Table 5.5. The largest of the minimum singular values for the possible signal pairs is highlighted. It can be observed that the most controllable pairs correspond to those with the active power delivered by the WPP (P_{wt}) as an input. The most observable pairs are those with the phase angle of the WPP connection point (θ_{wt}) as an output.

It can be concluded that the best signal pair is P_{wt}-θ_{wt} since it renders the largest of the minimum singular values for both matrices. Also, it can be seen that the worst signal pair is Q_{wt}-V_{wt}. However, the next best possible pair is not clear from the remaining options since the PBH test does not provide any joint controllability and observability measure.

P_{wt}-V_{wt}/P_{wt}-θ_{wt}	Q_{wt}-V_{wt}/Q_{wt}-θ_{wt}
78.9950	77.6115
8.3223	8.3224
1.6480	0.5251

Table 5.4: Singular Values of the matrix $\mathcal{C}(\lambda_1)$

P_{wt}-V_{wt}/Q_{wt}-V_{wt}	P_{wt}-θ_{wt}/Q_{wt}-θ_{wt}
77.461	77.462
8.329	8.323
0.002	**0.045**

Table 5.5: Singular Values of the matrix $\mathcal{O}(\lambda_1)$

Residue analysis

The magnitude of the residues are listed in Table 5.6. It can be observed that the maximum value corresponds to the pair P_{wt}-θ_{wt}. This is consistent with the information provided by the PBH test and this signal pair should be selected as a first option. It should be mentioned that a well-known PSSs design method to damp oscillations exists based on residue analysis [169].

	P_{wt}-V_{wt}	Q_{wt}-V_{wt}	P_{wt}-θ_{wt}	Q_{wt}-θ_{wt}
$\lvert R_i \rvert$	0.018	0.006	**0.349**	0.109

Table 5.6: Residue values

Conversely to the PBH test, the residue analysis clearly defines the best order of the signal pair due to its joint controllability and observability measurement test.

Geometric measures

The geometric measures for the system under study are in Table 5.7. The joint controllability and observability measure m_{co} shows that the signal pair to be selected must be P_{wt}-θ_{wt} since it has the maximum value among the possible input-output pairs. These results are consistent with those obtained

previously. However, in this case the information is clearer since the values are normalized.

	P_{wt}-V_{wt}	Q_{wt}-V_{wt}	P_{wt}-θ_{wt}	Q_{wt}-θ_{wt}
m_c	**0.9928**	0.9927	**0.9928**	0.9927
m_o	0.3842	0.3842	**0.9505**	**0.9505**
m_{co}	0.3815	0.3814	**0.9437**	0.9436

Table 5.7: Geometric Measures

5.4.3 RPHZs

The transfer function corresponding to the system under analysis is given by $G(s)$ in (5.15), where

$$\begin{aligned} g_{11}(s) &= -\frac{0.032727(s+0.5314)(s^2-0.08487s+78.87)}{(s+0.3985)(s^2+0.02391s+68.95)} \\ g_{12}(s) &= \frac{0.23117(s+0.4832)(s^2+0.01688s+69.35)}{(s+0.3985)(s^2+0.02391s+68.95)} \\ g_{21}(s) &= \frac{0.23766(s+0.4036)(s^2+0.0181s+93.34)}{(s+0.3985)(s^2+0.02391s+68.95)} \\ g_{22}(s) &= -\frac{0.021838(s+0.535)(s^2-0.2433s+151.9)}{(s+0.3985)(s^2+0.02391s+68.95)} \end{aligned} \tag{5.28}$$

Figure 5.4 shows the Bode plots of the individual transfer functions in (5.28). For clarity, Figure 5.4(a) features the diagonal elements $g_{ii}(s)$ and Figure 5.4(b) the off-diagonal entries $g_{ij}(s)$ of $G(s)$. It can be clearly seen that the damping controller should act in the region 8-11 rad/s (1.2-1.75 Hz).

In Equation (5.28), it can be seen a pair of complex RHPZs in the individual transfer functions $g_{11}(s)$ and $g_{22}(s)$ close to the lightly damped mode $\lambda_{12} = -0.01196 \pm j8.3038$. In the Bode plots in Figure 5.4(a), it can be observed the resonance peak caused by the low damping of λ_{12}. The contribution of 180 degrees of the non-minimum phase zeros is also clear in these plots. In the rest of the frequencies, the magnitudes of $g_{11}(s)$ and $g_{22}(s)$ are below -20 dB, suggesting a small contribution of input P_{wt} to output V_{wt} and input Q_{wt} to output θ_{wt}. Figure 5.4(b) shows $g_{12}(s)$ and $g_{21}(s)$.

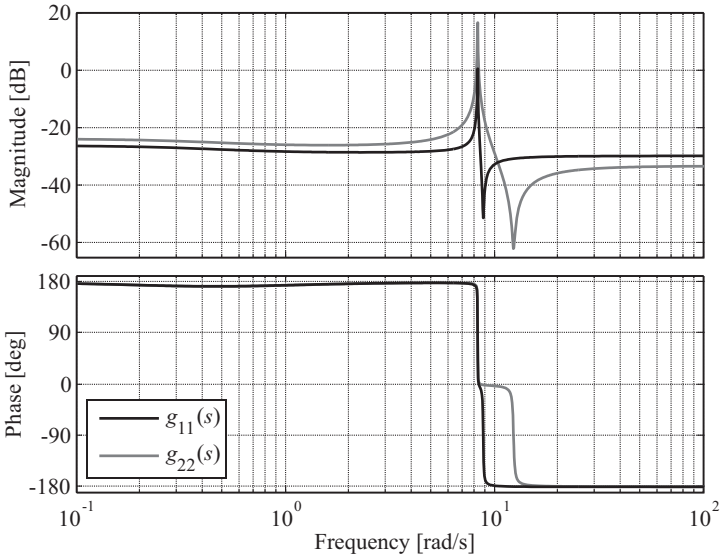

(a) $g_{11}(s)$ and $g_{22}(s)$

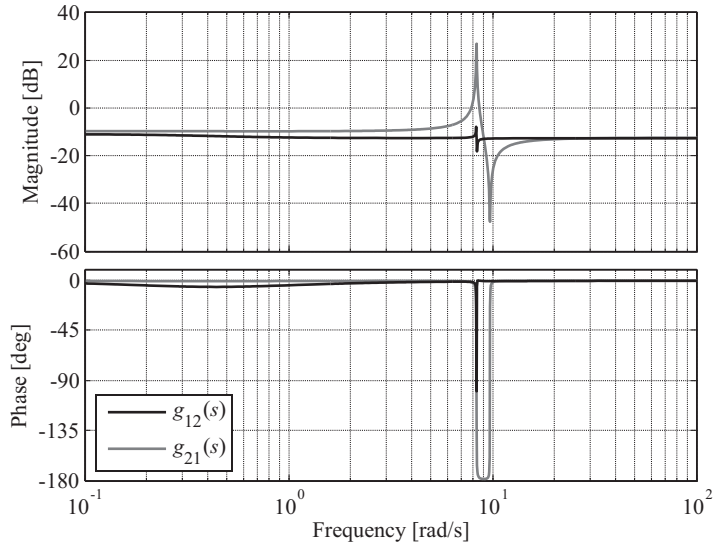

(b) $g_{12}(s)$ and $g_{21}(s)$

Figure 5.4: Bode diagrams of transfer functions $g_{ij}(s)$

The proximity of the oscillation mode λ_{12} to the lightly damped zeros tends to cancel the resonances peaks; however, in these cases the minimum phase

zeros contribute with positive phase. The magnitude of transfer functions $g_{ij}(s)$ is higher compared to that $g_{ii}(s)$.

If disturbances at the voltage are considered, the closed-loop transfer is given by

$$g_{cl,ij}(s) = (1 + K_{ij}(s)g_{ij}(s))^{-1}.$$

Due to the RHPZs in g_{11} and g_{22} ($\xi_{11} = 0.0424 \pm 8.8808j$ and $\xi_{22} = 0.1216 \pm 12.3242j$) regardless the controller

$$g_{cl,11}(\xi_{11}) = g_{cl,22}(\xi_{22}) = 1.$$

This implies that it will be difficult to reduce the resonance peak and thus increasing the damping of the oscillation mode λ_{12}, especially in case of g_{11} where the ξ_{11} is quite close to λ_{12} [171].

This preliminary analysis suggests avoiding signal pairs directly associated to individual elements $g_{11}(s)$ and g_{22} due to the limitations imposed by the presence of RHPZs; i.e., P_{wt}-V_{wt} and Q_{wt}-θ_{wt}. Nevertheless, since no conclusion has been made about the internal coupling of the plant it is not apparent how the RHPZs of $g_{11}(s)$ and $g_{22}(s)$ will reflect on the signal pairs P_{wt}-θ_{wt} and Q_{wt}-V_{wt} associated to off-diagonal transfer functions $g_{12}(s)$ and $g_{21}(s)$.

5.4.4 Input-output interactions

RGA

The elements of matrix H for the 2×2 system under study are

$$\eta_{11} = \frac{-0.0132\,(s+0.54)\,(s+0.53)\left(s^2-0.085s+77.87\right)\left(s^2-0.24s+154.9\right)}{(s+0.484)\,(s+0.398)\,(s^2+0.0239s+68.95)\,(s^2+0.018s+92.85)}$$

$$\eta_{12} = \frac{1.013\,(s+0.48)\,(s+0.4)\left(s^2+0.017s+69.35\right)\left(s^2+0.018s+93.34\right)}{(s+0.484)\,(s+0.398)\,(s^2+0.0239s+68.95)\,(s^2+0.018s+92.85)} \tag{5.29}$$

Figure 5.5 shows the Bode diagrams of the diagonal and off-diagonal RGA entries. It can be seen that $\eta_{11}(s)$ (diagonal elements of H) are negative for most frequencies and their magnitude small. This can be concluded after examination of (5.29) and the phase plot in Figure 5.5. Phases of 180 deg and -540 deg correspond to negative magnitudes, and overall $\eta_{11}(s)$ will only be positive for a narrow margin of frequencies between $8 - 10$ rad/s. Conversely, the magnitude of $\eta_{12}(s)$ (off-diagonal elements of H) is close to unity (i.e., 0 dB), as shown by Figure 5.5. Simple inspection of (5.29) shows

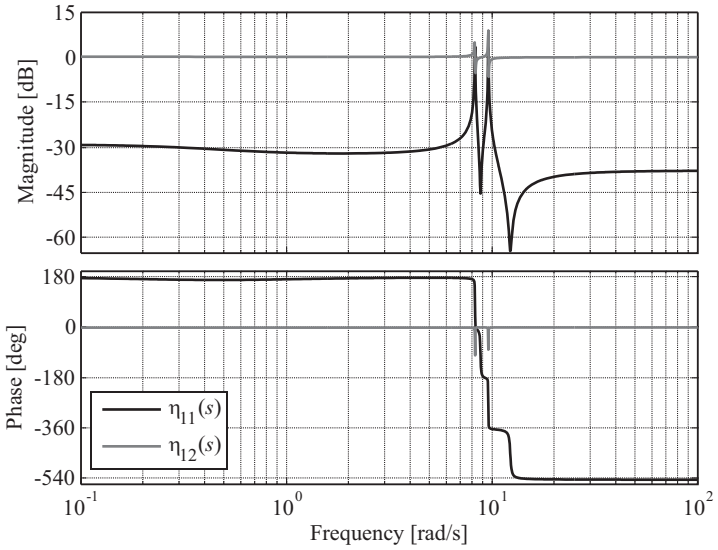

Figure 5.5: Bode diagrams of RGA matrix H

that off-diagonal entries $\eta_{12}(s)$ have a positive magnitude for all frequencies. This is corroborated by the nearly constant phase of 0 deg in Figure 5.5.

As outlined in Section 5.3.3, in case of using decentralized controllers with independently designed elements, input-output pairs where the diagonal (or off-diagonal) entries are positive are recommended. Since the magnitude of $\eta_{11}(s)$ elements is negative for most frequencies, pairs P_{wt}-V_{wt} and Q_{wt}-θ_{wt} should be avoided. Furthermore, since the magnitude of off-diagonal entries η_{12} is close to unity, the corresponding input-output pairs (i.e., P_{wt}-θ_{wt} and Q_{wt}-V_{wt}) could be treated as SISO plants. It should be noted that the change of sign at some frequencies in elements $\eta_{11}(s)$ implies that RHPZs are present in plant $G(s)$, which is consistent with (5.28). However, it is not clear how those non-minimum phase zeros will affect the control system design and performance arising from the possible signal pairs.

MSF

Using equations (5.20) and (5.23), the MSFs of plant (5.28) are given as

$$\gamma_a = \frac{76.87\,(s+0.483)\,(s+0.404)\left(s^2+0.017s+69.35\right)\left(s^2+0.018s+93.34\right)}{(s+0.535)\,(s+0.531)\,(s^2-0.0849s+77.87)\,(s^2-0.243s+151.9)}$$

$$\gamma_b = \frac{0.013\,(s+0.535)\,(s+0.531)\left(s^2-0.085s+77.87\right)\left(s^2-0.24s+151.9\right)}{(s+0.483)\,(s+0.404)\,(s^2+0.0169s+69.35)\,(s^2+0.0183s+93.34)} \tag{5.30}$$

An adequate interpretation of the MSF allows a complete evaluation of the control system design limitations arising both from the presence of RHPZs and the multivariable character of the plant, which goes beyond the information provided by the RGA analysis [164]. Since $G(s)$ was obtained from a state-space representation, the number of RHPZs of $(1 - \gamma_a(s))$ is given by [176]

$$Z = N + P - Q, \tag{5.31}$$

where Z is the number of RHPZs of $(1-\gamma_a(s))$, P is the number of right hand plane poles (RHPPs) of $\gamma_a(s)$, N is the number of clockwise encirclements to the (1,0) point in the Nyquist plot of $\gamma_a(s)$, and Q is the number of eigenvalues in the right hand plane of the state-space representation. This is an application of the Nyquist stability criterion [176].

Figure 5.6 shows the Bode and Nyquist plots of MSF $\gamma_a(s)$. From Figure 5.6(a), it can be seen that the coupling resulting from pairing P_{wt}-V_{wt} and Q_{wt}-θ_{wt} is high for all frequencies, as evidenced by the magnitude of $\gamma_a(s)$ above 20 dB. From (5.30), it is evident that $\gamma_a(s)$ has four RHPPs; i.e., $P = 4$. As shown by (5.28), for this system $Q = 0$. Since $\gamma_a(0) = 28.85$, the Nyquist plot starts at the right side of $(1, 0)$. Figure. 5.6(b) shows the positive frequencies for the Nyquist trajectory of $\gamma_a(s)$. The plot of $\gamma_a(s)$ encircles $(1, 0)$ four times in counter-clockwise direction, implying that $N = -4$. Thus, applying (5.31) $(1 - \gamma_a(s))$ contains no RHPZs; i.e., $Z = 0$.

The information obtained from the previous analysis is revealing. When considering the signal pairings P_{wt}-V_{wt} and Q_{wt}-θ_{wt}, the associated individual channels defined by (5.19) are non-minimum phase. This is not a consequence of the multivariable character of the plant, as evidenced by the lack of RHPZs in $(1-\gamma_a(s))$, but to those RHPZs appearing in the diagonal transfer functions $g_{11}(s)$ and $g_{22}(s)$ (equation(5.28)). Examination of the Bode plots $g_{ii}(s)$ in Figure. 5.4 shows that the frequency of those RHPZs is around the frequency of the oscillation mode λ_1. In order to avoid instability, the bandwidth of the oscillation damper should be restricted below

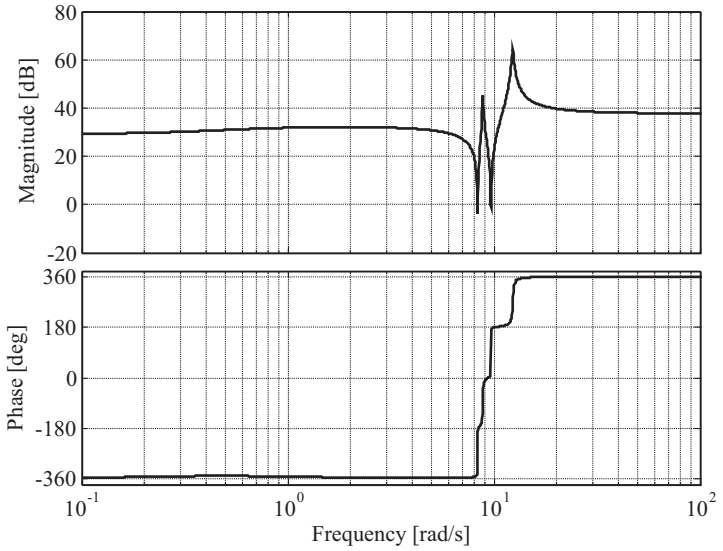

(a)

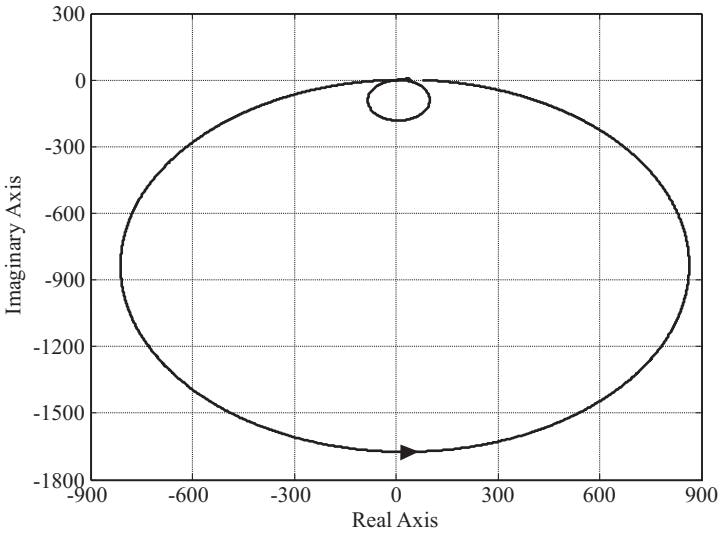

(b)

Figure 5.6: Assessment of MSF $\gamma_a(s)$: (a) Bode plot; (b) Nyquist plot.

the range of frequencies at which it should act to damp electromechanical oscillations. These are two conflicting and irreconcilable control design objectives and, therefore, the damper design employing signal pairings P_{wt}-V_{wt}

or Q_{wt}-θ_{wt} is not recommended. Even if this was not the case, the fact that $\gamma_a(s)$ has four RHPPs implies that $(1-\gamma_a(s))$ will preserve such structure. Thus, the damper controller would require the stabilization of an unstable plant with non-minimum phase zeros, which is by no means a trivial task [167].

Figure 5.7 shows the Bode and Nyquist plots of MSF $\gamma_b(s)$. As shown by Figure 5.7(a), the internal coupling the plant arising from pairing P_{wt}-θ_{wt} and Q_{wt}-V_{wt} is weak: the magnitude of $\gamma_b(s)$ is below -20 dB for most frequencies except for those where the damping controller should act. From (5.30) it is evident that $\gamma_b(s)$ has no RHPPs ($P=0$). As it can be seen from Figure. 5.7(b), the Nyquist trajectory of $\gamma_b(s)$ (only positive frequencies shown) starts to the left of $(1,0)$ and no encirclements to this point occur, implying that $N=0$. Applying (5.31), $Z=0$ and thus $(1-\gamma_b(s))$ contains no RHPZs. Moreover, transfer functions $g_{12}(s)$ and g_{21} have no RHPZs. In spite of the presence of RHPZs in $g_{11}(s)$ and $g_{22}(s)$, this does not reflect on the input-output channel definition associated to $\gamma_b(s)$ in (5.19).

Based on this analysis, the input-output pairing P_{wt}-θ_{wt} or Q_{wt}-V_{wt} should be considered for the damping controller design.

5.4.5 Simulations

In order to illustrate the previous results, time domain simulations were carried out. The test system of Figure 5.3 was implemented in MATLAB/Simulink. The PSS controller for the wind power plants was designed using a root locus approach,

$$K_{pss} = K\frac{sT_w}{sT_w+1} \tag{5.32}$$

where K_{pss} was formed by a washout filter with a time constant $T_w = 2$s, a gain $K=3$ which has been selected from the root locus diagrams shown in Figures 5.8 and a limiter.

Such a controller structure was used for the case of independent four input-output SISO pairs and when evaluating MIMO configurations. The controller parameters remained the same to offer a meaningful comparison while ensuring system stability for all SISO cases. In other words, for the following results $K_{pss} = k_{11} = k_{22} = k_{12} = k_{21}$.

Figure 5.9 shows the simulation results (input and output variables) for SISO designs considering input-output pairs P_{wt}-V_{wt} and Q_{wt}-θ_{wt} and for the case of a decentralized MIMO design considering the pairs defined by $\gamma_a(s)$ (i.e., $C_1(s)$: P_{wt}-V_{wt} and $C_2(s)$: Q_{wt}-θ_{wt}). The simulation starts with

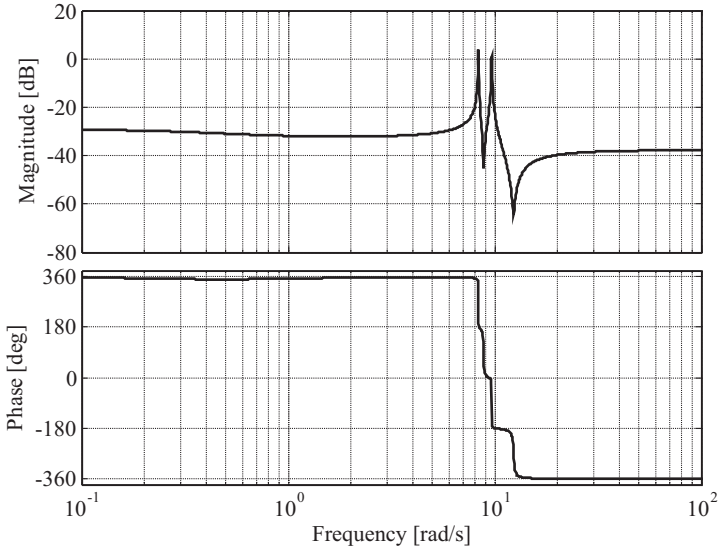

(a)

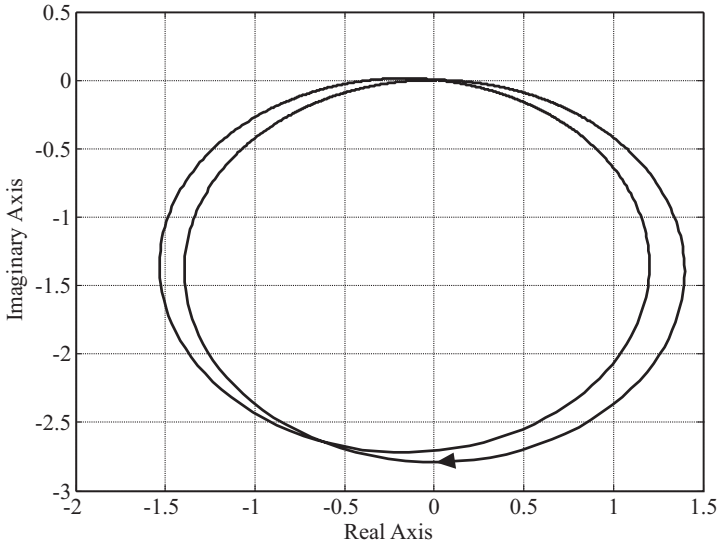

(b)

Figure 5.7: Assessment of MSF $\gamma_b(s)$: (a) Bode plot; (b) Nyquist plot.

the system at steady state. At 5s, an impulse variation on the mechanical power reference of the synchronous machine is done, in order to excite the

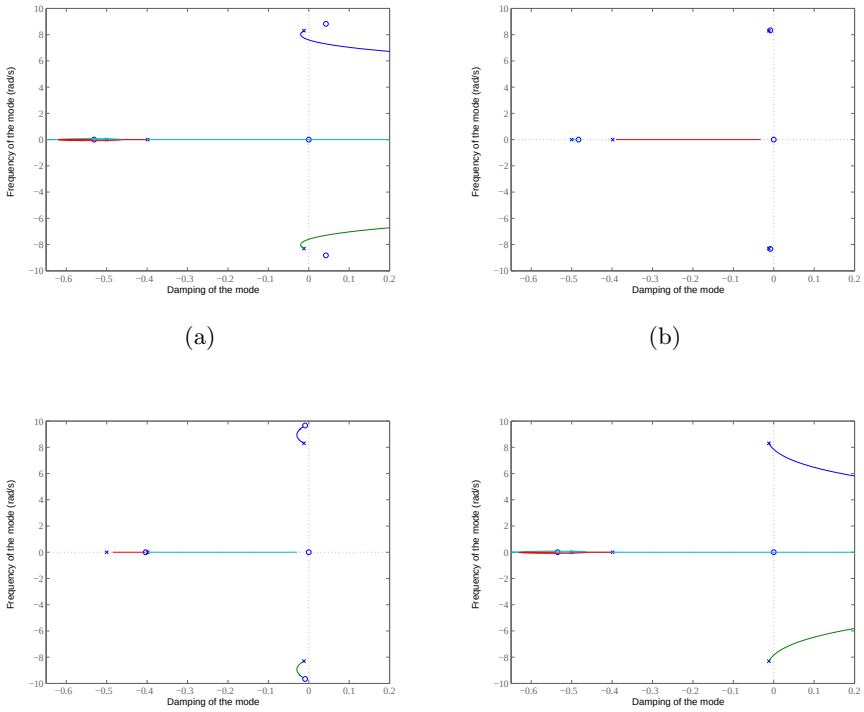

Figure 5.8: Root Locus diagrams showing eigenvalue modification for a variation of the gain K from 0 to 50. The gain selected is chosen the same for the four study cases: (a) P_{wt}-V_{wt}; (b) Q_{wt}-V_{wt}; (c) P_{wt}-θ_{wt}; (d) Q_{wt}-θ_{wt}

oscillation mode existing on the system. As it can be observed, the system becomes unstable for the MIMO design. This was expected since MSF $\gamma_a(s)$ features RHPPs and the simple controllers used are not able to modify its structure. It could be argued that a more complex MIMO controller may stabilize the plant, but this is out of the scope of this work. Conversely, the system is stable when considering the designs for the SISO pairs, but non-minimum phase zeros are present. Moreover, the damping contribution is weak in either SISO case and the oscillations are not damped during the simulation horizon. It could be argued that the performance may be improved by increasing the proportional gain of the controller, but care should

be exercised since the system may become unstable due to the presence of RHPZs.

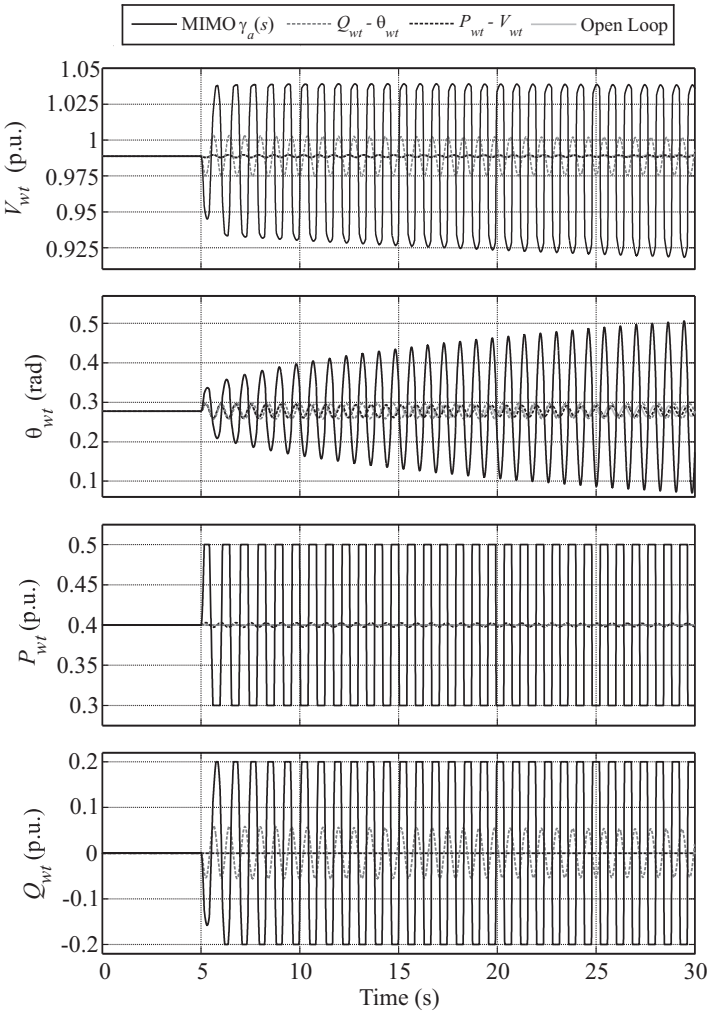

Figure 5.9: Simulation responses (voltage magnitude, phase angle of the voltage, active power, and reactive power at WPP bus) for SISO and MIMO designs involving input-output pairs P_{wt}-V_{wt} and Q_{wt}-θ_{wt}.

Figure 5.10 shows the simulation results for the SISO designs considering input-output pairs P_{wt}-θ_{wt} and Q_{wt}-V_{wt} and for the case of a decentralized MIMO design considering the pairs defined by $\gamma_b(s)$ (i.e., $C_1(s)$: P_{wt}- θ_{wt} and

$C_2(s)$: Q_{wt}-V_{wt}). As it can be seen, in both SISO cases the oscillations are damped after a transient period. When considering the SISO pair P_{wt}-θ_{wt}, the magnitude of the voltage, its phase angle and the reactive power show less oscillations than for the SISO case with Q_{wt}-V_{wt}. This was expected from the analysis carried out in previous sections. When using the same controller in both individual channels, it can be seen that the MIMO design produces the best damping performance in all variables except for the case of active power, where the oscillations take a longer time to be eliminated. This superior performance was expected since the MIMO design takes the damping contribution of both feedback loops.

It should be emphasized that the results obtained in Figures 5.9 and 5.10 agree on well with the analyzes carried out with the controllability and observability tools and the frequency domain approaches from the previous sections. It is also apparent that the best performance for any possible SISO alternative is achieved when considering input-output pair P_{wt}-θ_{wt}.

5.4.6 Recommendations for input-output pair selection

From the analysis of the different selection methods previously presented, some recommendations can be outlined with the aim of finding the most adequate alternative for input-output signal pairing (depending on the desired control scheme).

Considering the SISO case, controllability, observability and the location of RHPZs determine the best signal pair. Various tools for controllability and observability analyaes have been presented. The most useful is the geometric measure since erroneous results caused by different magnitude scales are avoided through the normalization of the controllability and observability measures. The location of RHPZs must also be considered in the study since they might impose serious control restrictions if they appear nearby the oscillation mode to be damped.

For decentralized multivariable schemes, the interaction between input-output pairs is also a limiting factor. For this analysis, both RGA and MSF can be used; nevertheless, MSF is more suitable since it provides additional information about the achievable performance levels and limitations associated to RHPZs.

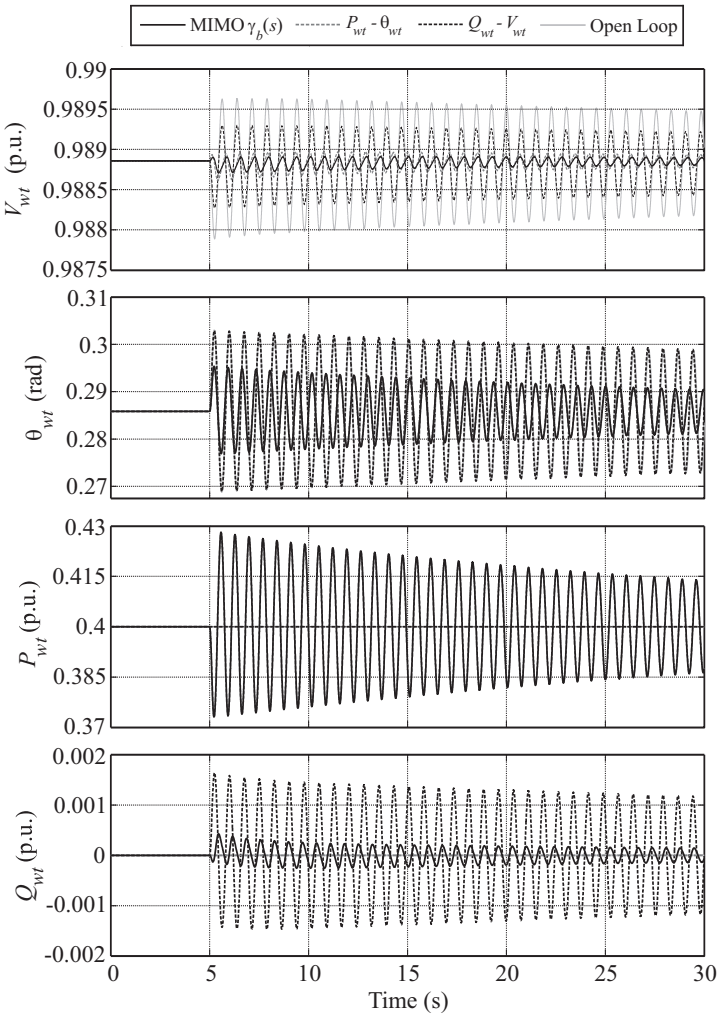

Figure 5.10: Simulation responses (voltage magnitude, phase angle of the voltage, active power, and reactive power at WPP bus) for SISO and MIMO designs involving input-output pairs P_{wt}-θ_{wt} and Q_{wt}-V_{wt}.

5.5 Conclusion of the chapter

Several tools have been used to decide which input-output configuration is more adequate to damp oscillations in power systems with WPPs. Controllability and observability tests have been analyzed – in particular, those allowing the evaluation of specific oscillation modes (PBH, residues and geometric measures). Among them, the most recommended are the geometric measures since they provide a normalized joint controllability and observability measure. The normalization is useful for the input-output selection because in general the input-output pairs have different scales.

In addition to the controllability and observability, the limitations imposed by the presence of RHPZs on performance have been considered. The stabilization of a plant with RHPZs gives rise to fixed points in the frequency response. As a consequence, if the RHPZs are close to the oscillation modes, there is no controller capable of achieving a substantial increment in damping.

Interactions among inputs and outputs were also analyzed with the aim to evaluate multivariable control schemes. RGA and MSF are useful tools to determine the most adequate pair for decentralized multivariable controls. An advantage of using the MSF approach over the RGA analysis, in addition to the definition of signal pairs afforded through both approaches, is that the potential dynamic performance and control system design of the oscillation damper can be evaluated. Moreover, through a careful analysis of the MSFs a clear effect of the RHPZs and limitations arising from them can be clearly defined.

In order to illustrate the different alternatives, a power system including a WPP was analyzed. A simple oscillation damper obtained through classic control design was employed to carry out time domain simulations. Simulation results show a system behavior in agreement with the previous analyzes.

6 Control signal selection for damping oscillations with wind power plants based on fundamental limitations

6.1 Introduction

The location of WPPs is a relevant factor in the capability of power system stabilizers (PSSs) to damp oscillations [177]. However, the location of wind power cannot be defined by the requirement of the power system contributions. The location is based mainly on energy capture possibilities and other economic aspects. As a consequence, WPPs may be far away from synchronous generators in which power system oscillations arise. For this reason, signals measured at the connection point of the WPP (local signals) may not be the most adequate ones to detect oscillations at remote locations where the synchronous generators are placed [177]. Recently, wide-area measurement systems (WAMSs) have emerged again allowing the use of remote signals in damping system based on WPPs and thus providing a solution to the previous issues [159]. However, WAMSs present some drawbacks in terms of signal delays and reliability [178, 179], aspects that can produce negative effects on oscillation damping.

In recent years, several papers have proposed different methodologies to determine the most adequate control signals and location for a PSS; they are

mainly focused on either FACTS, HVDC-links, or both at the same time [**?**, 157, 161, 60]. However, these analyses cannot be used for WPPs, since their location is not determined for oscillation damping purposes. Furthermore, in WPPs, the analysis must consider the fact that the disturbances and the remote signals to be damped might not be available, making local signals preferred. Therefore, the plant to be considered may be understood as the general control configuration (shown in Fig. 6.1), in which the oscillating signal cannot be fed back into the PSS. This control scheme, which imposes additional constraints on the controller design, results in limitations in the capability to attenuate disturbances [172, 180].

The aim of this paper is to propose an input-output selection criterion for the design of PSS for WPPs. The criterion especially considers the control limitations imposed by the impossibility of direct measurement of the signals to be controlled. Unlike previous works, the proposed criterion takes into account the controllability and observability of the local input-output pairs and the lower bound on the disturbance attenuation caused by the use of local signals in the PSS scheme as described in Fig. 6.1.

The chapter is organized as follows. Section 6.2 introduces the problem statement with some mathematical background. Section 6.3 presents different methods to predict control design limitations: a classical method to analyze the controllability and observability of a determined mode is presented in Section 6.3.1 and a methodology to determine the fundamental design limitations of a controller is presented in Section 6.3.2. In Section 6.4, a general criterion for input-output pair selection is proposed. The application of the criterion into two case of study is presented in Sections 6.5 and 6.6. Finally, the conclusions are summarized in Section 6.7.

6.2 Power System Stabilization based on WPPs

The dynamic behavior of a power system is described by a set of nonlinear differential and algebraic equations [36]. For small signal analyses, the nonlinear system is linearized around an operating point. Then, after some mathematical manipulations, the dynamics around the operating point is given by

$$\begin{aligned} \dot{x}(t) &= Ax(t) + B_w w(t) + B_u u(t), \\ z(t) &= C_z x(t) + D_{zw} w(t) + D_{zu} u(t), \\ y(t) &= C_y x(t) + D_{yw} w(t) + D_{yu} u(t), \end{aligned} \tag{6.1}$$

where $A, \ldots, D_{yu}$ are matrices of adequate dimensions, x denotes the state vector, w the disturbance and u the control input. The outputs z and y are

signals in which the oscillations can be observed. The signal z represents, for example, the angle of the synchronous machines and w a disturbance in the mechanical torque reference of the synchronous generator. These are remote signals that cannot be used by the PSS in order to avoid delays and reliability issues. Therefore, the local signal y (*e.g.* voltage or angle at the connection point) is the only information about the oscillations that the PSS can use to compensate them by injecting the correction signal u (*e.g.* active or reactive power).

The transfer function $G(s)$ corresponding to (6.1) can be partitioned as

$$\begin{bmatrix} z(s) \\ y(s) \end{bmatrix} = G(s) \begin{bmatrix} w(s) \\ u(s) \end{bmatrix} = \begin{bmatrix} G_{zw}(s) & G_{zu}(s) \\ G_{yw}(s) & G_{yu}(s) \end{bmatrix} \begin{bmatrix} w(s) \\ u(s) \end{bmatrix}. \tag{6.2}$$

From the previous definitions, the problem of designing a PSS based on WPP consists in computing a controller K to damp the oscillations in the signal z, as shown in Figure 6.1. From (6.2), the closed loop transfer

$$T_{zw} = G_{zw} + G_{zu}K\left(1 - G_{yu}K\right)^{-1} G_{yw} \tag{6.3}$$

should exhibit a more damped behavior than the open loop transfer G_{zw}.

This control problem is known as general control configuration and presents more limitations than the case in which the signal z is measured (*i.e.* when $z = y$) [172]. The performance achieved by any controller is limited by the need of guaranteeing stability of the closed loop system. These fundamental limitations are only dependent on the properties of the open loop system and not on the particular controller. The main purpose of the paper is to provide a criterion that using the fundamental limitations of the system permits to select the most adequate input-output pairs (u, y) to achieve the best oscillation damping.

6.3 Fundamental limitations in control design

The idea in the study of fundamental limitations of control design is to predict the performance of the closed loop system without computing the controller. Before presenting the input-output selection criterion, some background concepts are presented in this section.

6.3.1 Controllability and Observability

Controllability gives a measure of the possibility of modifying the location of an oscillation mode by state feedback. Observability provides a measure

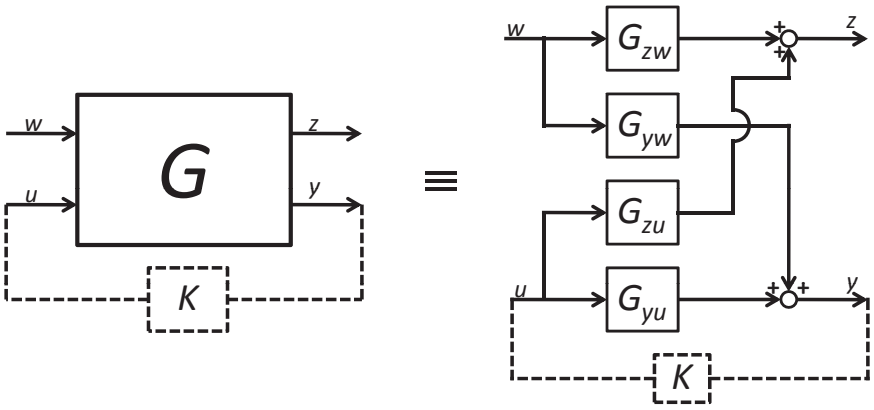

Figure 6.1: General control configuration

of the visibility of a particular oscillation mode on a given output. To select the best input-output pair, both properties are important since the control is assumed based on output feedback. The residues or the geometric joint controllabilty/observability analyses are the commonly used methods in an input-output selection procedure. Both analyses are close connected and basically state that for good controllability/observability characteristics, the matrices B_u and C_y should not be orthogonal to the eigenvectors corresponding to the oscillation mode [181].

In particular, the geometric approach allows evaluating the controllability/observability of each eigenvalue of the system. In addition, the measures are normalized which is an important factor to compare transfer functions with different units. The geometric joint controllability/observability measure is given by

$$\mathrm{m}_{\mathrm{co},k} = \mathrm{m}_{\mathrm{c},k}\mathrm{m}_{\mathrm{o},k} \tag{6.4}$$

where

$$\mathrm{m}_{\mathrm{c},k} = \frac{|B_u^T f_k|}{\|f_k\|\|B_u\|},$$
$$\mathrm{m}_{\mathrm{o},k} = \frac{|C_y e_k|}{\|e_k\|\|C_y\|},$$

are the controllability and observability measures, respectively, and e_k and f_k are the right and left eigenvectors, respectively, associated to the eigenvalue

λ_k. A value near zero indicates that the eigenvalue is poorly controllable or observable. On the other hand, a value close to one corresponds to good controllability and observability features [182].

The input-output pair more controllable and observable will be the pair that allows to damp the oscillation mode with lower control effort. Controllability and observability are common criterion in the selection of the most adequate input-output pair. However, in the general control configuration in Figure 6.1, controllability and observability are not the only limitations on the achievable damping.

6.3.2 Design limitations caused by feedback

The capability of attenuating a signal by feedback is limited by the necessity of ensuring closed loop stability. In the case of the general control configuration, these limitations depend not only on the transfer G_{yu} but also on the transfers G_{yw} and G_{zu}. The last transfer functions are not in the loop but they may affect the control effectiveness to attenuate the disturbance w effects on the output of interest z. The term fundamental design limitations refers to the fact that the value of T_{zw} at certain frequencies is fixed independently of the stabilizing controller. These limitations arise when G_{yu}, G_{zu} and G_{yw} have non-minimum phase (NMP) zeros (*i.e.*, in the closed right hand plane (CRHP)) or G has poles in CRHP. These limitations have been extensively studied, the case of standard feedback problem ($z = y$) can be found in [183]. The general control configuration case is analyzed in [172]. Next, a brief summary is presented to ease the understanding of the proposed selection criterion.

To solve the ideal disturbance attenuation problem means to make arbitrarily small the magnitude of the frequency response of T_{zw}. If $G_{zu} \not\equiv 0$, $G_{yw} \not\equiv 0$ and the determinant $\det G = G_{zw}G_{yu} - G_{zu}G_{yw} \not\equiv 0$, then the controller

$$K^C(s) = \frac{G_{zw}(s)}{\det G(s)} \tag{6.5}$$

leads to a T_{zw} equal to zero for all s, where the symbol $f \not\equiv 0$ means that f is not identical to zero (it can be zero for a set of s but not for all s). The controller K^C is not useful in practice because of its strong dependence on the plant model can yield a closed loop system sensitive to modeling errors. The importance of K^C is that shows the existence or not of theoretical limitations to achieve ideal disturbance attenuation. In case of G_{yu}, G_{zu} and G_{yw} with zeros in CRHP or unstable poles in G, the controller K^C is not always able to ensure stability and thus ideal disturbance attenuation.

In these cases, independently of controller choice, the magnitude of T_{zw} will not be arbitrary small.

Systems reducible to a feedback loop

In case of $\det G \equiv 0$, the system is said to be reducible to a feedback loop and

$$T_{zw} = G_{zw}S,$$

where $S = (1 - G_{yu}K)^{-1}$ is the sensitivity function. It is well known that if ξ in CRHP is a zero of G_{yu} then $S(\xi) = 1$ [183]. Therefore, $T_{zw}(\xi) = G_{zw}(\xi)$ and

$$\|T_{zw}\|_\infty = \max_\omega |T_{zw}(j\omega)| \geq |G_{zw}(\xi)|.$$

This is a fundamental limitation and does not depend on a particular controller.

Case $\det G \not\equiv 0$

If the system is not reducible to a feedback loop, the fundamental limitations are caused by the presence of zeros of G_{zu} or G_{yw} in CRHP or by unstable poles of G.

CRHP zeros of G_{zu} and G_{yw} If $\det G \not\equiv 0$ and ξ in CRHP is a zero of G_{zu} or G_{yw} but it is not a pole of G and the following condition

$$m_{zw}(\xi) < m_{zu}(\xi) + m_{yw}(\xi) \tag{6.6}$$

is satisfied, where m_{zw}, m_{zu} and m_{yw} are the multiplicities of ξ as a zero of G_{zw}, G_{zu} and G_{yw}, respectively, then

$$||T_{zw}||_\infty \geq |G^0_{zw}(\xi)| > 0, \tag{6.7}$$

where G^0_{zw} is a transfer function such that $G_{zw} = G^0_{zw}\mathcal{B}_\xi$ where $\mathcal{B}_\xi$ is a Blaschke product with $m_{zw}(\xi)$ zeros at ξ and, if ξ is complex, at its complex conjugate, *i.e.*

$$\mathcal{B}_\xi = \prod_{l=1}^{m_{zw}} \frac{(\xi - s)}{(\xi + s)}.$$

The lower bound (6.7) implies that no matter the controller, the disturbance attenuation cannot be lower than $|G^0_{zw}(\xi)|$. Moreover, independently of the controller the closed loop transfer T_{zw} will pass through the point $G^0_{zw}(\xi)$. This can be a serious limitation if the oscillation mode is close to the zero ξ and $|G^0_{zw}(\xi)|$ is not small.

Unstable poles of G Assuming that T_{zw} is stable and that $\det G \not\equiv 0$ and let p be an open RHP pole of G with multiplicity $\gamma_G(p) \geq 1$, if $\gamma_G(p) > \gamma_{zw}(p)$ and p is a transmission zero of G with multiplicity $m_G(p) > 0$ and either $G_{zw} \equiv 0$ or

$$m_G(p) < m_{zw}(p) + \gamma_G(p) - \gamma_{zw}(p), \tag{6.8}$$

then

$$||T_{zw}||_\infty \geq \lim_{s \to p} \left| \frac{\det G(s) \mathcal{B}_p^{-1}(s)}{G_{yu}(s)} \right| > 0, \tag{6.9}$$

where $\mathcal{B}_p$ is a Blaschke product with $m_G(p)$ zeros at p. As in the previous case, the lower bound (6.9) imposes a lower bound on the achievable attenuation at frequencies close to the unstable pole p.

Ideal disturbance attenuation

Previous results allow stating the necessary and sufficient conditions for solving the ideal disturbance attenuation problem. Removing any CRHP pole-zero cancelation, the controller (6.5) results in

$$K^C = \frac{G_{zw}}{\det G}. \tag{6.10}$$

Then, assuming that $\det G \not\equiv 0$, that each zero ξ of G_{zw} and G_{yw} is not a pole of G and does not satisfy the condition (6.6), and that each unstable pole of G does not satisfy the condition (6.8), then the controller (6.10) stabilizes the closed loop system. Otherwise, a stabilizing controller that achieves a perfect disturbance attenuation does not exist, and the closed loop system cannot be arbitrary small.

6.4 Input-Output Selection Criterion

In the light of the concepts summarized in the previous section, a criterion for the selection of the most adequate input-output pair is proposed. The idea is to find the local output y in which the oscillation to be damped is more visible and the local input u more effective to cancel the oscillations. The proposed criterion is based on small signal analysis therefore the first step consists in linearizing the model of the power system. With the linear model (6.1), the criterion consists in evaluating the controllability/observability of G_{yu} and the fundamental limitations imposed by G. The first test permits to determine the input-output pair that would demand less control effort to

damp the oscillations. In general, if the oscillation mode is clearly visible from y and the input u has a strong effect on the controlled variable, less correction terms would be necessary to damp the oscillation.

The fundamental limitations provide a criterion to determine the lower limits in the achievable attenuation. As mentioned in the previous section, the presence of zeros of G_{zu} and G_{yw} in the CRHP or unstable poles impose a lower limit on the magnitude of the frequency response of the closed loop system. If the zeros or poles are close to an oscillation mode, such analysis reveals that no matter the controller the mode cannot be arbitrarily damped.

The proposed input-output selection criterion can be summarized as follows.

1. Obtain the linear description of the power systems (6.1). This can be done by an analytic procedure if the mathematical expressions are available or by numerical linearization if the nonlinear model is provided by an electrical simulation software (*e.g.* SimPowerSystem Toolbox or DigSilent, etc.). Besides the disturbance w and the signal z located where the oscillation must be damped, the model must include all the signals that can be used as control action u and local measure y.

2. Check the controllability and observability for the mode λ_k to be damped in order to determine the input-output pair in which the control is more effective to increase the damping. The best pair will be the one with the higher geometric measure $\mathrm{m_{co}}$.

3. Determine if the system is reducible to a feedback loop and find the zeros of G_{yu}, G_{yw} and G_{zu} and poles of G. If there exist zeros or poles in the CRHP, use the formulae in Section 6.3.2 to compute the lower limits in the attenuation. The best input-output pair will be the one with a lower limit in $||T_{zw}||_\infty$.

4. The most adequate pair will be the one with better controllability / observability characteristic and the lower limit in the attenuation.

The criterion is applicable to power systems of considerable complexity. It must be reminded that the analysis should be limited to those oscillation modes considered critical. Moreover, the remote signals considered will depend on the synchronous generator with larger participation factor on such oscillations.

It is interesting to mention that the criterion can be extended to consider $\mathcal{D}$-stability regions. These regions are subsets of the left half plane with

additional stability conditions, such as a cone in which all poles present a damping coefficient greater than a given value. In case of including $\mathcal{D}$-stability regions, in the previous analysis, the CRHP should be replaced by the complement of the $\mathcal{D}$-stability region.

6.5 Case of study 1: Single machine infinite bus system with wind power plant generation

In order to illustrate the application of the proposed input-output selection criterion, the power system shown in Figure 6.2, and already used in Chapter 5, is analyzed. The system in Figure 6.2 is a generic network used to show the interaction between conventional generation and wind power plants. The electrical network is assumed to be lossless (only inductances). The nonlinear expression for this system can be found by means of synchronous generator and standard power flow equations. The synchronous generator is described with a standard one-axis model without controllers. It is assumed that the WPP with converter-based wind turbines behaves as a negative load, since the converter dynamics is much faster than the electromechanical dynamics [49]. The power delivery by the WPP is assumed saturated in $\pm 15\%$ of its nominal power. The equations and parameters used in the power system modeling can be found in [71].

The nonlinear power system is governed by the synchronous generator equations [36].

$$\begin{aligned} \dot{\delta} &= \omega - \omega_s, \\ \dot{\omega} &= \frac{\omega_s}{2H}\left(P_m - \frac{E'V_1}{X'}\sin(\delta - \theta_1) - D\omega\right), \\ \dot{E}' &= \frac{1}{T_0}\left(E_f - \frac{X}{X'}E' + \frac{X - X'}{X'}V_1\cos(\delta - \theta_1)\right), \end{aligned} \tag{6.11}$$

where δ, ω and E' are the rotor angle, the rotor frequency and the internal electromagnetic field (EMF) of the synchronous generator, respectively. The transient reactance and the rotor reactance of the synchronous generator are given by X' and X,respectively, T_0 is the open-circuit time constant, P_m is the mechanical input power, ω_s denotes the synchronous reference, D is the mechanical damping, H refers to the inertia constant and E_f excitation voltage. The parameters values related to the synchronous generator are introduced in Table 6.1 [133].

The power flow equations of the power system under analysis are given

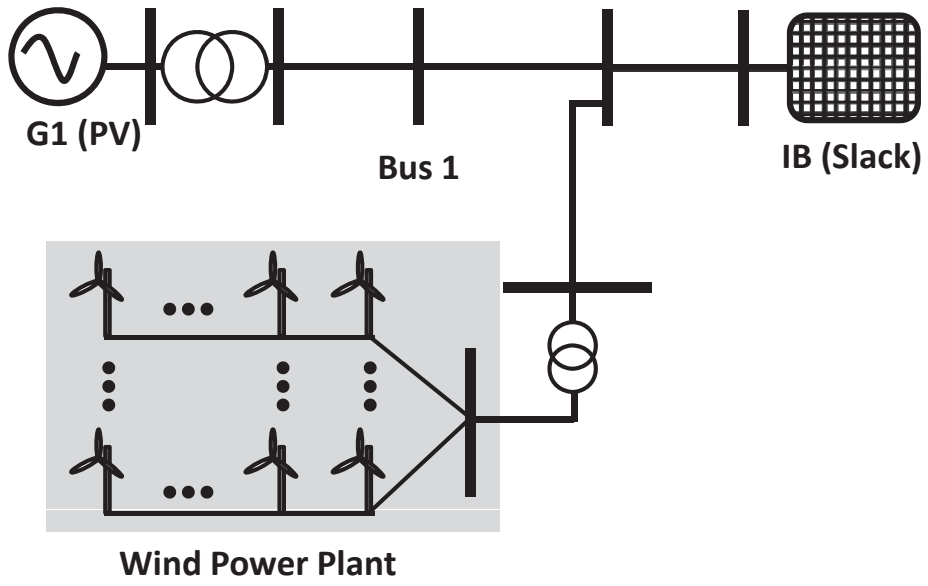

Figure 6.2: Synchronous Machine Infinite Bus System with a Wind Power Plant connected

T_0	H (s)	X_{ta}	X'
6	4	1.1	$0.15 + X_{ta}$

Table 6.1: Synchronous machine parameters (in p.u. except indicated)

by

$$
\begin{aligned}
P_g &= \frac{E'V_1}{X'}\sin(\delta-\theta_1),\\
Q_g &= \frac{E'^2}{X'}-\frac{E'V_1}{X'}\cos(\delta-\theta_1),\\
P_{12} &= \frac{V_1V_2}{X_{12}}\sin(\theta_1-\theta_2),\\
Q_{12} &= \frac{V_1^2}{X_{12}}-\frac{V_1V_2}{X_{12}}\cos(\theta_1-\theta_2),\\
P_{wt2} &= \frac{V_{wt}V_2}{X_{wt2}}\sin(\theta_{wt}-\theta_2),\\
Q_{wt2} &= \frac{V_{wt}^2}{X_{wt2}}-\frac{V_{wt}V_2}{Xwt2}\cos(\theta_{wt}-\theta_2),\\
P_{2\infty} &= \frac{V_2V_\infty}{X_{2\infty}}\sin(\theta_2-\theta_\infty),\\
Q_{2\infty} &= \frac{V_2^2}{X_{2\infty}}-\frac{V_2V_\infty}{X_{2\infty}}\cos(\theta_2-\theta_\infty),
\end{aligned}
\tag{6.12}
$$

where P_i and Q_i ($i \in \{g, 12, wt2, 2\infty\}$) are the active and reactive power transferred through the electrical lines, [V_i and θ_i ($i \in \{g, 12, wt2, 2\infty\}$) represent the voltage magnitude and phase angle of the power system busses, and X_i ($i \in \{g, 12, wt2, 2\infty\}$) are the reactances of the lines. The parameters values related to the power system are presented in Table 6.2 [71].

P_g	P_{wt}	Q_{wt}	E'	ω_s (rad/s)	X_{12}	X_{wt2}	$X_{2\infty}$
0.8	0.4	0	1	100π	0.1	0.1	0.2

Table 6.2: Power system parameters (in p.u. except indicated)

As disturbance w causing the oscillations is considered the mechanical power reference of the synchronous generator T_m. The signal to be controlled, that is the signals on which the oscillation must be damped, is the angle of the synchronous machine $z = \delta$. As possible control signals u are considered the active power P_{wt} and the reactive power Q_{wt} and as local measure y the voltage magnitude measured at the WPP connection point V_{wt} and the phase angle of the voltage WPP bus θ_{wt}.

6.5.1 Selection of the most adequate input-output pair

Linearization

After linearizing the nonlinear model compound by (B.1) and (B.2), the following state equations are obtained

$$\begin{aligned} \dot{x} &= Ax + B_w w + B_u u, \\ z &= C_z x, \\ y &= C_y x + D_{yu} u, \end{aligned} \tag{6.13}$$

where $x = [\Delta\delta \ \Delta\omega \ \Delta E']^T$, with Δ denoting the incremental values,

$$\begin{aligned} A &= A_1 + M_1 A_2, \\ B_u &= M_1 N_1 M_5 N_2, \\ B_w &= \begin{bmatrix} 0 & 0 \\ \\ \dfrac{1}{M} & 0 \end{bmatrix}, \\ C_z &= \begin{bmatrix} 1 & 0 & 0 \end{bmatrix}, \\ C_y &= -M_6^{-1} M_7 N_2 (M_2 - M_3 N_1 M_2), \\ D_{yu} &= M_6^{-1} - M_6^{-1} M_7 N_2, \end{aligned} \tag{6.14}$$

The rest of the matrix parameters are defined in the Appendix B.

The eigenvalues of A are listed in Table 6.3. It can be observed a lightly-damped local oscillation mode at $\lambda_{1,2} = -0.012 \pm j8.3038$, hereafter this is the oscillation mode to be damped.

Eigenvalue	Value	Freq. (Hz)	Damping (%)
$\lambda_{1,2}$	$\mathbf{-0.012 \pm j8.3038}$	**1.3216**	**0.1445**
λ_3	-0.3985	0	1

Table 6.3: Eigenvalues of the matrix A

Controllability and observability test

There are four input-output pairs to be analyzed according to the possible configurations mentioned before. Since the mode to be damped is λ_1, the controllability and observability test is applying only to this case. The geometric measures of controllability and observability are listed in Table 6.4. It can be seen that the four pairs exhibit good controllability characteristics. The main differences are in the observability. The measures in Table 6.4 suggest that the best measured signal y is the angle of the voltage at the connection point θ_{wt}. Therefore, the pairs (P_{wt}, θ_{wt}) and (Q_{wt}, θ_{wt}) are the best options from the controllability and observability view. The slightly difference in the value of $\mathrm{m_{co}}$ indicates that when the pair (P_{wt}, θ_{wt}) is chosen, it is expected that the oscillation will be more visible and the controller will need less control effort to increase the damping. Then, from the controllability/observability point of view, the input-output pairs can be ordered as follows

1. (P_{wt}, θ_{wt}),
2. (Q_{wt}, θ_{wt}),
3. (P_{wt}, V_{wt}),
4. (Q_{wt}, V_{wt}).

Fundamental limitations

In the four cases analyzed, $\det G \not\equiv 0$ therefore the system is not reducible to a feedback loop. The transfer function G has not unstable poles but

I/O pairs	m_c	m_o	m_{co}
(P_{wt}, V_{wt})	0.99282	0.38425	0.38149
(Q_{wt}, V_{wt})	0.99276	0.38425	0.38147
(P_{wt}, θ_{wt})	0.99282	0.95051	0.94369
(Q_{wt}, θ_{wt})	0.99276	0.95051	0.94363

Table 6.4: Geometric measures of the controllability and observability for the four I/O pairs

there exist NMP zeros. The zeros of G_{yw} and G_{zu} are listed in Table 6.5 for each case. The multiplicity of the CRHP zeros in the four cases satisfy condition (6.6) and they are not zeros of G_{zw}. Therefore, independently on the controller, the close loop transfer T_{zw} will not be arbitrary zero at the frequencies of the zeros. These lower limits can be seen in the last column in Table 6.5. From these values, it can be concluded that the best pair from the limitation point of view are the pairs (P_{wt}, θ_{wt}) and (Q_{wt}, θ_{wt}). Hence, under the analysis of fundamental limitations, the the order of input-output pairs results the order of

1. (P_{wt}, θ_{wt}) and (Q_{wt}, θ_{wt}),
2. (P_{wt}, V_{wt}) and (Q_{wt}, V_{wt}).

I/O Pairs	Zeros of G_{zu}	Zeros of G_{yw}	$\lvert G^0_{zw}(\xi)\rvert$
(P_{wt}, V_{wt})	-0.4271	$\pm j8.4081$	0.3751
(Q_{wt}, V_{wt})	-0.7659	$\pm j8.4081$	0.3751
(P_{wt}, θ_{wt})	-0.4271	± 12.1903	0.002
(Q_{wt}, θ_{wt})	-0.7659	± 12.1903	0.002

Table 6.5: Zeros of G_{yw} and G_{zu} and lower limits of $\|T_{zw}\|_\infty$

Input/output signal selection

The intersection of both criterion suggests the final order for the input-output pairs

1. (P_{wt}, θ_{wt}),
2. (Q_{wt}, θ_{wt}),
3. (P_{wt}, V_{wt}),
4. (Q_{wt}, V_{wt}).

According to the previous analysis, the pair (P_{wt}, θ_{wt}) presents the best controllability and observability characteristics, which indicates that the damping can be achieved with less control effort. This pair presents also the lower limit on the $\|T_{zw}\|_\infty$ pointing out the existence of a controller capable of achieve the best damping response of the oscillation mode λ_1. Moreover, since the zero ξ in the CRHP is not near the oscillation mode, the attenuation is not so affected by the presence of a NMP zero.

6.5.2 Frequency and transient responses

In order to illustrate the meaning of the previous results, the PSS controllers for WPPs have been designed by means of the H_∞ approach to minimize $||T_{zw}||_\infty$. By using this method, it is ensured that the controller obtained is stabilizing. The controller transfer function for each case studied are as follows:

$$K_{01\infty} = \frac{243.7s^4+1.1e4s^3+2.8e4s^2+7.1e5s+3e5}{s^5+470.5s^4+822.9s^3+6.68e4s^2+5.2e4s+2.3e6},$$

$$K_{02\infty} = \frac{-465.8s^4-1.51e004s^3-4.45e4s^2-1e6s-4.1e5}{s^5+369.9s^4-2740s^3+5.6e4s^2-1.9e5s+2.2e6},$$

$$K_{03\infty} = \frac{-1010s^4-2902s^3-7.4e4s^2-1.4e5s-5.5e4}{s^5-139.3s^4+1642s^3+604.2s^2+1.3e5s+7.6e5},$$

$$K_{04\infty} = \frac{658.4s^4-693.8s^3+4.5e4s^2-6.7e4s-3.2e4}{s^5+14.51s^4+518.2s^3+2455s^2+3.16e4s+1e5},$$

where $K_{01\infty}$, $K_{03\infty}$, $K_{03\infty}$ and $K_{04\infty}$ are the control designed for the $P_{wt} - V_{wt}$, $Q_{wt} - V_{wt}$, $P_{wt} - \theta_{wt}$ and $Q_{wt} - \theta_{wt}$ signal pairings, respectively.

The output z was weighted with

$$W_z = \frac{1}{s^2 + 0.02391s + 68.95},$$

to enforce the damping of the mode λ_1, and the control signal u was also weighted with $W_u = 1$ to avoid numerical issues.

It is worth to remark that the proposed criterion does not require the computation of the controller, in this chapter they are computed only to

illustrate that the prediction provided by the proposed criteria corresponds with frequency and transient responses. Notice that the cancelation controller K^C (6.10) in this case does not guarantee closed loop stability due to the presence of NMP zeros.

The magnitude of the frequency responses of the open loop system G_{zw} and the closed loop system with the four controllers corresponding to each input-output pair can be seen in Figure 6.3. At $\omega = j8.4081$ the magnitude of T_{zw} is 0.3794 in the case of pairs (P_{wt}, V_{wt}) and (Q_{wt}, V_{wt}) and 0.002 at $s = 12.1903$ in the case of pairs (P_{wt}, θ_{wt}) and (Q_{wt}, θ_{wt}), as predicted by the fundamental limitation analysis. It can be observed that the attenuation achieved in the case of the pairs (P_{wt}, V_{wt}) and (Q_{wt}, V_{wt}) is rather poor as a consequence of the proximity of the NMP zeros to the oscillation mode λ_1. With these two input-output pairs, the ∞-norm result 0.3794. On the other hand, with the pairs (P_{wt}, θ_{wt}) and (Q_{wt}, θ_{wt}), with NMP zeros more distant from λ_1, the limitation is not a serious constraint to achieve the attenuation of the oscillation mode. Figure 6.3 clearly shows that from the fundamental limitations view, the best measured signal y is θ_{wt}.

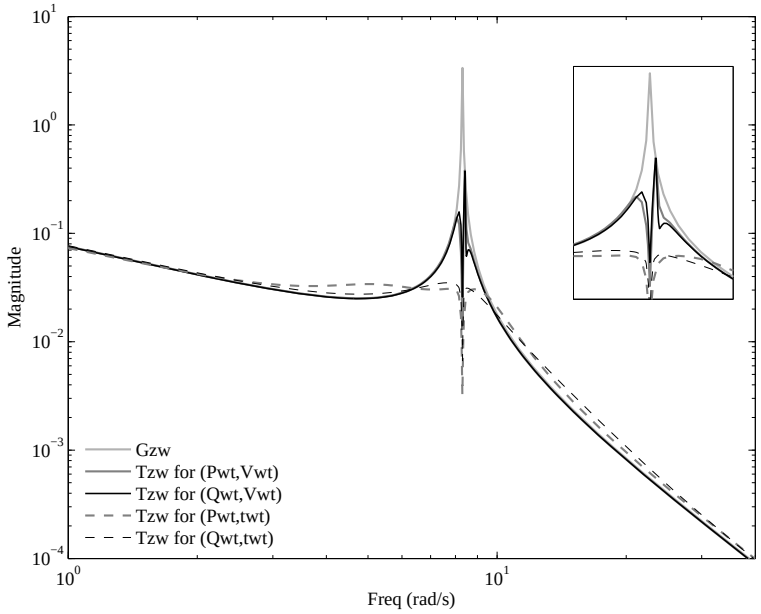

Figure 6.3: Magnitude of the open loop transfer G_{zw} and the closed loop transfer T_{zw} for the four possible input-output pairs with H_∞ controllers

Figure 6.4 shows the transient responses of the open loop and the closed loop for the pairs (P_{wt}, θ_{wt}) and (P_{wt}, V_{wt}). The simulations were performed using the nonlinear expressions of the power system and the corresponding H_∞ controllers. The responses correspond to an impulse on the mechanical power reference of the synchronous generator T_m. As predicted by the selection criterion, the choice of the angle θ_{wt} as measured signal y is a better choice than the voltage V_{wt}. The control using the pair (P_{wt}, θ_{wt}) is clearly more effective in damping the oscillations. In Figure 6.4, it is also clear that with the pair (P_{wt}, θ_{wt}) less control effort $(u = P_{wt})$ is necessary as established by the controllability/observability analysis. It is interesting to remark that the upper and lower saturation limits imposed on the active power delivered by the WPP are not achieved.

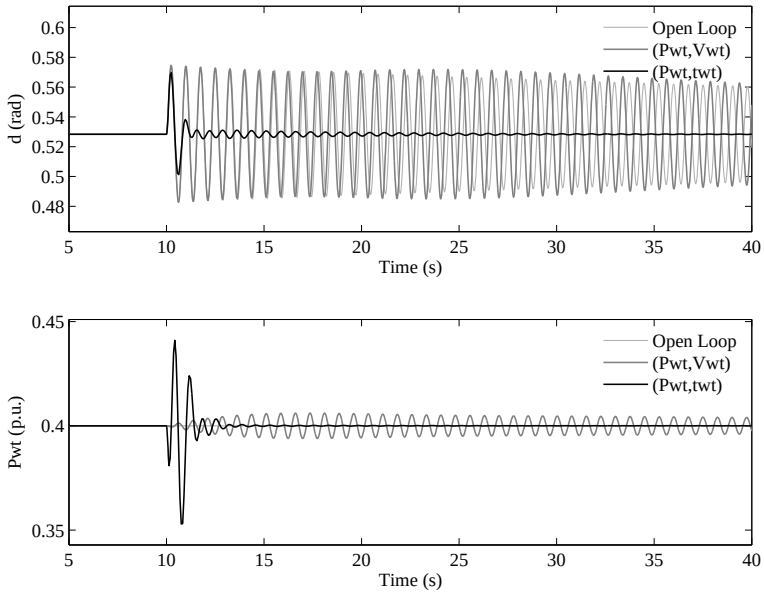

Figure 6.4: Transient responses of the open loop and closed loop for the pairs (P_{wt}, V_{wt}) and (P_{wt}, θ_{wt})

In Figure 6.5, it can be observed the transient responses of the open loop system and the closed loop system for the pairs (Q_{wt}, θ_{wt}) and (Q_{wt}, V_{wt}). Again, the control configuration using the angle of the voltage at the connection point θ_{wt} as measured signal y is the best choice. Clearly, the damping achieved with the pair (Q_{wt}, θ_{wt}) is better than the one obtained with the pair (Q_{wt}, V_{wt}). Again it can be seen that the upper and lower saturation

limits imposed on the reactive power delivered by the WPP are not reached. Comparing Figs. 6.4 and 6.5, it can be observed a slightly less control effort and slightly faster damping of the oscillation in the case of the pair (P_{wt}, θ_{wt}) with respect to (Q_{wt}, θ_{wt}). This also fit with the proposed selection criterion.

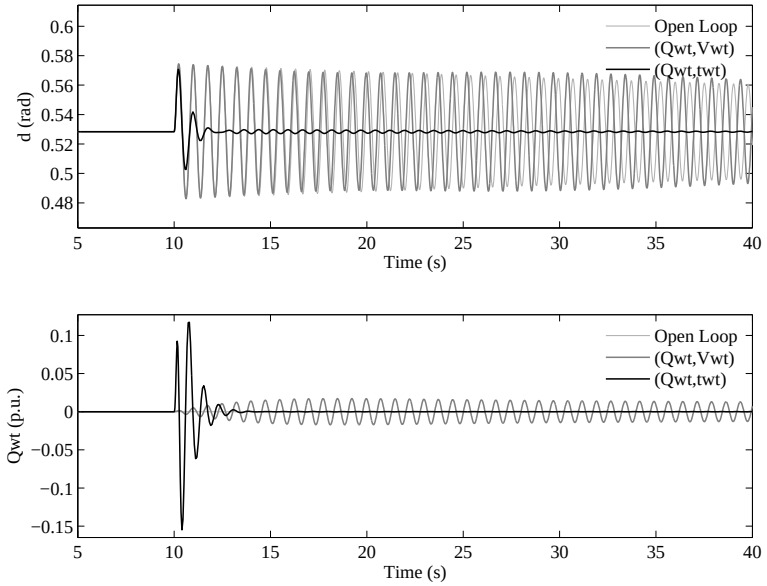

Figure 6.5: Transient responses of the open loop and closed loop for the pairs (Q_{wt}, V_{wt}) and (Q_{wt}, θ_{wt})

6.6 Case of study 2: Three machines system with wind power plant generation

In this section, to demonstrate the applicability of the proposed criteria to a large power system, it has been applied to the power system shown in Figure 6.6. As occurs in the previous case, the electrical network is considering the lines as only inductances. The synchronous generator is modelled as a standard one-axis model without controllers, and the converter-based WPP is represented as a controlled negative load. This is acceptable since electromechanical dynamics of the WPP are hidden due to power converter, and converter frequency range is much faster than the power system dynamics [49]. The power delivery by the WPP is assumed saturated in $\pm 25\%$ of its nominal power. The equations and parameters used in the power system

modeling can be found in [133].

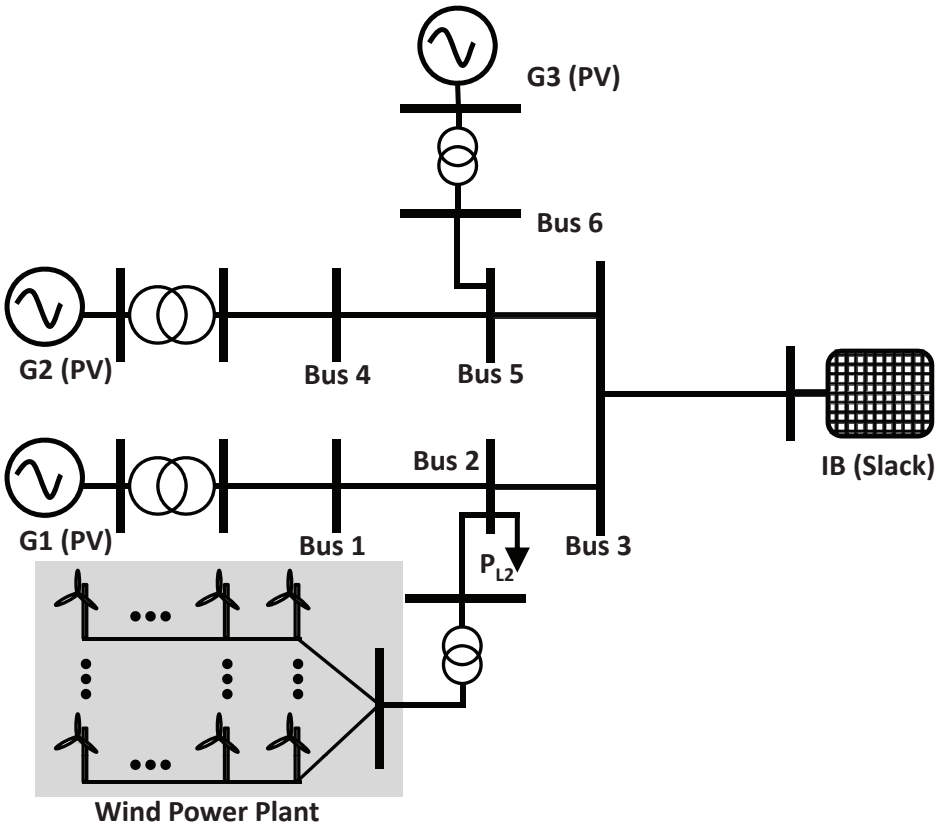

Figure 6.6: Three machines system with a wind power plant connected

The nonlinear power system is governed by the equations of the synchronous generators connected into the power system [36]

$$\begin{aligned}
\dot{\delta}_i &= \omega_i - \omega_s, \\
\dot{\omega}_i &= \frac{\omega_s}{2H_i}\left(P_{mi} - \frac{E_i' V_k}{X_i'}\sin(\delta_i - \theta_k) - D_i\omega_i\right), \\
\dot{E}_i' &= \frac{1}{T_{0i}}\left(E_{fi} - \frac{X_i}{X_i'}E_i' + \frac{X_i - X_i'}{X_i'}V_k\cos(\delta - \theta_k)\right),
\end{aligned} \tag{6.15}$$

where $i = 1, 2, 3$ refer to the synchronous generators, and δ_i, ω_i and E_i' are the rotor angle, the rotor frequency and the internal electromagnetic field (EMF) of all the synchronous generators, respectively. The transient

reactance and the rotor reactance of the synchronous generators are given by X_i' and X_i, respectively, T_{0i} is the open-circuit time constant, P_{mi} is the mechanical input power, ω_s denotes the synchronous reference, D_i is the mechanical damping, H_i refers to the inertia constant and E_{fi} excitation voltage, for each generator implemented in the system. The parameters values used in the power system modeling including synchronous generator, lines and reference values of power and voltage, are given in Tables 6.6 and 6.7.

T_{01}	T_{02}	T_{03}	H_1 [s]	H_2 [s]	H_3 [s]	
6	3	3	4	2	4.6	
D_1	D_2	D_3	X_{ta}	X_1'	X_2'	X_3'
0.01	0.0125	0.005125	0.1	$1.15 + X_{ta}$	$1.15 + X_{ta}$	$1.15 + X_{ta}$

Table 6.6: Synchronous machines parameters (in p.u. except indicated)

The power flow equations for this power system can be written as

$$\begin{aligned} P_{gi} &= \frac{E_i' V_j}{X_i'} \sin(\delta_i - \theta_j), \\ Q_{gi} &= \frac{E_i'^2}{X_i'} - \frac{E_i' V_j}{X_i'} \cos(\delta_i - \theta_j), \\ P_{kl} &= \frac{V_k V_l}{X_{kl}} \sin(\theta_k - \theta_l), \\ Q_{kl} &= \frac{V_k^2}{X_{kl}} - \frac{V_k V_l}{X_{kl}} \cos(\theta_k - \theta_l), \end{aligned} \tag{6.16}$$

where P_{gi} and Q_{gi} ($i \in \{1, 2, 3\}$) are the active and reactive power transferred from the synchronous generators through the power transformer, P_{kl} and Q_{kl} ($k \in \{1, 2, 3, 4, 5, 6, wt\}$ and $l \in \{2, 3, 5, \infty\}$) are the active and reactive power transferred through the power lines, V_j and θ_j ($j \in \{1, 4, 6\}$) represent the voltage magnitude and phase angle of the busses after the power transformers, V_k, V_l, θ_k and θ_l ($k \in \{1, 2, 3, 4, 5, 6, wt\}$ and $l \in \{2, 3, 5, \infty\}$) represent the voltage magnitude and phase angle of the power system busses, X_i' ($i \in \{1, 2, 3\}$) are the reactances of the power transformers, and X_{kl} ($k \in \{1, 2, 3, 4, 5, 6, wt\}$ and $l \in \{2, 3, 5, \infty\}$) are the reactances of the lines. The sum of all the active and reactive power at each bus must be equal to zero.

P_{gs1}	P_{gs2}	P_{gs3}	P_{wt}	P_{L2}	Q_{L2}
0.8	0.8	0.6	0.8	2	0.5

E'_1	E'_2	E'_3	V_{wt}	ω_s [rad/s]	X_{12}
1.03	1.03	1.01	1	100π	0.1

X_{wt2}	X_{23}	X_{53}	X_{65}	X_{45}	$X_{3\infty}$
0.1	0.1	0.1	0.1	0.1	0.2

Table 6.7: Power system parameters (in p.u. except indicated)

In this study case, the mechanical power reference of the synchronous generator T_{m1} is assumed as system disturbance and the signal to be controlled, that is the signals on which the oscillation must be damped, is the angle of the synchronous machine $z = \delta_1$. Finally, the possible control signals u and local measure y are the same as in the previous study case.

6.6.1 Selection of the most adequate input-output pair

Linearization

After linearizing the nonlinear model compound by (6.15) and the power flow equations, the following state equations are obtained

$$\begin{aligned} \dot{x} &= Ax + B_w w + B_u u, \\ z &= C_z x, \\ y &= C_y x + D_{yu} u, \end{aligned} \tag{6.17}$$

where $x = [\Delta\delta_1\ \Delta\omega_1\ \Delta E'_1\ \Delta E'_2\ \Delta\delta_2\ \Delta E'_3\ \Delta\delta_3\ \Delta\omega_2\ \Delta\omega_3]^T$, with Δ denotes the incremental values. The power system has been linearized through numerical computation.

The eigenvalues of A are listed in Table 6.3. It can be observed two lightly-damped local oscillation modes at $\lambda_{2,3} = -0.0776 \pm j4.7011$ and $\lambda_{4,5} = -0.0633 \pm j4.4687$, hereafter these are the oscillation modes to be damped.

Eigenvalue	Value	Freq. (Hz)	Damping (%)
$\lambda_{1,2}$	$-0.3244 \pm j6.5644$	1.0448	4.9358
$\boldsymbol{\lambda_{3,4}}$	$\mathbf{-0.0776 \pm j4.7011}$	**0.7482**	**1.6505**
$\boldsymbol{\lambda_{5,6}}$	$\mathbf{-0.0633 \pm j4.4687}$	**0.7112**	**1.4164**
λ_7	-0.2180	0	1
λ_8	-0.3062	0	1
λ_9	-0.4511	0	1

Table 6.8: Eigenvalues of the matrix A

Controllability and observability test

There are four input-output pairs to be analyzed according to the possible configurations mentioned before. Since the modes to be damped are $\lambda_{3,4}$ and $\lambda_{5,6}$, the controllability and observability test is applying only to these cases. The geometric measures of controllability and observability are listed in Table 6.9. It can be seen that the four pairs exhibit good controllability characteristics for $\lambda_{5,6}$; however, they are slightly lower in the case of $\lambda_{3,4}$. Nevertheless, all the values are similar. The main differences are in the observability. The measures in Table 6.4 suggest that the best measured signal y for $\lambda_{3,4}$ is the voltage magnitude at the connection point V_{wt}. On the other hand, considering the mode $\lambda_{5,6}$, the best measured signal y is the phase angle of the voltage at the connection point θ_{wt}. Therefore, the pair (Q_{wt}, θ_{wt}) is the best option in the $\lambda_{5,6}$ case; and (Q_{wt}, V_{wt}) in the $\lambda_{3,4}$ case. Remember that it is expected that the oscillation will be more visible and the controller will need less control effort to increase the damping when the pair with higher $\mathrm{m_{co}}$ is chosen. Then, from the controllability/observability point of view, the input-output pairs depending on the oscillation mode can be ordered as follows.

- For $\lambda_{3,4}$ case
  1. (Q_{wt}, V_{wt}),
  2. (P_{wt}, V_{wt}),
  3. (Q_{wt}, θ_{wt}),
  4. (P_{wt}, θ_{wt}).
- For $\lambda_{5,6}$ case

1. (Q_{wt}, θ_{wt}),
2. (P_{wt}, θ_{wt}),
3. (Q_{wt}, V_{wt}),
4. (P_{wt}, V_{wt}).

Case	I/O pairs	m_c	m_o	m_{co}
$\lambda_{3,4}$	(P_{wt}, V_{wt})	0.1148	0.0859	0.0099
	(Q_{wt}, V_{wt})	0.1212	0.0859	0.0104
	(P_{wt}, θ_{wt})	0.1148	0.0559	0.0064
	(Q_{wt}, θ_{wt})	0.1212	0.0559	0.0068
$\lambda_{5,6}$	(P_{wt}, V_{wt})	0.3807	0.0942	0.0359
	(Q_{wt}, V_{wt})	0.4483	0.0942	0.0422
	(P_{wt}, θ_{wt})	0.3807	0.1161	0.0442
	(Q_{wt}, θ_{wt})	0.4483	0.1161	0.0521

Table 6.9: Geometric measures of the controllability and observability of $\lambda_{3,4}$ and $\lambda_{5,6}$ modes for the four I/O pairs

Fundamental limitations

In the four cases analyzed, $\det G \not\equiv 0$ therefore the system is not reducible to a feedback loop. The transfer function G has not unstable poles but there exist NMP zeros in all cases except for the pair (P_{wt}, V_{wt}). The zeros of G_{yw} and G_{zu} are listed in Table 6.10 for each case. As all NMP zeros have multiplicity 1, the three cases satisfy condition (6.6) and they are not zeros of G_{zw}. Therefore, except for the pair (P_{wt}, V_{wt}), independently on the controller, the closed loop transfer T_{zw} will not be arbitrary zero at the frequencies of the zeros. These lower limits can be seen in the last column in Table 6.10. From these values, it can be concluded that the best pair from the limitation point of view is (P_{wt}, V_{wt}). Nevertheless, the NMP zero in the pair (Q_{wt}, V_{wt}) does not impose a strong limitation since $|G^0_{zw}(\xi)|$ is small and it is distant from the oscillation modes $\lambda_{3,4}$ and $\lambda_{5,6}$. Hence, under the analysis of fundamental limitations, the input-output pairs result ordered as follows.

1. (P_{wt}, V_{wt})

2. (Q_{wt}, V_{wt}),
3. (P_{wt}, θ_{wt}) and (Q_{wt}, θ_{wt}).

I/O Pairs	Zeros of G_{zu}	Zeros of G_{yw}	$\lvert G^0_{zw}(\xi)\rvert$
(P_{wt}, V_{wt})	$-0.3198 \pm j6.617$	$-0.316 \pm j6.577$	–
	$-0.0067 \pm j4.654$	$-0.0014 \pm j4.561$	–
	-0.2028	-0.2285	–
	-0.3011	-0.2517	–
	-0.4510	-0.4508	–
(Q_{wt}, V_{wt})	$-0.3218 \pm j6.607$	$-0.316 \pm j6.577$	–
	$-0.0076 \pm j4.610$	$-0.0014 \pm j4.561$	–
	0.0262	-0.2285	**0.7868**
	-0.3029	-0.2517	–
	-0.4509	-0.4508	–
(P_{wt}, θ_{wt})	$-0.3198 \pm j6.617$	$-0.31 \pm j6.585$	–
	$-0.0067 \pm j4.654$	$\mathbf{0.008 \pm j4.614}$	**16.074**
	-0.2028	-0.2176	–
	-0.3011	-0.3176	–
	-0.4510	-0.4516	–
(Q_{wt}, θ_{wt})	$-0.3218 \pm j6.607$	$-0.31 \pm j6.585$	–
	$-0.0076 \pm j4.610$	$\mathbf{0.008 \pm j4.614}$	**16.074**
	0.0262	-0.2176	**0.7868**
	-0.3029	-0.3176	–
	-0.4509	-0.4516	–

Table 6.10: Zeros of G_{yw} and G_{zu} and lower limits of $\|T_{zw}\|_\infty$

Input/output signal selection

According to the previous analysis and considering the oscillation modes $\lambda_{3,4}$ and $\lambda_{5,6}$ simultaneously, the pairs (P_{wt}, V_{wt}) and (Q_{wt}, V_{wt}) present similar controllability and observability characteristics (slightly lower than

the other cases). The pair (P_{wt}, V_{wt}) presents no limitations associated to NMP zeros pointing out the existence of a controller capable of achieving the ideal disturbance attenuation of the oscillation modes $\lambda_{3,4}$ and $\lambda_{5,6}$. Since the zero ξ in the CRHP appearing in the (Q_{wt}, V_{wt}) pair is not close to the oscillation modes, the attenuation is not seriously affected by the presence of this NMP zero.

Considering that the NMP zeros in the pairs (P_{wt}, θ_{wt}) and (Q_{wt}, θ_{wt}) impose stronger a limitation to increase the damping due to the proximity to the modes $\lambda_{3,4}$ and $\lambda_{5,6}$, this aspect prevails over the controllability/observability measures. The choice between (P_{wt}, θ_{wt}) and (Q_{wt}, θ_{wt}) is so clear since the NMP zero in (Q_{wt}, θ_{wt}) distant from the oscillations mode. The geometric measures can be used to obtain the final order of the pair. Based on the previous arguments, the following order is suggested.

1. (Q_{wt}, V_{wt}),
2. (P_{wt}, V_{wt}),
3. (Q_{wt}, θ_{wt}),
4. (P_{wt}, θ_{wt}).

6.6.2 Frequency and transient responses

Again, the controllers were design using H_∞ optimal control tools [183]. The objectives were to enforce the damping of both modes $\lambda_{3,4}$ and $\lambda_{5,6}$ therefore the signal z was weighted with

$$W_z = \frac{\kappa \omega_{osc}^2 s}{s^2 + 2\xi_{damp}\omega_{osc} s + \omega_{osc}^2},$$

with $\kappa = 0.125$, $\omega_{osc} = 4.6$ and $\xi_{damp} = 0.3$. The control u was also penalized with

$$W_u = \frac{0.15s^2 + 1.65s + 1.5}{0.1s^2 + 10.01s + 1}$$

to limit the control effort and thus avoiding numerical issues. As previously stated the proposed criterion does not require the computation of the controller; however, they are computed to illustrate the prediction done. For this reason the controller design is not explained in detail, a more extensive description on the application of H_∞ optimal control tools in power systems can be found in [**?**].

The magnitude of the frequency responses of the open loop system G_{zw} and the closed loop system with the four controllers corresponding to each

input-output pair can be seen in Figure 6.7. At $s = 0.008 \pm j4.614$ the magnitude of T_{zw} is 16.074 in the case of pairs (P_{wt}, θ_{wt}) and (Q_{wt}, θ_{wt}) and 0.7868 at $s = 0.0262$ in the case of pairs (Q_{wt}, V_{wt}), as predicted by the fundamental limitation analysis. It can be observed that the attenuation achieved in the case of the pairs (P_{wt}, θ_{wt}) and (Q_{wt}, θ_{wt}) is rather poor as a consequence of the proximity of the NMP zeros to the oscillation modes $\lambda_{3,4}$ and $\lambda_{5,6}$. On the other hand, with the pair (Q_{wt}, V_{wt}), with NMP zeros more distant from oscillation modes, the limitation is not a serious constraint to achieve the attenuation of the oscillation modes. In the case (P_{wt}, V_{wt}) there is no limitations caused by NMP zeros. Figure 6.3 clearly shows that from the fundamental limitations view, the best measured signal y is V_{wt}.

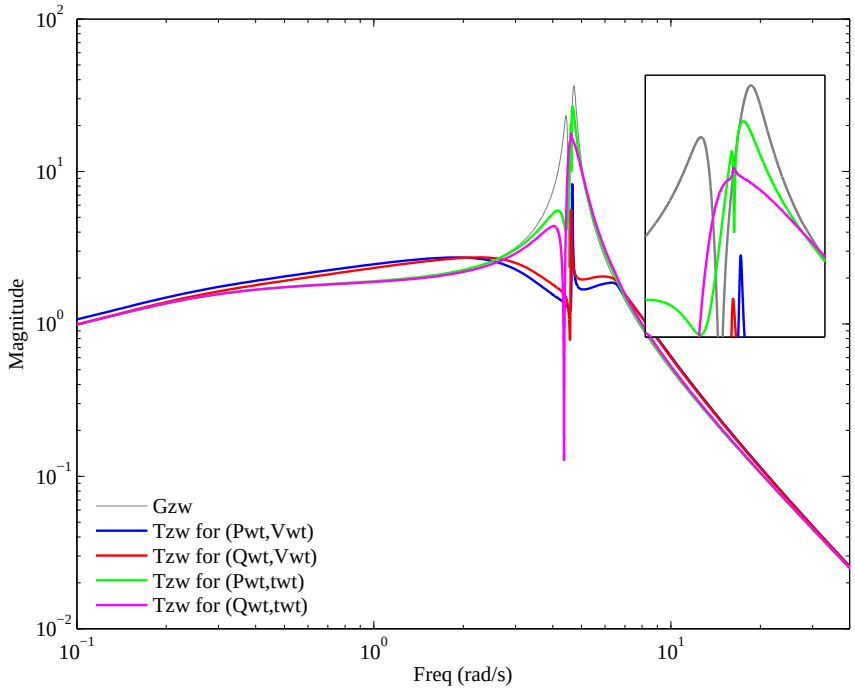

Figure 6.7: Magnitude of the open loop transfer G_{zw} and the closed loop transfer T_{zw} for the four possible input-output pairs with H_∞ controllers

Figure 6.8 shows the transient responses of the open loop and the closed loop for the pairs (P_{wt}, θ_{wt}) and (P_{wt}, V_{wt}). The simulations were performed using the linear expressions of the power system and the corresponding H_∞ controllers. The responses correspond to an impulse on the mechanical power

reference of the synchronous generator T_{m1}. As predicted by the selection criterion, the choice of the voltage V_{wt} as measured signal y is a better choice than the angle θ_{wt}. The control using the pair (P_{wt}, V_{wt}) is clearly more effective in damping the oscillations and the upper and lower saturation limits imposed on the active power delivered by the WPP are not reached during the entire simulation.

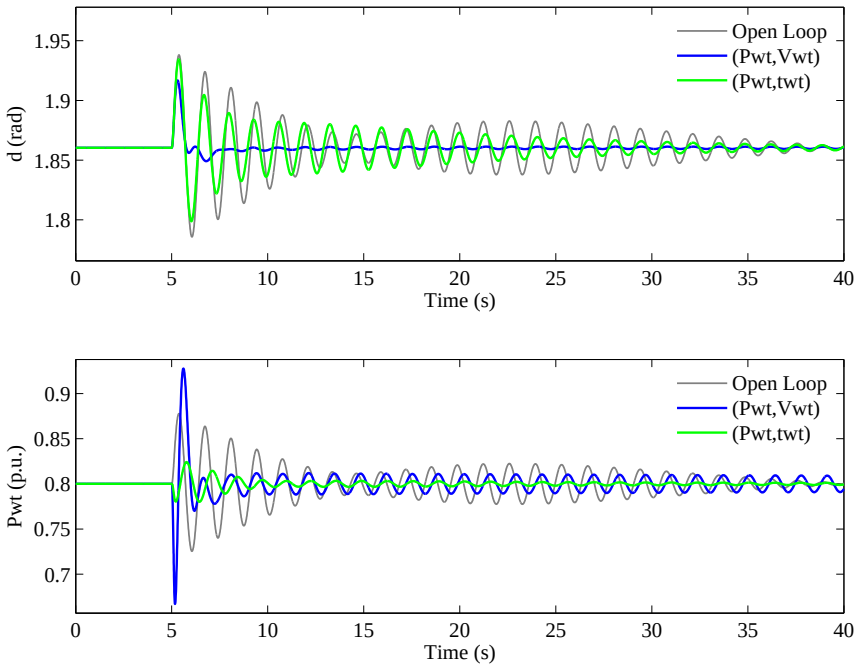

Figure 6.8: Transient responses of the open loop and closed loop for the pairs (P_{wt}, V_{wt}) and (P_{wt}, θ_{wt})

In Figure 6.9, it can be observed the transient responses of the open loop system and the closed loop systems for the pairs (Q_{wt}, θ_{wt}) and (Q_{wt}, V_{wt}). Again, the control configuration using the magnitude of the voltage at the connection point V_{wt} as measured signal y is the best choice. Clearly, the damping achieved with the pair (Q_{wt}, V_{wt}) is better than the one obtained with the pair (Q_{wt}, θ_{wt}). Again it can be seen that the upper and lower saturation limits imposed on the reactive power delivered by the WPP are not reached. Comparing Figs. 6.8 and 6.9, it can be observed a similar response to damp the oscillation modes in the case of the pair (P_{wt}, V_{wt}) with respect to (Q_{wt}, V_{wt}). This also fit with the proposed selection criterion.

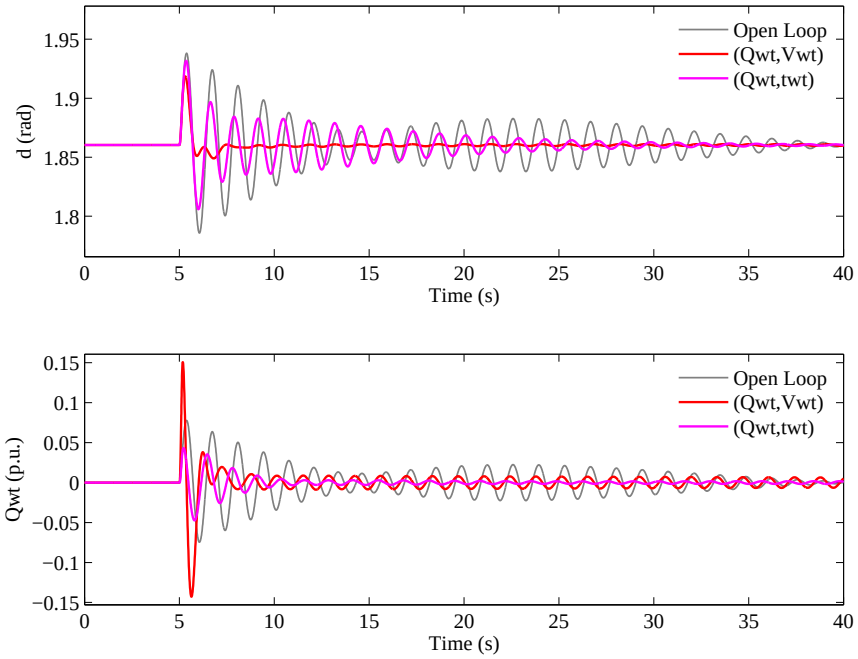

Figure 6.9: Transient responses of the open loop and closed loop for the pairs (Q_{wt}, V_{wt}) and (Q_{wt}, θ_{wt})

6.7 Conclusions of the chapter

A criterion to select the most adequate input-output pair for the design of PSS for WPP has been proposed. The main difference with previous criteria is in considering the use of local signals to damp remote oscillations. When WPP are employed to assist in the enhancement of the power system stability, the PSS might be far away from the location where the rotor oscillations of the synchronous generators arise. The proposed selection criterion analyzes fundamental limitations of the system to predict, without designing the controller, the capability of a particular choice of local signals to damp an oscillation mode. The study of the controllability and observability characteristics allows to determine the input-output pair that will require less control effort to achieve the oscillation damping. The analysis of the fundamental limitations permits to identify frequencies at which is not possible to reduce the magnitude of the frequency response of the closed loop system. If these frequencies are close to the oscillation modes to be damped, it will be difficult, no matter the controller choice, to achieve a noticeable increase

of damping. The application of the selection criterion to a set of candidate input-output pairs produces a ranking of the input-output local signals to achieve the best oscillation damping according to open loop characteristics of the system.

In order to illustrate the use of the selection criterion, a single machine system with a WPP has been analyzed. Frequency responses and simulation results have been presented to connect the fundamental limitation with the more intuitive transient responses of the power system to an impulse disturbance.

7

Effect of non-standard operating frequencies on the economic cost of offshore AC networks

7.1 Introduction

A European SuperGrid [184, 185, 186, 187] will allow the connection of offshore renewable energy sources in remote locations to existing onshore networks. It has been recognized that offshore wind resources will play an important role in determining the design and placement of SuperGrid infrastructure. In order to provide large power transmission capacity over long distances it is proposed that the connection of offshore wind farms to onshore networks is performed by high-voltage direct-current (HVDC) links [188], as it is shown in Figure 7.1.

Multi-terminal HVDC (MT-HVDC) technology [27, 189, 190] is one technical solution that allows the connection of multiple offshore wind farms to one or more onshore connection points. In order to provide adequate system reliability, a MT-HVDC system must be capable of blocking faults that occur in the DC grid [191, 192]. Advances in hybrid DC breaker technology have recently been reported [193], however, the lack of a commercially proven DC circuit breakers may be a major barrier to the implementation of MT-HVDC systems. Some VSC topologies have been proposed that promise inherent

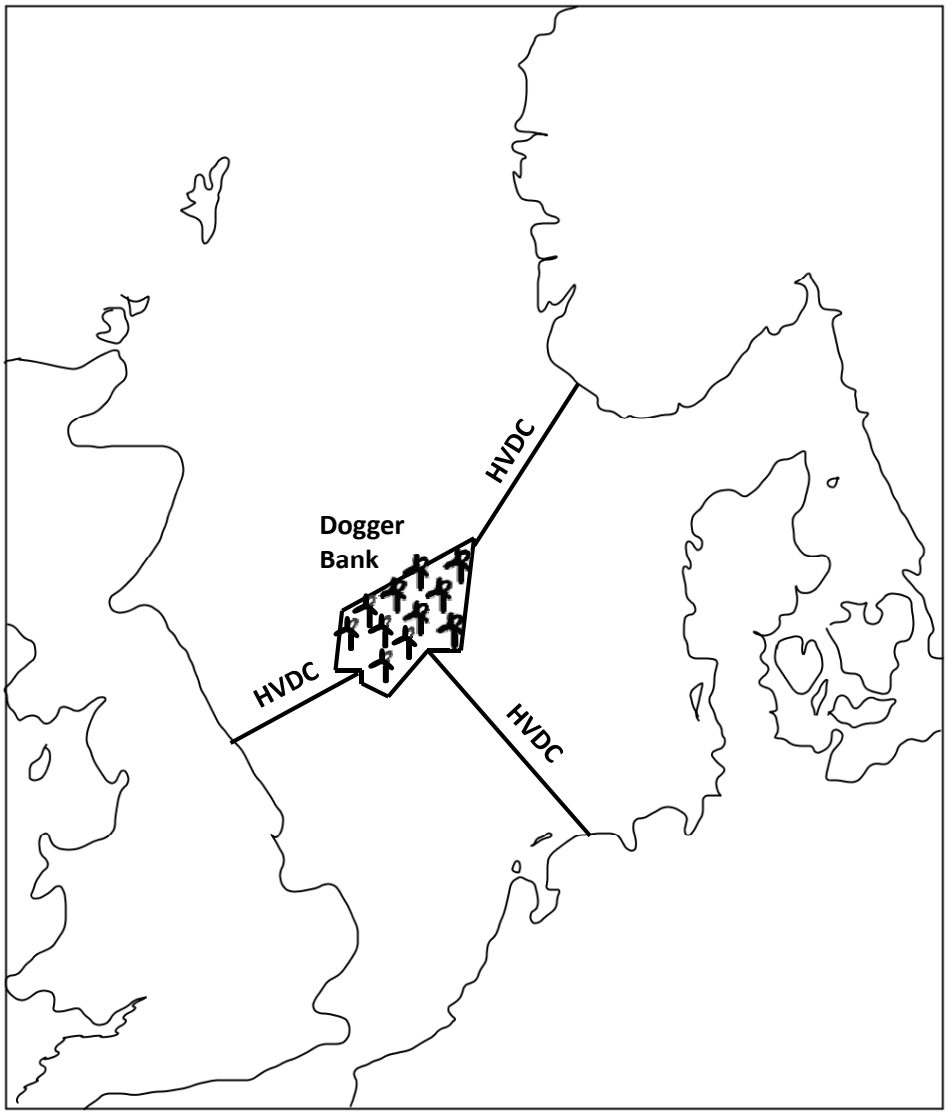

Figure 7.1: Map representation of the location of one of the interconnections proposals: Dogger Bank

fault blocking capability, however these remain to be commercially proven and suffer additional complexity and potentially higher losses [194, 195].

An alternative or complementary option for the European SuperGrid is the "SuperNode concept" and is the focus of this chapter. A SuperNode is

an offshore network which allows the connection of multiple wind arrays and HVDC substations via an AC-hub arrangement and which does not require DC fault blocking capability [196]. Figure 7.2 is a high-level representation of the SuperNode concept. The AC-hub arrangement eliminates the requirement for DC circuit breaking by employing only point-to-point HVDC links [197]; in this case AC circuit breakers located on the AC-hub and in the onshore AC network may be used to isolate faults occurring on any individual HVDC link whilst leaving other links operational. A further potential advantage of the AC-hub arrangement is the opportunity to use current-source converter (CSC) point-to-point technology in place of more costly voltage source converter (VSC) MT-HVDC technology. CSCs generally offer higher power transfer capability and greater efficiencies at a given cost point than VSCs [197] although they require significant reactive compensation and additional harmonic filtering which increases their overall space requirements. It should be noted that in an AC grid composed only of power electronic converters, at least one VSC or STATCOM will be required in order to provide a reference voltage source and enable black-start capability.

As the SuperNode is connected to onshore AC networks only through point-to-point HVDC links, the offshore AC-hub may run unsynchronized with onshore networks, as in the case shown in Figure 7.1. Indeed, in some cases synchronism with one onshore AC network (e.g., mainland Europe) may preclude synchronism with another (e.g. the UK). A further observation is that there is no requirement for the hub to operate at the same nominal frequency as any onshore network and that operation at non-standard frequencies (i.e., not 50 or 60 Hz) may confer technical and economic advantages. For instance, an operational frequency below 50 Hz can offer lower transmission losses and allow the use of longer cables, whilst an operational frequency above 50 Hz can reduce transformer sizes, in turn reducing offshore platform sizes.

This chapter considers operation of a SuperNode at non-standard fixed nominal operating frequencies in the range 20–120 Hz (dynamic variable frequency operation is not considered). An analysis of some of the technical and economic effects of operating at a non-standard frequency are examined. Tranche A of Dogger Bank [198] is used as a case study to highlight the potential economic advantages of operating at non-standard frequencies.

The chapter is organized as follows. Section 2 introduces the "SuperNode concept". Section 3 proposes and develops different economic functions to evaluate the frequency-cost dependence of SuperNode components. Section 4 investigates which is the nominal operating frequency that provides a minimum costs for a Dogger Bank Tranche A SuperNode. Finally, the

conclusions are summarized in Section 5.

7.2 What is the SuperNode?

The SuperNode scheme proposed in this chapter is loosely based on the HVDC2000 scheme appearing in [199]. The HVDC2000 scheme suggests the connection of several wind arrays to one offshore HVDC substation with one HVDC link to deliver the generated power onshore. The SuperNode concept as described here is an extension of the HVDC2000 scheme: It includes additional HVDC point-to-point links and a greater number of wind arrays. At a high level, the SuperNode may be described as a group of wind farms connected radially to their wind array substation, which are in turn connected radially to the main offshore substation containing multiple HVDC converters, as shown in Figure 7.2.

In the analysis presented here, all wind turbine interfaces are assumed to be of the fully rated converter type, allowing the assumption that the offshore AC hub is completely isolated from both the wind turbine instantaneous dynamics and the onshore grid by means of power electronic converters.

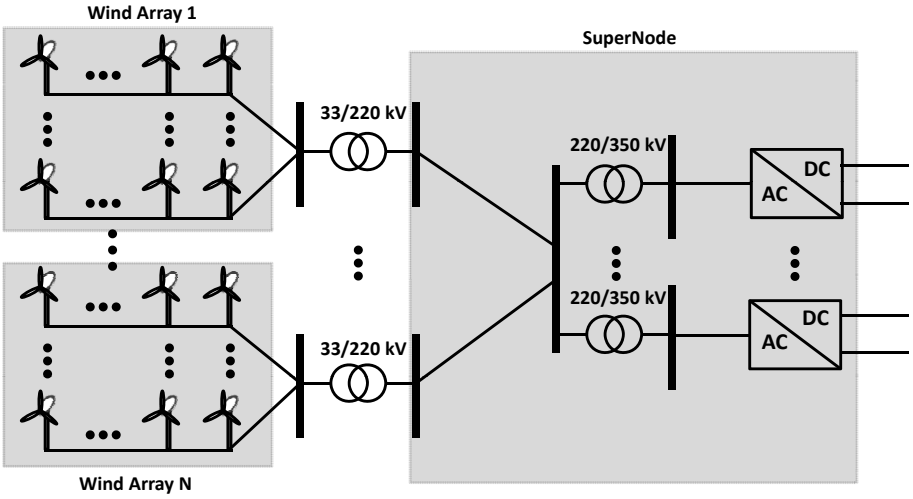

Figure 7.2: Single line diagram of the SuperNode based on the HVDC2000 scheme from National Grid

7.3 Frequency-cost dependence of SuperNode components

7.3.1 Cables

Operation at non-standard frequency implies variation in the impedances and the ratings of the cables due to factors such as skin effect, proximity factor and thermal capacity as discussed in IEC60287 [200]. The wind array to transformer substation connections are proposed at MV, whereas the transformer substation is connected to the SuperNode substation at HV (see Figure 7.2). It is important to note that parameters for standard 50/60Hz cables are used in the following analysis and that the cable designs have not been modified to reflect use at non-standard operating frequencies. This analysis is based upon cable data found in [199, 201, 202] and values including the effect of cable geometry from [203].

The system has been analysed assuming a cable utilisation factor between 0.85 and 0.99 [198, 204]. The cable utilisation factor (ρ) is defined as [205]

$$\rho = \frac{I_{amp}^2 - I_c^2}{I_{amp}^2} \tag{7.1}$$

where I_{amp} is the ampacity of the cable and I_c is the cable charging current. The reactive current is considered to be solely the result of cable capacitance for both HV and MV cables (i.e., cable inductance is neglected [202, 203]). In this study, the cable charging current is assumed to be shared equally between both ends of the cable, therefore I_c is maximum and equal at either end of the cable. For a fixed cable utilisation factor, this assumption results in a cable twice as long when compared to a scenario in which the charging current is delivered only by one end of the cable (e.g., if the cable were to feed a simple resistive load [206]).

Cable ampacity variation with frequency

IEC60287 provides standard formulas for calculating the maximum current capacity (ampacity) of a cable for varying frequency and for different cable geometries. In Figure 7.3, the relationship between the ampacity of several cables and the operating frequency is plotted. The dotted lines represent the frequencies above which the accuracy of IEC60287 is not assured [200]. Segmented conductors with $k_s = 0.435$ and $k_p = 0.37$ are assumed as defined in IEC60287.

From the ampacity curve corresponding to the cable of 220 kV with a cross section of 1600 mm^2 (shown in Figure 7.3(a)), it can be seen that the frequency limit which ensures the accuracy of the calculations is around 70 Hz. The performance of this cable at higher frequencies would not be well modelled and for this reason such a cable is not included in the following analysis. The frequency limit for cables with cross sections of 1000 mm^2 is 108 Hz, but these cables are included in the analysis as the majority of the frequency range of interest (20-120 Hz) is covered.

Cable length

The relationship between cable utilisation factor ρ and cable length l (km) may be calculated using

$$l = \sqrt{3} I_{amp} \left(\frac{\sqrt{1-\rho^2}}{\pi f C_c U} \right) \tag{7.2}$$

where I_{amp} (kA) is the ampacity of the cable, C_c (F/km) is the cable capacitance, U (kV) is the sending end voltage and f (Hz) is the frequency of the system.

Using (7.2) and considering the ampacity variation of IEC60287, cable length for different frequencies and utilisation factors can be calculated and is shown in Figures 7.4, 7.5, 7.6 and 7.7 for HV cables, and 7.8, 7.9, 7.10 and 7.11 for MV cables, respectively.

Number of cables

The necessary number of cables (N_{cables}) to transfer an active power (P) can be calculated from the active power capacity of one cable (P_{cable}). P_{cable} depends upon the cable ampacity (I_{amp}), the desired length (l) and the frequency (f):

$$P_{cable} = \sqrt{3} U I_{amp} \sqrt{1 - \left(\frac{\pi f C_c U l}{\sqrt{3} I_{amp}} \right)^2} \tag{7.3}$$

Knowing P and P_{cable}, the required number of cables can be calculated as

$$N_{cables} = \frac{P}{P_{cable}}. \tag{7.4}$$

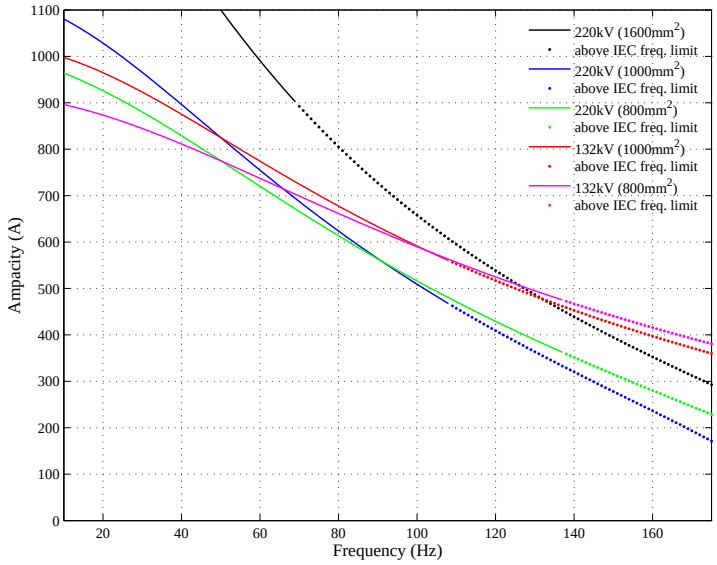

(a) HV cables ampacity

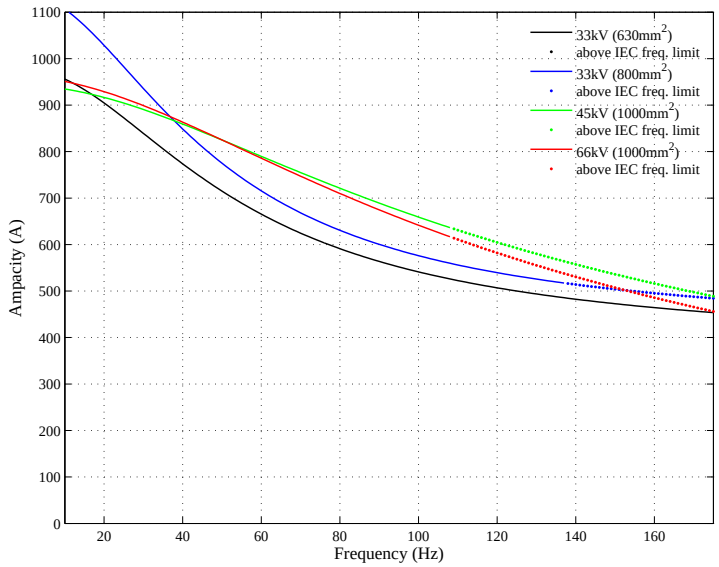

(b) MV cables ampacity

Figure 7.3: Maximum current capacity (ampacity) of HV and MV cables as function of frequency under different cable geometries

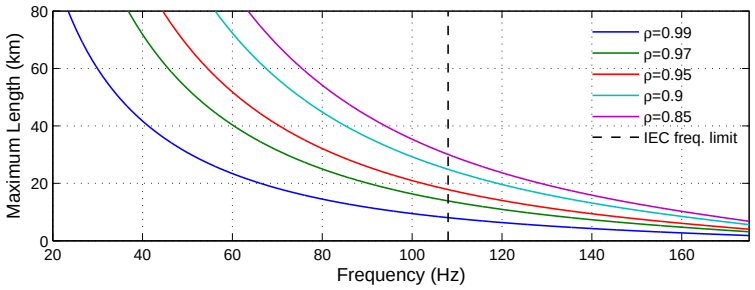

Figure 7.4: Maximum length variation of 220 kV-1000 mm^2 cables as a function of frequency and cable utilisation factor

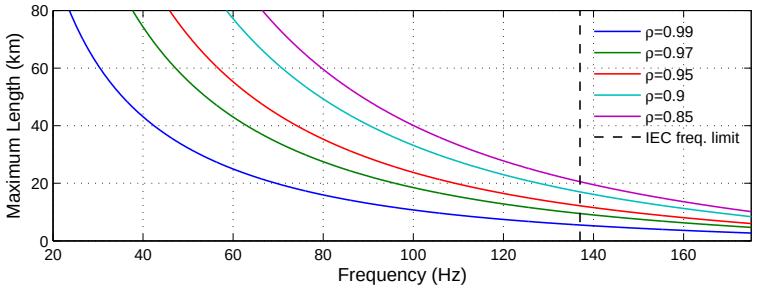

Figure 7.5: Maximum length variation of 220 kV-800 mm^2 cables as a function of frequency and cable utilisation factor

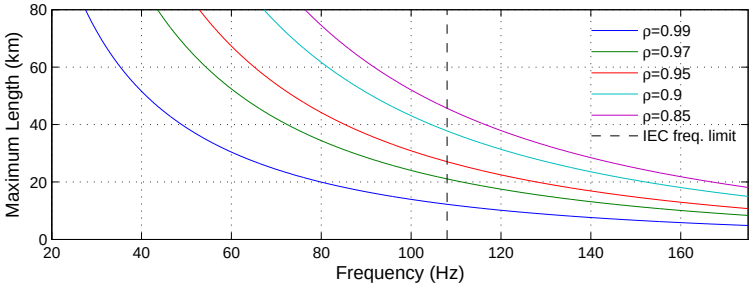

Figure 7.6: Maximum length variation of 132 kV-1000 mm^2 cables as a function of frequency and cable utilisation factor

Cost of cables

For offshore installations, cross-linked polyethylene (XLPE) cables are usually installed. The cost of XLPE submarine cables can be calculated with

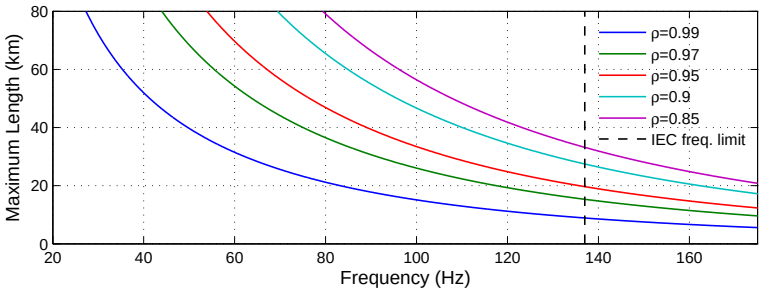

Figure 7.7: Maximum length variation of 132 kV-800 mm^2 cables as a function of frequency and cable utilisation factor

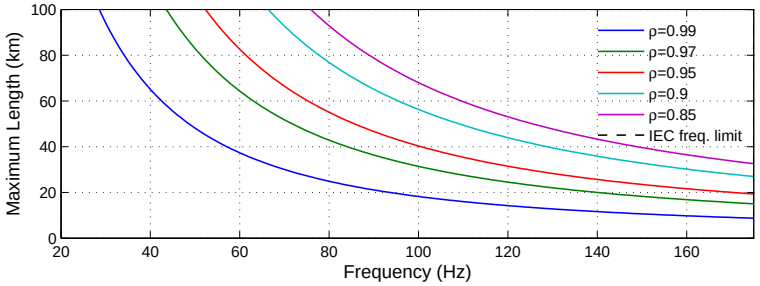

Figure 7.8: Maximum length variation of 33 kV-630 mm^2 cables as a function of frequency and cable utilisation factor

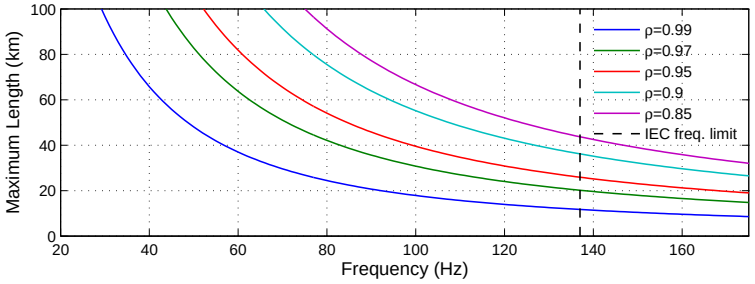

Figure 7.9: Maximum length variation of 33 kV-800 mm^2 cables as a function of frequency and cable utilisation factor

the following formula [207, 208]

$$C_c = K_1 + K_2 \cdot e^{K_3 \cdot I_{amp}} \tag{7.5}$$

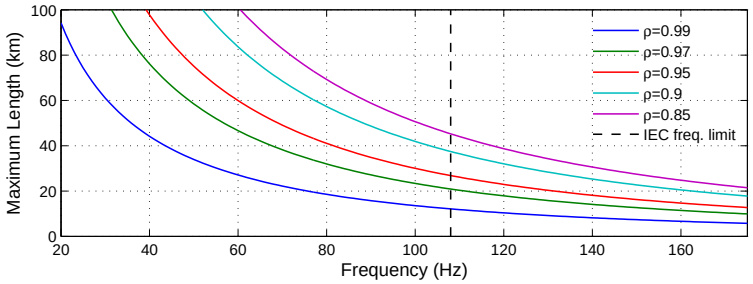

Figure 7.10: Maximum length variation of 45 kV-1000 mm^2 cables as a function of frequency and cable utilisation factor

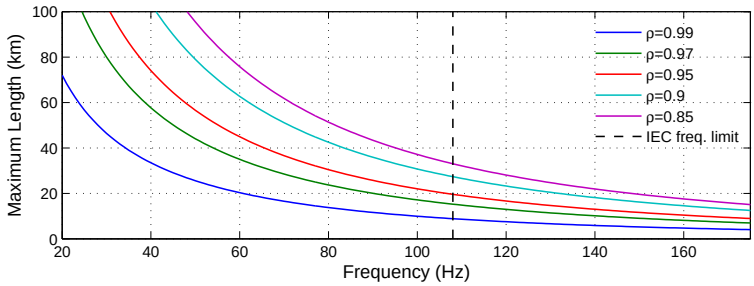

Figure 7.11: Maximum length variation of 66 kV-1000 mm^2 cables as a function of frequency and cable utilisation factor

where C_c is the cost of the cable in k€/km, the constant values (K_1, K_2, K_3) are defined in Table 7.1 which are dependent on the cable voltage rating. I_{amp} is the ampacity of the cable in Amperes. It is important to remark that the I_{amp} figure used to calculate the cable cost is the ampacity of the cable at 50 Hz, not the ampacity at a particular (non-standard) operating frequency.

7.3.2 Transformer design

All power transformers incorporated into the SuperNode are affected by the change in system operational frequency, since the core area of a transformer (A_{core}) is related with the nominal frequency (f) by the following equation [209]:

$$A_{core} \approx \frac{E}{4.44 f N B_{sat}} \tag{7.6}$$

kV	K_1	K_2	K_3
33	45.6	66.1	$2.34{\cdot}10^{-3}$
45	57.2	67.8	$2.33{\cdot}10^{-3}$
66	76.3	69.3	$2.34{\cdot}10^{-3}$
132	219	23.3	$3.80{\cdot}10^{-3}$
220	353	12.2	$4.62{\cdot}10^{-3}$

Table 7.1: Coefficients for XLPE submarine AC cables

where E is the applied voltage, N is the number of turns and B_{sat} is the saturation flux density of the core material (it is assumed that the full flux swing of the core material is utilised). Assuming the applied voltage, the number of turns and the saturation flux density of the core material remain constant, a relationship between core area and frequency can be determined. From these assumptions it is possible to approximate the way in which core volume V_{core}, winding volume $V_{winding}$ and enclosure surface area A_{enc} scale with frequency. This is developed in 7.3.2 and the resulting size-frequency scalings shown in Table 7.2.

Frequency	V_{core}	$V_{winding}$	A_{enc}
25 Hz	2	2	$\sqrt[3]{2^2}$
50 Hz	1	1	1
100 Hz	$\frac{1}{2}$	$\frac{1}{2}$	$\frac{1}{\sqrt[3]{2^2}}$

Table 7.2: Core volume, winding volume and enclosure surface area scaling factors of a transformer for different operating frequencies

Transformer sizing

Under the assumptions made in Section 7.3.2, transformer core area (A_c) is inversely proportional to operating frequency. In order to establish the scaling of core and winding volumes and enclosure surface area with frequency it is necessary to make three further assumptions in the design of the transformer: Winding DC resistance (R_w), the number of turns (N) and

the winding aspect ratio a are all to be kept constant with frequency. The winding aspect ratio determines the relative sizing of core and winding such that $t_w = at_c$, where t_w is the thickness of the winding and t_c is the thickness of the core, as shown in Figure 7.12. For typical power transformers, the winding aspect ratio is

$$a \approx \frac{1}{2}. \tag{7.7}$$

The winding wire thickness (t_{cu}) is related to winding DC resistance (R_w) by

$$R_w = \frac{l_w}{t_{cu}^2 \sigma} = \frac{4(t_c + t_w)N}{t_{cu}^2 \sigma} \tag{7.8}$$

where l_w is the length of the winding, which is simply N times the average perimeter of the winding and σ is the conductivity of the winding material. On examination of Figure 7.12 the height of the winding may be found as

$$h_w = \frac{t_{cu}^2}{t_w} N = \frac{4\left(t_c + t_w\right) N^2}{R_w \sigma t_w} = \frac{4\left(1 + \frac{1}{a}\right) N^2}{R_w \sigma} \tag{7.9}$$

which demonstrates that, under the above assumptions, winding height is independent of frequency. The core volume is simply

$$V_c = h_w A_c \tag{7.10}$$

and the winding volume is

$$V_w = h_w \left[\left(t_c + 2t_w\right)^2 - t_c^2\right] = h_w 4a\left(a+1\right) t_c^2 = 4a\left(a+1\right) h_w A_c \tag{7.11}$$

Thus both core and winding volumes scale inversely proportional to frequency (as $A_c \propto 1/f$). Note that this analysis provides a first-order approximation of transformer scaling laws only. The constraints imposed result in transformers that will become increasingly 'thin and tall' at higher frequencies. It may be expected that the aspect ratio will be adjusted to achieve a more optimized design in practical systems.

The area of the enclosure (A_{enc}) of the transformer is also frequency dependant. To a first approximation, the enclosure area may be expected to scale with the square of the linear dimensions of the transformer. Assuming the transformer is equal in all linear dimensions, and with the knowledge that core and winding volumes scale as $1/f$ it should be expected that $A_{enc} \propto 1/f^{2/3}$.

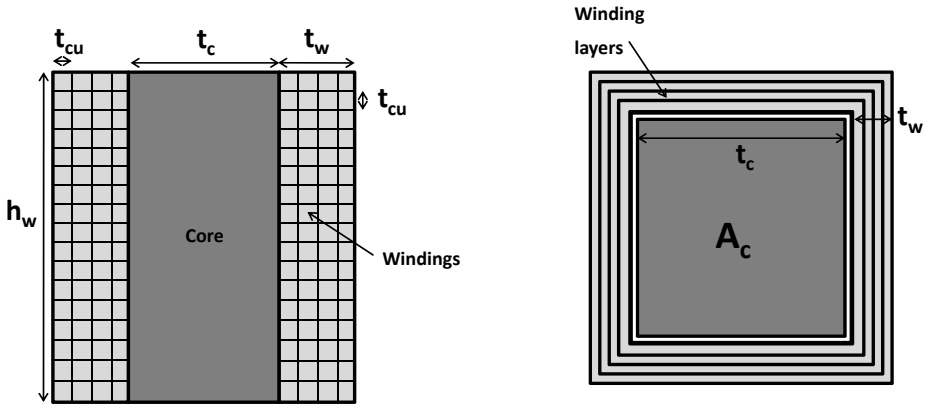

Figure 7.12: Transformer representation showing a single core arm and winding construction (left: side view, right: top view)

Transformer cost

The cost of transformers designed for use at at 50 Hz, depending on their size, can be calculated with the following formulas [207]:

$$\begin{array}{ll} LV/MV: & C_{Tr50} = -153 + 131 \cdot T_r^{0.447} \\ MV/HV: & C_{Tr50} = 42.7 \cdot T_r^{0.751} \end{array} \tag{7.12}$$

where C_{Tr50} is the transformer cost in k€ and T_r is the rated power of the transformer in MVA. From Table 7.2, it can be seen that the materials used in the manufacture of the transformer vary depending on the nominal frequency. Therefore, considering the percentages of the transformer cost presented in Table 7.3 [210], a variation on the total cost of different parts of the transformer can be computed depending on the frequency as follows

$$C_{Tr} = \frac{0.325 f_r + 0.22 f_r + 0.164 \sqrt[3]{f_r^2}}{0.325 + 0.22 + 0.164} C_{Tr50} \tag{7.13}$$

where f_r is the normalized frequency, calculated as a ratio between the standard frequency and the analysed frequency ($f_r = 50\,\text{Hz}/f$). Figure 7.21 represents the total capital cost of each type of transformer. It can be seen that the cost of the transformer is less at higher frequencies due to the reduction in construction material quantity.

Transformer Material	Cost (%)
Magnetic Steel	32.5 ± 5.5
Windings	22 ± 6
Insulation	14.1 ± 5.5
Carbon Steel	16.4 ± 8.5
Fabricated Parts	15 ± 9

Table 7.3: Percentages of the overall cost for each material used in the manufacture of a transformer

7.3.3 Reactive power compensation

The reactive nature of all undersea cables is dominated by their large capacitance per unit length [211] and therefore shunt reactors may be used to provide reactive compensation. The required inductance is related to cable capacitance by

$$L = \frac{1}{C_c(2\pi fl)^2} \tag{7.14}$$

The peak charging current of the cable $I_{c(pk)}$ is proportional to frequency [211]:

$$I_{c(pk)} = 2\sqrt{2}\pi C_c U f l \tag{7.15}$$

The peak stored energy in the shunt reactor (E) can be calculated as

$$E = \frac{1}{2} L I_{c(pk)}^2 \tag{7.16}$$

By substituting (7.14) and (7.15) into (7.16), it can be concluded that the energy storage requirements (and hence physical size) of compensating shunt reactors per cable of a fixed length is frequency independent.

Cost of reactive power compensation

The cost of the reactive power compensation, a shunt reactor in this case, can be calculated as 2/3 of the cost of a transformer with the same rating [207, 208]. The cost of shunt reactors may be evaluated as follows:

$$C_{rpc} = C_{50} \frac{N_{cf}}{N_{c50}} \tag{7.17}$$

where C_{50} is the cost of shunt reactor at 50 Hz, N_{cf} is the number of required cables at a given frequency and N_{c50} is the number of required cables at 50 Hz.

7.3.4 Offshore infrastructure

Cost of MV/HV substation platform

As a first order approximation, it is estimated that the total weight of transformers consumes roughly 2/3 of the rated load of the MV/HV substation platform. Using the transformer reduction ratios obtained in Table 7.2 and assuming that transformer core and winding weight is dominant, the variation of the platform rated mechanical load with frequency may be approximated as

$$W_{pf} = W_{pf50}\left(\frac{1}{3} + \frac{2}{3}f_r\right) \tag{7.18}$$

where f_r is the normalized frequency, calculated as a ratio between the analysed frequency and the standard frequency ($f_r = 50\,\text{Hz}/f$) and W_{pf50} is the platform rated mechanical load at 50 Hz. Equation (7.18) is contains a constant value (since there are some elements in the platform which must always be installed, and their size is not frequency dependant) and a frequency dependant value which is directly proportional to transformer core and winding volume.

In order to evaluate the offshore substation platform cost C_{ss} in k€ the following equation is used:

$$C_{ss} = 2530 + 88.7 n_{wt} P_{wt}\left(\frac{1}{3} + \frac{2}{3}f_r\right) \tag{7.19}$$

where n_{wt} is the number of wind turbines, P_{wt} is the rated power of wind turbines and f_r is the normalized frequency. Equation (7.19) is derived from [207], modified to reflect the frequency dependency of transformer size and consequently the frequency dependency of platform cost.

Cost of HVDC substation platform

The capital cost of the HVDC substation can be divided into three main parts: the cost of converters, the cost of transformers and the cost of ancillary equipment. The cost of converters and ancillary equipment is considered to be constant because their ratings are expected to be relatively independent of operating frequency. They are therefore neglected from the frequency-cost analysis. However, transformer cost is a strong function of frequency

and so HVDC substation overall cost will behave in a similar manner to the MV/HV substation cost described by (7.19).

7.4 Evaluation of costs for a Dogger Bank Tranche A SuperNode

The first stage of Dogger Bank (so-called Tranche A) is used to demonstrate the SuperNode concept as shown in Figure 7.13. In Tranche A, an area of 2000 km^2 is defined and three wind farms with a power capacity of 1.4 GW each are to be installed.

For this study, an identical area is used (2000 km^2). However, 4 wind arrays of 1 GW each are assumed instead of three wind farms of 1.4 GW. This assumption increases the power transmission requirement of the HV cables from 1.4 to 2 GW, in line with the assumptions made in the HVDC2000 design [199]. Capital costs are divided into electrical device costs and offshore infrastructure costs, which are addressed separately in the following sections.

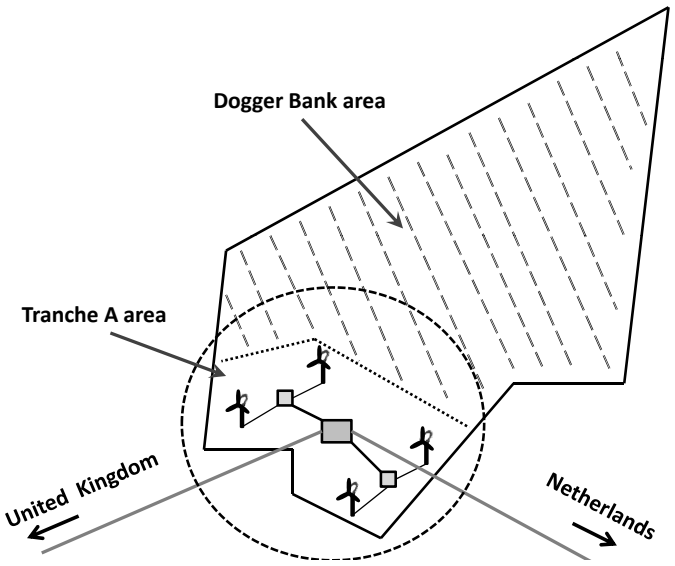

Figure 7.13: Dogger Bank geographical representation with the SuperNode implemented in Tranche A

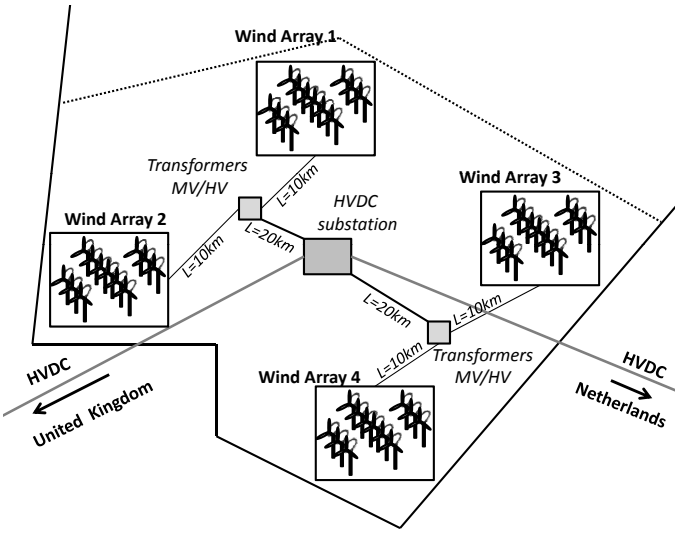

Figure 7.14: Close-up view of Tranche A showing the cable length requirements with a HVDC substation located at the center of the area

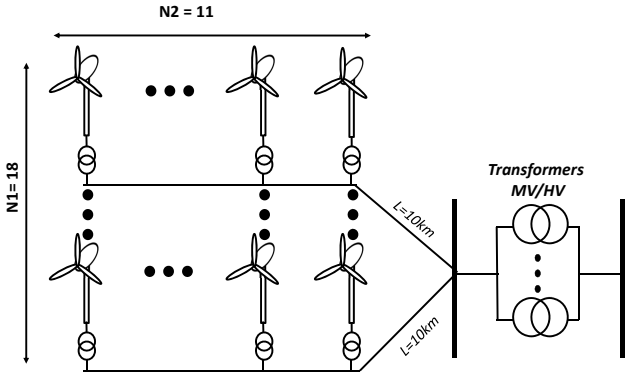

Figure 7.15: Individual 1 GW wind array layout in Tranche A

7.4.1 Cables

Cable lengths

The closest point of the Tranche A area is 125 km away from the UK, whilst the farthest point is 182 km [212]. Approximating the Tranche A area as a rectangle with one side of length equal to the difference between the closest and the farthest point of the area ($h_1 = 57$ km), the breadth of the area can be simply determined ($h_2 = 35$ km). The HV cable lengths will be approximately half this length if the HVDC substation is located in the centre of this area. Each wind array has its own area calculated as detailed in 7.4.1. Taking into account the positioning of the wind arrays relative to the MV and HV substations, the HV cables must be approximately 20 km long, whereas the MV cables are approximately 10 km long. Individual wind arrays shown in Figure 7.14 are illustrated in more detail in Figure 7.15.

Wind farm design

The wind farm sizes have been defined according to [199], where the horizontal (h) and vertical (v) distance among wind turbines are $h = 4D$ and $v = 7D$, where D is the wind turbine diameter. A wind turbine of 5 MW with $D = 126$ m was selected. Each wind farm should generate 1 GW, therefore there are necessarily 200 wind turbines on each wind farm. In order to occupy a square area, the wind farms are located as 18 rows with 11 wind turbines on each. This wind farm configuration leads to a 9.1 km horizontal length (h_{tot}) and 9.7 km vertical length (v_{tot}), as shown in Figure 7.16.

Number of cables

The necessary number of cables to transfer the desired power (2 GW through the HV cables and 1 GW through the MV cables) with different operational frequencies are shown in Figures 7.17 and 7.18 (both fractional and integer (rounded up) values are shown). As the frequency increases both the and the amapacity of the cables (Figure 7.3) and cable utilisation factors decrease (Figures 7.4, 7.5, 7.6 and 7.7 for HV cables, and 7.8, 7.9, 7.10 and 7.11 for MV cables, respectively), requiring a greater number of cables to transmit the rated power.

Cable costs

Equation (7.5) may be used to calculate the capital cost of the HV and MV cables and is shown in Figures 7.19 and 7.20 respectively. The lowest

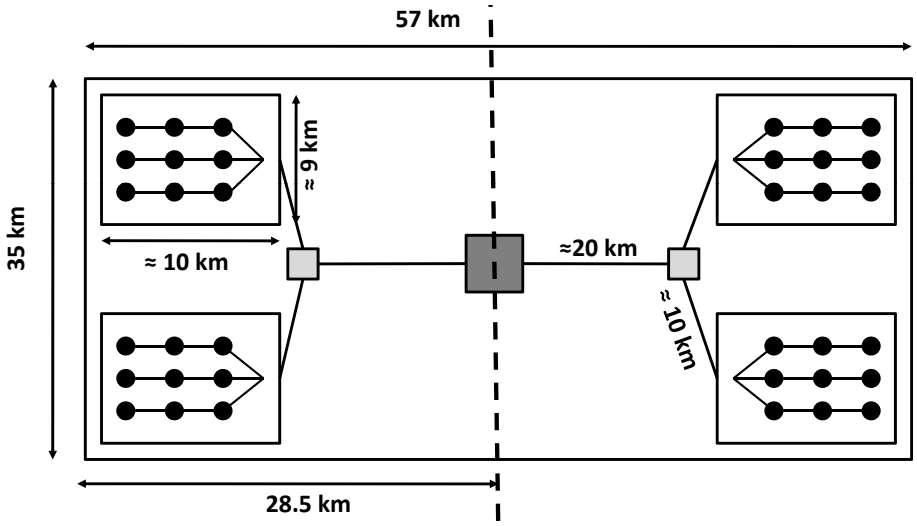

Figure 7.16: Dogger Bank Tranche A approximation for the SuperNode Design

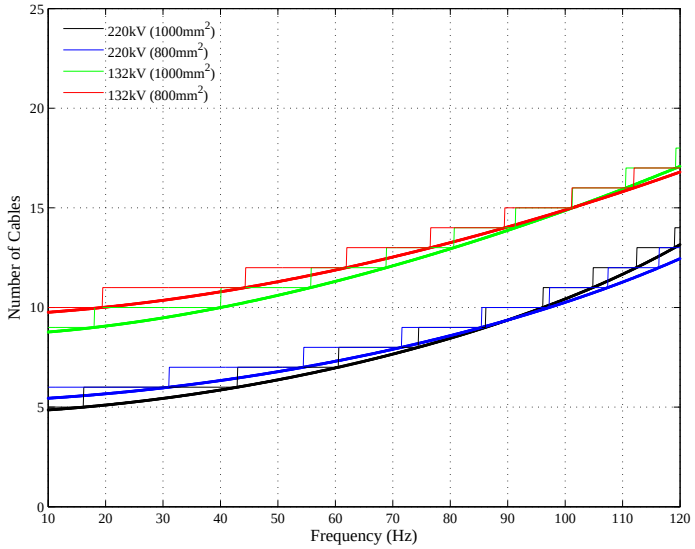

Figure 7.17: Number of HV cables required (fractional and integer) for different geometries as a function of operating frequency

cost MV cable is the 66 kV with a cross section of 1000 mm^2, for all fre-

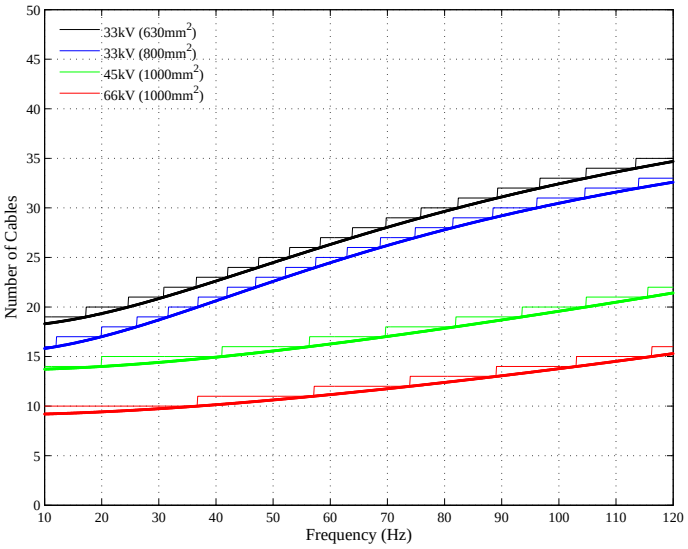

Figure 7.18: Number of MV cables required (fractional and integer) for different geometries as a function of operating frequency

quencies, and the lowest cost HV cable is the 220 kV with a cross section of 800 mm^2, also for all frequencies, which are therefore the selected cables for this analysis.

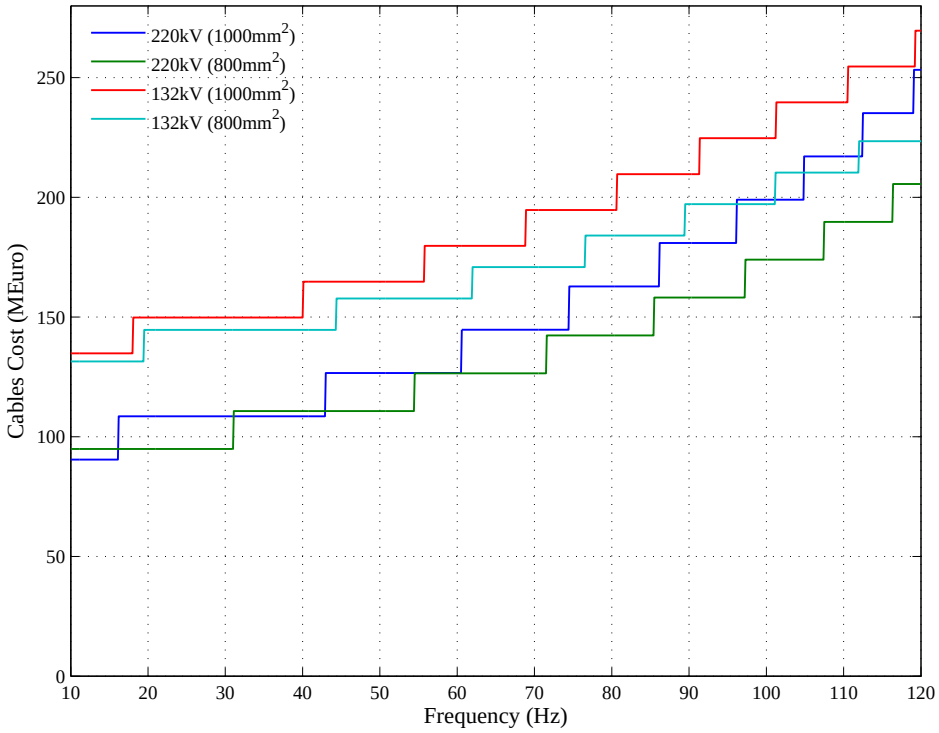

Figure 7.19: Capital cost in M€ of the HV-cables for each wind array as a function of frequency for different cable geometries

7.4.2 Main electrical devices

Cost of transformers

The necessary number of transformers can be calculated by dividing the the maximum power to be transferred by the rated power of the transformer, except in the case of the LV/MV transformers which are installed in each wind turbine. The selected transformers are: 200×LV/MV 8 MVA one of which is located in each wind turbine, 8×MV/HV 280 MVA, which are placed in the wind array substations, and 4×HV/HV 520 MVA, which are installed on the HVDC platform. The total cost of all wind turbine, MV/HV and HVDC substations transformers evaluated using (7.13) is shown in Figure 7.21.

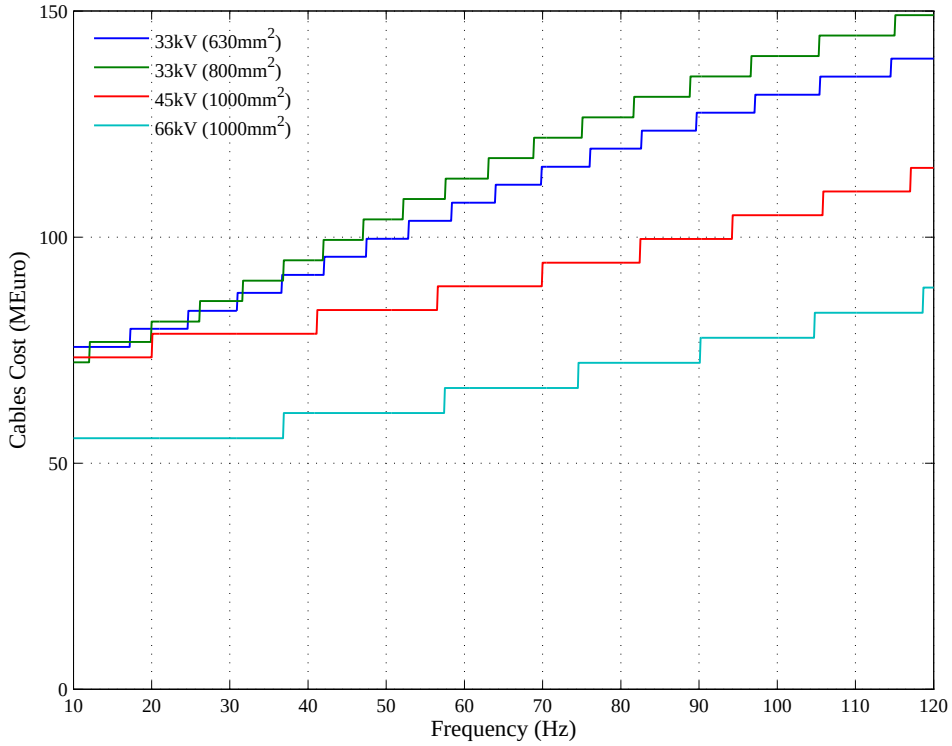

Figure 7.20: Capital cost in M€ of the MV-cables for each wind array as a function of frequency for different cable geometries

Cost of reactive power compensation

The cost of reactive power compensation increases proportionally with number of installed cables, therefore the cost increases with frequency as shown in Figure 7.22.

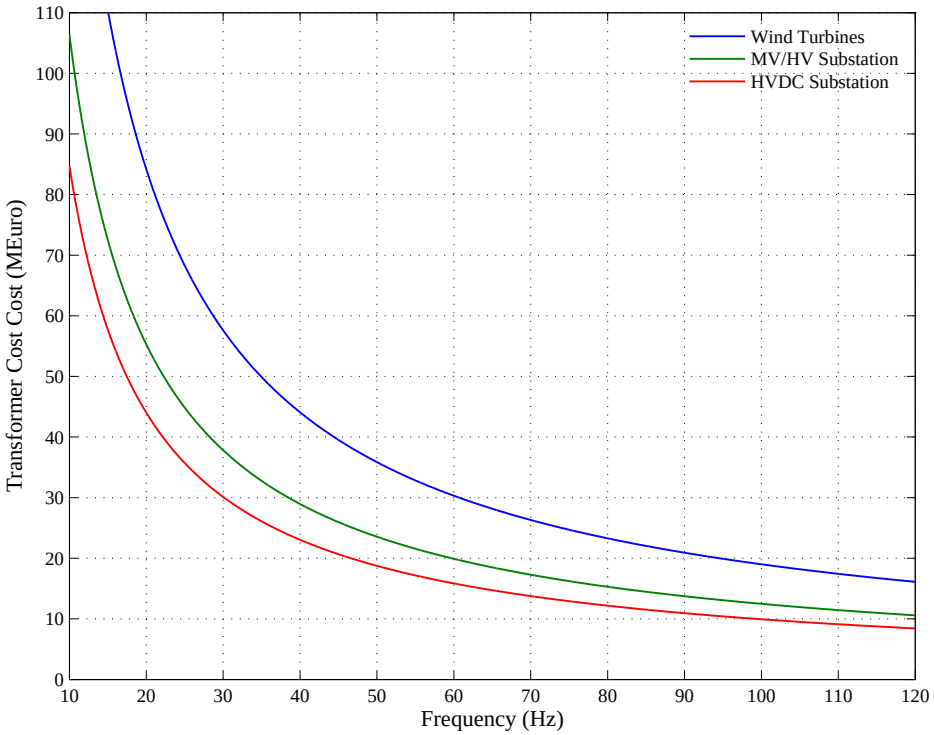

Figure 7.21: Capital cost in M€ for each type of power transformers as a function of frequency

Total capital cost of main electrical devices

The costs calculated in previous sections may be summed in order to investigate the total cost of the cables, transformers and reactive compensation. Figure 7.23 shows a minimum in the integer cable number curve at 54 Hz with a cost of 677 M€, whereas the minimum cost with a fractional number of cables is at 60 Hz. The use of 25 Hz is approximately 22% and 100 Hz 10% more expensive than the 50 Hz case.

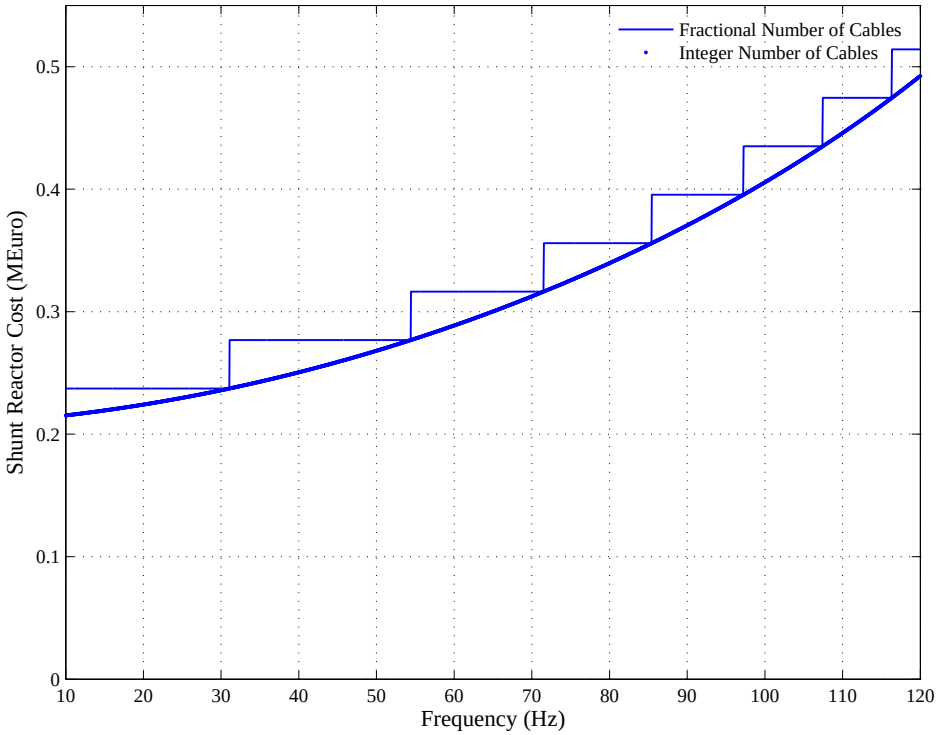

Figure 7.22: Capital cost in M€ for the reactive power compensation (shunt reactor) as a function of frequency

7.4.3 Infrastructure costs

Each MV/HV substation platform should be designed to house 8 transformers of 280 MVA rated power. The HVDC substation platform should be designed to house 8 HVDC converters and 8 step-up transformers with 520 MVA rated power. Equation (7.19) may be used to evaluate individual substation platform costs as shown in Figure 7.24, where a considerable reduction on the platform cost with frequency can be observed.

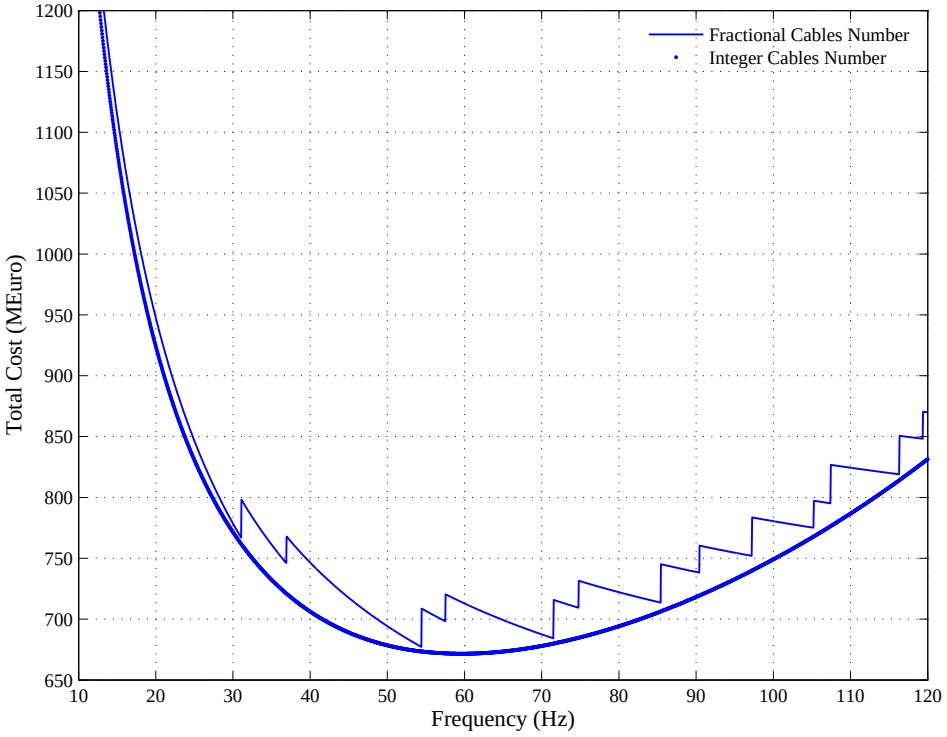

Figure 7.23: Total capital cost of main electrical devices. The integer cable number curve does not meet the curve obtained by using the fractional number of cables; this is because the change in the required number of cables for HV and MV do not occur at the same instance.

7.4.4 Total capital cost of the SuperNode

Adding the total cost of the electrical devices and the offshore infrastructure, an approximate idea of the global capital cost of the whole system may be arrived at. Figure 7.25 shows a minimum in the integer cable number curve of at 85 Hz with a cost of 1234 M€, whereas the minimum cost with a fractional number of cables is at 93 Hz. The use of 25 Hz is approximately 45% more expensive than the 50 Hz case, whereas the 100 Hz case is around 13% less expensive. The cost curve is quite shallow in the vicinity of the minimum and therefore it may be expected that any selection in the range 65–110 Hz would be a good choice for system operating frequency.

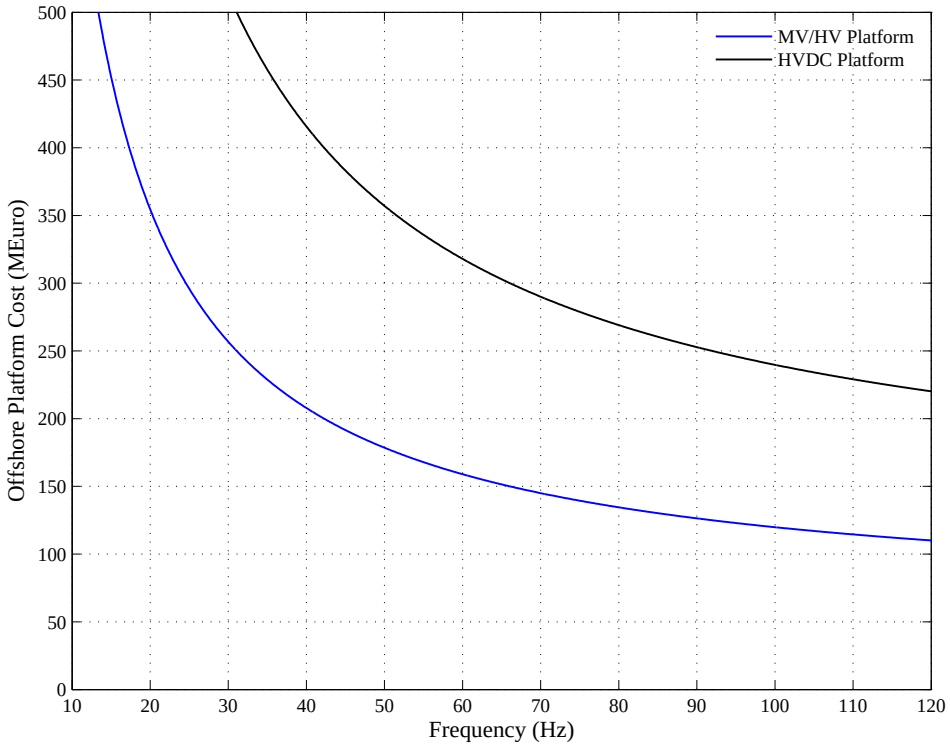

Figure 7.24: Offshore substation platforms capital cost in M€ as a function of frequency

7.5 Conclusions of the chapter

The SuperNode concept has been presented as an alternative to the use of MT-HVDC systems for the aggregation of geographically close wind power resources in a European SuperGrid, The SuperNode have been validated by using Dogger Bank Tranche A as a case study. The effect of choosing non-standard operating frequencies on the costs of major electrical components (such as cables, transformers and reactive compensation) and in offshore infrastructure (platforms) has been investigated. To conduct such operating frequency comparison, frequency dependent cost functions of the electrical components required for SuperNode concept installation have been developed.

The advantage of choosing lower operating frequencies are the large transmission distances which may be reached, however for the Dogger Bank case study presented here, large transmission distances are not required and the

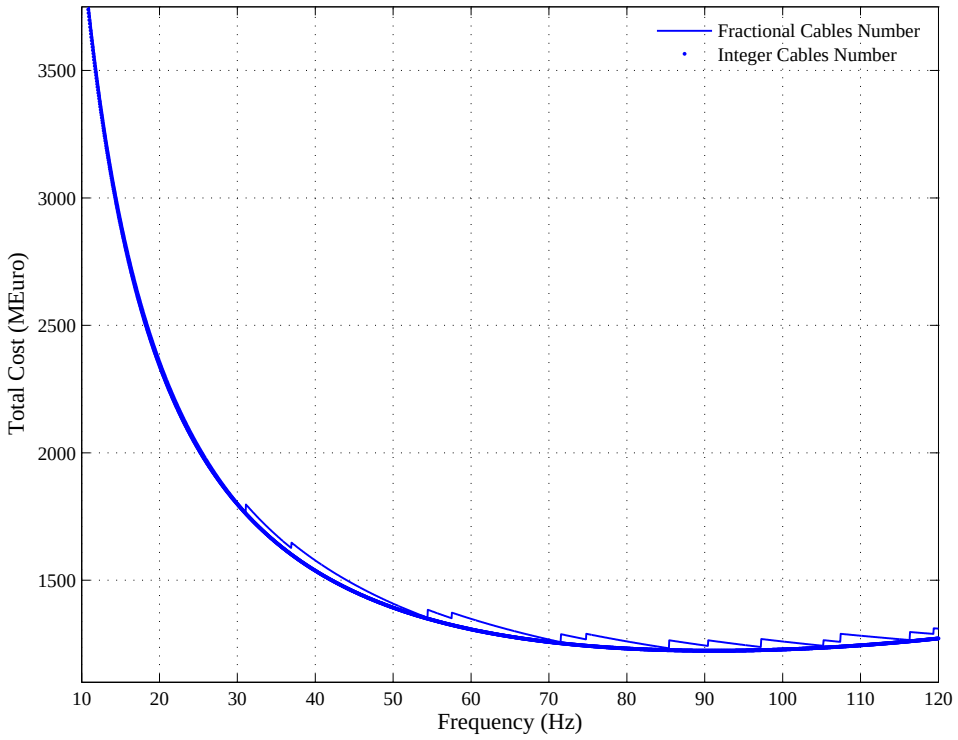

Figure 7.25: Total capital cost of the SuperNode in M€ as a function of frequency

increased costs of other electrical components and infrastructure outweighs the benefits of the slight increase in transfer capacity per cable. This may in general be expected to be the case in SuperNode designs where geographically close wind farms are to be interconnected. The principal advantage of higher frequency operation (e.g., 100 Hz) is the substantial reduction in size of the major electrical elements and supporting platforms, the penalty being the reduced power transfer capacity per cable and therefore the need for a greater number of cables. However, as cable costs constitute the largest fraction of overall cost, even a relatively small increase in the required number of cables is seen to substantially balance out the savings made elsewhere, meaning that a cost minimum is found at some intermediate point. Whilst the economic analysis presented here is of a first-order nature only it serves to demonstrate the design tradeoffs that may be made when designing geographically small AC networks that may work unsynchronized from the

wider grid. The conclusions of the present work are based on an analysis of component rating and associated capital costs and do not consider the operational challenges that may arise in such systems. Further detailed power flow and transient stability analyses will be required to capture the influence of the proposed non-standard operating frequencies on overall system performance.

Not present in the analysis presented here is a consideration of installation costs. The decrease in transformer and substation size at high operating frequencies also implies a reduction of costs for their offshore installation; in other words, additional savings may be achieved beyond those considered here. For example, the size and/or the number of special purpose marine vessels used to transport and install offshore electrical infrastructure may be reduced since transformers and substations will be smaller at higher frequencies. Thus the cost savings associated with high operating frequencies may be expected to be somewhat greater than those already outlined here and in this case the cost minimum would be pushed towards a higher frequency.

It can be concluded that higher operational frequencies, such as 100 Hz, could be economically advantageous for offshore AC networks such as the SuperNode. More detailed models of the cost dependence of electrical infrastructure on frequency as well as further analysis considering the costs of infrastructure transport and installation on a case-by-case basis will allow a more exact optimum frequency to be selected.

8 Conclusions

The thesis has covered important issues related to power system dynamics arising from the rapid increase of wind power into the power generation share. This thesis has addressed how wind power plants are able to contribute to keep power system stability from the electromechanical point of view; since transmission system operators (TSOs) will require, in a near future, to wind power plants to provide damping to the power system oscillations.

The influence of each wind turbine technology on power system small signal stability has been investigated. The oscillation damping capability of wind power plants using local signals has been demonstrated by means of the implementation of different power system stabilizers. From the comparison of such controllers and the analysis of how different aspects related to the grid such as cable length and wind power plant location in the power system have been studied. From such analysis, some critical factors influencing in their controller response have been highlighted.

Although, previous results have provided some information about the possible contribution of wind power plants to damp power system oscillations, such results are fully dependent on particular considerations including power system, the design of power system stabilizers, the signals used as input and outputs of such controller, among others. To be able to draw more general conclusions, power oscillation damping provided by the WPPs have been analyzed using tools which are independent from the particular controller.

First, the selection of the best local input-output signals for the controller design has been analyzed assuming that all the signals required are available by measuring. Different analysis techniques considering both controllability

and observability measures and input-output interactions have been compared. From this comparison and after a critical analysis, recommendations have been given in order to select the best signal pairs to damp power system oscillations considering different approaches, such as single-input single-output (SISO) and multivariable control (MIMO). These recommendations include geometric measures and RHPZs for SISO case, and for MIMO case, geometric measures and MSF.

Further, a new criterion to select the most adequate input-output pair for the design of PSS for WPP has been proposed. Unlike previous results, the proposed criterion have considered explicitly local and remote signals in the analysis, since the use of WPP local signals to damp remote oscillations (occurring in synchronous generators) has been treated. Using fundamental design limitations and controllability and observability concepts, the criterion is able to identify the most adequate pair of input-output local signals without designing the controller. The study of the controllability and observability characteristics have allowed to determine the input-output pair that will require less control effort to achieve the oscillation damping; whilst, the analysis of the fundamental limitations have permitted to identify frequencies at which is not possible to reduce the magnitude of the frequency response of the closed loop system. It is worth to remark that if such frequencies are close to the oscillation modes to be damped, it will be difficult, no matter the controller choice, to achieve a noticeable increase of damping.

In order to validate these input-output selection methods, some study cases have been analyzed. In such cases, wind power plants with converter-based wind turbines are assumed to behave as a negative load. This hypothesis is adequate under small signal analysis since a full rate power converter isolates both generator and wind turbine from the grid; besides, these analyses consider small variations around an operating point which can be taken into account as a constant value in wind power. Neglect these effects can have little impact in power system oscillations due to the fact that wind turbine technologies do not work synchronously with conventional generators. However, it is worth to remark that wind turbines could present their own oscillations modes.

Finally, the analysis and design of an offshore AC network (The SuperNode), as an alternative to the use of MT-HVDC systems, in order to make possible the implementation of an European "Supergrid" with current technologies has been analyzed studying the frequency dependence of wind power component costs. Higher operating frequencies than 50 Hz have demonstrated a substantial reduction in size of the major electrical elements and supporting platforms required for the offshore AC network implementation;

however, there is a penalty such as the reduction of the power transfer capacity per cable, implying both the requirement of a greater number of cables and a reduction on transmission distances. Since the distances between wind farms has been assumed not longer than 20 km, such length restriction has not arisen as a critical factor. Conversely, the increase in the required number of cables affect substantially the overall cost of the wind power plant. Thus, a minimum of the overall cost has been found in a frequency over 50 Hz. It is worth to remark that the such results have been based on component rating analysis and capital costs associated to these components, but have not considered the operational challenges that may arise in such systems.

8.1 Further work

From this thesis, future research lines have arisen, which appear listed in the following:

- Within this thesis, the selection of the most adequate input-output signals to damp power system oscillations from wind power plants for both SISO and MIMO controls, considering system limitations has been analyzed. However, other aspects could be of interest, for instance:
  - The design of controllers with other advanced control methods, for example optimal control. Moreover, there is the need of including uncertainty in the system to make the controller more robust.
  - To include in the system definition, the use of wide area measurement systems (WAMS) considering their time delays.
  - To consider in the control design, the physical limitations of the electric components.
- Throughout this thesis, wind power plants mainly considering converter-based wind turbines technologies (DFIG and FRCWT) have been assumed as a single aggregate wind turbine. It is a well-established assumption to analyze rotor-angle stability issues in power system; nonetheless, it could be interesting to study:
  - The small signal interaction of various wind turbines in a wind power plant.

  - How to distribute the active or reactive power extra responses to support power systems.
  - The use of more detailed aggregated wind turbines (including mechanics) models to ensure that any converter-based wind turbine technologies do not interact with power system electro-mechanical oscillations.
  - The effect of larger penetration of wind power into weak grids stability.

- From the offshore AC network design analysis, several improvements could be included:
  - To consider power losses costs in the analysis of the more interesting operational frequency.
  - To include in the study, the efficiency of the electric components and to analyze the effect of higher frequency on power converters switching.
  - To analyze of the effect of low frequencies for transmission proposes.
  - To study the opportunity of creating an offshore DC grid.

Bibliography

[1] United Nations Framework Convention on Climate Change. Kyoto protocol to the united nations framework convention on climate change, 1998. 1

[2] European Commission. Communication from the commision: Energy efficiency: delivering the 20% target, November 2008. 1

[3] S. Heier. *Grid Integration of Wind Energy Conversion Systems*. John Wiley and Sons, 1998. 1

[4] WWEA. World wind energy report 2010, 2011. 1

[5] J. Wilkes and J. Moccia. Wind in power: 2012 European statistics. Technical report, EWEA, 2013. 1

[6] S. Sawyer and K. Rave. Global wind report - annual market update 2012. Technical report, Global Wind Energy Council (GWEC), 2013. 1

[7] R. Wiser and M. Bolinger. Wind technologies market report. Technical report, U.S. Department of Energy, 2012. 1

[8] Thomas Ackermann. *Wind Power in Power Systems*. Wiley, 2005. 1, 14

[9] J. L. Domínguez-García, D.J. Rogers, C.E. Ugalde-Loo, J. Liang, and O. Gomis-Bellmunt. Effect of non-standard operating frequencies on

the economic cost of offshore AC networks. *Renewable Energy*, 44:267–280, 2012. 1

[10] M. Tsili, Ch. Patsiouras, and S. Papathanassiou. Grid code requirements for large wind farms: A review of technical regulations and available wind turbine technologies. In *Proc. of the European Wind Energy Conference & Exhibition (EWEC'08)*, 2008. 1, 4, 14

[11] Ministerio de Industria Turismo y Comercio: Secretaria de Estado de Energía. Procedimientos de operación 12.3, Octubre 2006. 1, 4, 14

[12] B. Fox, D. Flynn, L. Bryans, N. Jenkins, D. Milborrow, M. O'Malley, R. Watson, and O. Anaya-Lara. *Wind Power Integration: Connection and system operational aspects*. The Institution of Engineering and Technology, 2007. 1, 4

[13] O. Gomis-Bellmunt, A. Junyent-Ferre, A. Sumper, and J. Bergas-Jane. Ride-through control of a doubly fed induction generator under unbalanced voltage sags. *IEEE Transactions on Energy Conversion*, 23:1036–1045, 2008. 1

[14] Z. Chen and F. Blaajberg. Wind farm - a farm source in future power systems. *Renewable and Sustainable Energy Reviews*, 13:1288–1300, 2009. 1

[15] A. Sumper, O. Gomis-Bellmunt, A. Sudri-Andreu, R. Villafafila-Robles, and J. Rull-Duran. Response of fixed speed wind turbines to system frequency disturbances. *IEEE Transactions on Power Systems*, 24:181–192, 2009. 1

[16] M. Stiebler. *Wind Energy Systems for Electric Power Generation*. Springer-Verlag, 2008. 1

[17] O. Anaya-Lara, N. Jenkins, J. Ekanayake, P. Cartwright, and M. Hughes. *Wind Energy Generation: Modelling and Control*. Wiley, 2009. 1, 3, 14, 24, 25, 28, 29, 31, 33

[18] J. L. Domínguez-García, O. Gomis-Bellmunt, L. Trilla-Romero, and A. Junyent-Ferré. Indirect vector control of a squirrel cage induction generator wind turbine. *Computer & Mathematics with Applications*, 64(2):102–114, 2012. 1, 64

[19] Ministerio de Industria Turismo y Comercio: Secretaria de Estado de Energía. Instalaciones conectadas a la Red de Transporte y equipo generador: requisitos minimos de diseño, equipamiento, funcionamiento, puesta en servicio y seguridad. Technical report, Red Eléctrica, October 2008. 2, 4

[20] ENTSO-E. Entso-e network code for requirements for grid connection applicable to all generators, March 2013. 3, 4, 14

[21] J.G. Slootweg. *Wind Power, Modelling and Impact on Power System Dynamics*. PhD thesis, Delft University of Technology, 2003. 3, 24, 25, 26

[22] G. M. J. Herbert, S. Iniyan, E. Sreevalsan, and S. Rajapandian. A review of wind energy technologies. *Renewable and Sustainable Energy Reviews*, 11:1117–1145, 2007. 3

[23] A.R. Jha. *Wind Turbine Technology*. CRC Press, 2011. 3

[24] R. Eriksson and L. Söder. Widearea measurement system-based subspace identification for obtaining linear models to centrally coordinate controllable devices. *IEEE Transactions on Power Delivery*, 26:988–997, 2011. 3

[25] H.F. Latorre and M. Ghandhari. Improvement of power system stability by using a VSC-HVDC. *Internation Journal of Electrical Power & Energy systems*, 33:332–339, 2011. 3

[26] O. Gomis-Bellmunt, A. Junyent-Ferré, A. Sumper, and S. Galceran-Arellano. Maximum generation power evaluation of variable frequency offshore wind farms when connected to a single power converter. *Applied Energy*, 87:3103–3109, 2010. 3

[27] O. Gomis-Bellmunt, J. Liang, J. Ekanayake, R. King, and N. Jenkins. Topologies of multiterminal HVDC-VSC transmission for large offshore wind farms. *Electric Power Systems Research*, 81:271–281, 2011. 3, 119

[28] M. De-Prada-Gil, O. Gomis-Bellmunt, A. Sumper, and J. Bergas-Jane. Analysis of a multi turbine offshore wind farm connected to a single large power converter operated with variable frequency. *Energy*, 36:3272–3281, 2011. 3

[29] M. De Prada-Gil, O. Gomis-Bellmunt, A. Sumper, and J. Bergas-Jane. Power generation efficiency analysis of offshore wind farms connected to a SLPC (single large power converter) operated with variable frequencies considering wake effects. *Energy*, 37(1):155–168, 2012. 3

[30] H.M. Ayres, I. Kopcak, M.S. Castro, F. Milano, and V.F. da Costa. A didaction procedure for designing power oscillation dampers of FACTS devices. *Simulatino Modelling Practice and Theory*, 18:896–909, 2010. 3

[31] C.R. Makkar and L. Dewan. Transient Stability Enhancement using Robust FACTS Controllers A Brief Tour. *Canadian Journal on Electrical & Electronics Engineering*, 1:150–155, 2010. 3

[32] F. Díaz-González, A. Sumper, O. Gomis-Bellmunt, and R. Villafafila-Robles. A review of energy storage technologies for wind power applications. *Renewable and Sustainable Energy Reviews*, 16(4):2154–2171, 2012. 3

[33] K. Elkington. *The Dynamic Impact of Large Wind Farms on Power System Stability*. PhD thesis, KTH, 2012. 4, 12, 13

[34] J. Machowski, J.W. Bialek, and J.R Bumby. *Power System Dynamics: Stability and Control*. Wiley, 2008. 7, 11, 18

[35] P. Kundur, J. Paserba, and S. Vitet. Overview on definition and classification of power system stability. In *Proc. of the Quality and Security of Electric Power Delivery Systems CIGRE/IEEE PES International Symposium*, 2003. 8

[36] P. M. Anderson and A. A Fouad. *Power System Control and Stability*. Iowa State University Press., 1977. 8, 11, 92, 99, 108, 177

[37] P. Kundur. *Power System Stability and Control*. CRC Press, 2007. 8

[38] IEEE/CIGRE Join Task Force on Stability Terms And Definitions. Definition and classification of power system stability. *IEEE Transactions on Power Systems*, Vol 19:1387–1388, 2004. 9

[39] M. Basler and R. Schaefer. Understanding power-system stability. *IEEE Transactions on Industry Application*, 44:463–474, 2008. 9

[40] G. Anderson. Modelling and analysis of electric power systems. Technical report, Swiss Federal Institute of Technology (ETH), Zurich, 2008. 11

[41] P. Kundur. *Power System Stability and Control.* McGraw-Hill, 1994. 11, 12, 19, 65, 68

[42] M.K. Pal. *Lecture Notes on Power System Stability.* MKPalConsulting, 2007. 12, 13

[43] N.R. Ullah. *Wind Power Added Value for Network Operation.* PhD thesis, Chalmers University of Technology, 2008. 14, 26, 28

[44] E.H. Camm, M.R. Behnke, O. Bolado, M. Bollen, M. Bradt, C. Brooks, W. Dilling, M. Edds, W. J. Hejdak, D. Houseman, S. Klein, F. Li, J. Li, P. Maibach, T. Nicolai, J. Patino, S.V. Pasupulati, N. Samaan, S. Saylors, T. Siebert, T. Smith, M. Starke, and R. Walling. Characteristics of wind turbine generators for wind power plants. In *Power Energy Society General Meeting, 2009. PES '09. IEEE*, pages 1–5, 2009. 14

[45] B. Wu, Y. Lang, N. Zargari, and S. Kouro. *Power Conversion and Control of Wind Energy Systems.* John Wiley & Sons, 2011. 14

[46] M. De Prada-Gil, J. L. Domínguez-García, F. Mancilla-David, E. Muljadi, M. Singh, O. Gomis-Bellmunt, and A. Sumper. Type2 wind turbine with additional subsynchronous resonance damping. In *Fifth Annual Green Technologies Conference (IEEE GreenTech 2013)*, 2013. 15

[47] J. G. Slootweg and W. L. Kling. Aggregated modelling of wind parks in power system dynamics simulations. In *Proc. of the IEEE Power Tech 2003*, pages 1–6, 2003. 17, 24

[48] V. Akhmatov and H. Knudsen. An aggregated model of a grid-connected, large-scale, offshore wind farm for power stability investigations - importance of windmill mechanical system. *Electrical Power & Energy systems*, 24:709–717, 2002. 17, 24

[49] E. Hagstrøm, I. Norheim, and K. Uhlen. Large-scale wind power integration in Norway and impact on damping in the Nordic grid. *Wind Energy*, 8:375–384, 2005. 17, 25, 26, 28, 45, 73, 99, 107

[50] M.I. García-Planas and J. L. Domínguez-García. *Introducción a las matrices positives.* Edicions UPC, 2013. 21

[51] C. Gallardo. *Estabilidad y amortiguamiento de Oscilaciones en Sistemas electricos con alta penetracion eolica.* PhD thesis, Universidad Carlos III de Madrid, 2009. 22

[52] J.G. Slootweg and W.L. Kling. The impact of large scale wind power generation on power system oscillations. *Electric Power Systems Research*, 67:9–20, 2003. 24, 25, 28, 45

[53] R. D. Fernández, R. J. Mantz, and P. E. Battaiotto. Impact of wind farms on a power system. an eigenvalue analysis approach. *Renewable Energy*, 32:1676–1688, 2007. 24, 26, 27, 28

[54] S. Brownless, B. Fox, D. Flynn, and T. Littler. Wind farm induced oscillations. In *Proc. of the Universities Power Engineering Conference (UPEC'06)*, pages 118–122, 2006. 24

[55] D.J. Volwes, C. Samarasinghe, M.J. Gibbard, and G. Ancell. Effect of wind generation on small-signal stability - a new zealand example. In *Proc. of the IEEE Power & Energy Society General Meeting*, pages 5217–5224, 2008. 24, 25, 26, 28

[56] L. Meegahapola, D. Flynn, J. Kennedy, and T. Littler. Impact of wind generation mix on transient stability for an interconnected power system. In *Proc. of the European Wind Energy Conference (EWEC'09)*, 2009. 24, 25, 28

[57] D. Thakur and N. Mithulananthan. Influence of constant speed wind turbine generator on power system oscillation. *Electric Power Components and Systems*, 37:478–494, 2009. 25, 28, 46

[58] H. Ahmadi, H. Ghasemi, and H. Lesani. A Comparative Small Signal Stability Analysis of PMSG and SCIG-Based Wind Farms. In *Proc. of the 25th Internation Power System Conference (PSC 2010)*, 2010. 25, 26, 28

[59] T. R. Ayodele, A. A. Jimoh, J. L. Munda, and J. T. Agee. The Influence of Wind Power on the Small Signal Stability of a Power System. In *Proc. of the International Conference on Renewable Energies and Power Tech 2007 Quality (ICREPQ'11)*, 2011. 25, 28

[60] J. Zhang, A. Dyśko, J. O'Reailly, and W.E. Leithead. Modelling and performance of fixed-speed induction generators in power system oscillation stability studies. *Electric Power Systems Research*, 78:1416–1424, 2008. 25, 28, 69, 92

[61] J. Arai, T. Dei, S. Takai, and K. Takagi. Study on application of Fixed Speed Generator for Wind Power Generation. In *Proc. of the International Conference on Electrical Engineering*, 2009. 25, 28

[62] H.A. Pulgar-Painemal. *Wind Farm Model for Power System Stability Analysis*. PhD thesis, University of Illinois at Urbana-Champaign, 2010. 25

[63] S. Yuanzhang, W. Lixin, L. Guojie, and L. Jin. A review on analysis and control of small signal stability of power systems with large scale integration of wind power. In *Proc. of the International Conference on Power System Technology (POWERCON2010),*, 2010. 25

[64] O. Anaya-Lara, F.M. Hughes, N. Jenkins, and G. Strbac. Influence of wind farms on power system dynamic and transient stability. *Wind Engineering*, 30:107–127, 2006. 25, 28

[65] C. Wang, L. Shi, L. Wang, and Y. Ni. Small Signal Stability Analysis Considering Grid-Connected Wind Farms of DFIG Type. In *Proc. of the IEEE Power and Energy Society General Meeting - Conversion and Delivery of Electrical Energy in the 21st Century*, pages 1–6, 2008. 25, 28

[66] E. Muljadi, C.P. Butterfield, B. Parsons, and A. Ellis. Effect of variable speed wind turbine generator on stability of a weak grid. *IEEE Transactions on Energy Conversion*, 22:29–36, 2007. 25, 28

[67] G. Tsourakis, B.M Nomikos, and C. Vournas. Effect of wind parks with doubly fed asynchronous generators on small-signal stability. *Electric Power Systems Research*, 79:190–200, 2009. 25, 26, 27, 28, 29

[68] J.L. Rueda and F. Shewarega. Small signal stability of power systems with large scale wind power integration. In *Proc. of the XIII Encuentro Regional Iberoamericano de CIGR*, number XIII/PI-C1 -22, 2009. 25, 28

[69] N. Boonpirom and K. Paithoonwattanakij. The small signal stability analysis of doubly-fed induction generator in wind farm system. In *Proc. of the Australasian Universities Power Engineering Conference (AUPEC'06)*, 2006. 25, 28

[70] A. Mendonça and J.A. Peças-Lopes. Impact of large scale wind power integration on small signal stability. In *Proc. of the International Conference on Future Power Systems,*, 2005. 26, 28

[71] K. Elkington, V. Knazkins, and M. Ghandhari. On the stability of power systems containing doubly fed induction generator-based gen-

eration. *Electric Power System Research*, 78:1477–1484, 2008. 26, 73, 99, 101

[72] R.D. Fernández, R.J. Mantz, and P.E. Battaiotto. Potential contribution of wind farms to damp oscillations in weak grids with high wind penetration. *Renewable and Sustainable Energy Reviews*, 12:1692–1711, 2008. 26, 27, 28, 40, 41, 42

[73] J.C. Muñoz and C.A. Cañizares. Comparative Stability Analysis of DFIG-based Wind Farms and Conventional Synchronous Generators. In *Proc. of the Power Systems Conference and Exposition*, 2011. 26, 27, 28

[74] Ch. Eping, J. Stenzel, M. Pöller, and H. Müller. Impact of large scale wind power on power system stability. In *Proc. of the Fifth International Workshop on Large-Scale Integration of Wind Power and Transmission Networks for Offshore Wind Farms*, 2005. 26, 27, 28, 46

[75] F. Wu, Z.P. Zhang, K. Godfrey, and P. Ju. Small signal stability analysis and optimal control of a wind turbine with doubly fed induction generator. *IET Generation. Transmission and Distribution*, 1:751–761, 2007. 27, 28, 37

[76] F. Wu, X.P. Zhang, and P. Ju. Small signal stability analysis and control of the wind turbine with the direct-drive permanent magnet generator integrated to the grid. *Electric Power Systems Research*, 79:1661–1667, 2009. 26, 28, 29

[77] N. Ullah and T. Thiringer. Effect of operational modes of a wind farm on the transient stability nearby generators and on power oscillations: a nordic grid study. *Wind Energy*, 11:63–73, 2008. 26, 28

[78] T. Knüppel, V. Akhmatov, J.N. Nielsen, K.H. Jensen, A. Dixon, and J. Østergaard. Small-Signal Stability Analysis of Full-Load Converter Interfaced Wind Turbines. In *Proc. of the 8th International Workshop on Large-Scale Integration of Wind Power into Power Systems as well as on Transmission Networks for Offshore Wind Farms*, pages 531–538, 2009. 26, 28

[79] T. Knüppel, V. Akhmatov, J.N. Nielsen, K.H. Jensen, A. Dixon, and J. Østergaard. On Small-Signal Stability of Wind Power System with Full-Load Converter Interfaced Wind Turbines. In *Proc. of the WINDPOWER 2010 Conference & Exhibition*, 2010. 26, 28

[80] H. Müller, M. Pöller, A. Basteck, M. Tilscher, and J. Pfister. Grid compatibility of variable speed wind turbines with directly coupled synchronous generator and hydro-dynamically controlled gearbox. In *Proc. of the 6th International Workshop on Large-Scale Integration of Wind Power and Transmission Networks for Offshore Wind Farms*, pages 307–315, 2006. 26

[81] A. Tabesh and R. Iravani. Transient behavior of a fixed-speed grid-connected wind farm. In *Proc. of the International Conference on Power Systems Transients (IPST'05)*, 2005. 27

[82] G. Ramtharan, N. Jenkins, O. Anaya-Lara, and E. Bossanyi. Influence of rotor structural dynamics representations on the electrical transient performance of fsig and dfig wind turbines. *Wind Energy*, 10:293–301, 2007. 27

[83] T. Burton, D. Shape, N. Jenkins, and E. Bossanyi. *Wind Eenergy: Handbook*. John Wiley and Sons, 2001. 28, 29, 31

[84] M. Rahimi and M. Parniani. Dynamic behavior and transient stability analysis of fixed speed wind turbines. *Renewable Energy*, 34:2613–2624, 2009. 29

[85] S. Papathanassiou and P. Papadopoulos. Mechanical stresses in fixed-speed wind turbines due to network disturbances. *IEEE Transactions on Energy Conversion*, 16:361–367, 2001. 29

[86] A.D. Hansen, F. Iov, P. Sørensen, N. Cutululis, C. Jauch, and F. Blaajberg. Dynamic wind turbine models in power system simulation tool DIgSILENT. Technical report, RISØ - Aalborg University, 2007. 29

[87] Erik Hau. *Wind Turbine: Fundamentals, Technologies, Applications, Economics*. Springer, 2006. 29

[88] Y. Ulianov-López and J.A. Dominguez-Navarro. Small signal stability analysis of wind turbines with squirrel cage induction generators. In *Proc. of the IEEE/PES Transmission and Distribution Conference and Exposition: Latin America,*, pages 1–10, 2008. 29

[89] F. Mei and B.C Pal. Modal analysis of a grid connected doubly-fed induction generator. *IEEE Transaction on Energy Conversion*, 22:728–736, 2007. 29

[90] L. Lin, L. Song, W. Li, and S. Jing. Modal analysis concerning the control mode of doubly-fed induction generator. In *Proc. of the International Conference on Sustainable Power Generation and Supply*, pages 1–6, 2009. 29

[91] J.R. Massing and H. Pinheiro. Small Signal Stability of DFIG with Series Grid-Side Converter. In *Proc. of the Brazilian Power Electronics Conference, (COBEP '09)*, pages 711–718, 2009. 29

[92] L.H. Yang, J. Østergaard, Z.Y. Dong, and X.K. Ma. Hopf bifurcation and eigenvalue sensitivity analysis of doubly fed induction generator wind turbine system. In *Proc. of the IEEE Power and Energy Society General Meeting*, pages 1–6, 2010. 29

[93] L. Yang, Z. Xu, J. Østergaard, Z.Y. Dong, K.P. Wong, and X. Ma. Oscillatory stability and eigenvalue sensitivity analysis of a dfig wind turbine system. *IEEE Transactions on Energy Conversion*, 26:328 – 339, 2011. 29

[94] H. Geng, D. Xu, B. Wu, and G. Yang. Comparison of oscillation damping capability in three power control strategies for PMSG-based WECS. *Wind Energy*, 14:389–406, 2011. 29, 37

[95] F. D. Bianchi, H. D. Battista, and R.J. Mantz. *Wind Turbine Control Systems*. Springer, 2007. 30, 32, 33

[96] J. Tamura, T. Yamazki, M. Ueno, Y. Matsumura, and S. Kimoto. Transient stability simulation of power system including wind generator by PSCAD/EMTDC. In *Proc. of the IEEE Porto Power Tech Conference*, 2001. 30

[97] J.F. Manwell, J.G. McGowan, and A.L. Rogers. *Wind Energy Explained: theory, design and application*. John Wiley and Sons, 2009. 30

[98] A.J.G. Westlake, J.R. Bumby, and E. Spooner. Damping the power-angle oscillations of a permanent-magnet synchronous generator with particular reference to wind turbine applications. *IEE Proceedings of Electric Power Applications*, 143(3):269–280, 1996. 30

[99] S.M. Muyeen, M.H. Ali, R. Takahashi, T. Murata, and J. Tamura. Damping of blade-shaft torsional oscillations of wind turbine generator. *Electric Power Components and Systems*, 36:195–211, 2008. 30, 42

[100] S.M. Muyeen, M.H. Ali, R. Takahashi, T. Murata, J. Tamura, Y. Tomaki, A. Sakahara, and E. Sasano. Blade-Shaft Torsional Oscillation Minimization of Wind Turbine Generator System by Using STATCOM/ESS. In *Power Tech 2007*, pages 1–6, 2007. 30, 42

[101] M.S. El-Moursi, B. Bak-Jensen, and M.H. Abdel-Rahman. Novel statcom controller for mitigating ssr and damping power system oscillations in a series compensated wind park. *IEEE Transactions on Power Electronics*, 25 (2):429–441, 2010. 31

[102] E. Bossanyi. Wind turbine control for load reduction. *Wind Energy*, 6:229–244, 2003. 31

[103] J. Conroy and R. Watson. Torsional damping control of gearless full-converter large wind turbine generators with permanent magnet synchronous machines. *Wind Engineering*, 31:325–340, 2007. 31

[104] B. Badrzadeh, S. K. Salman, and K. S. Smith. Assessment and enhancement of grid fault-induced torsional oscillations for induction generator-based wind turbines. In *Proc. of the IEEE/PES Power Systems Conference and Exposition.*, 2009. 31

[105] Z.X Xing, L.Z Liang, H.Y Guo, and X.D Wang. Damping Control Study of the Drive Train od DFIG Wind Turbine. In *Proc. of the International Conference on Energy and Environment Technology*, pages 576–579, 2009. 31

[106] E.B. Muhando, T. Senjyu, A. Yona, H. Kinjo, and T. Funabashi. Disturbance rejection by dual pitch control and self-tuning regulator for wind turbine generator parametric uncertainty compensation. *IET Control Theory & Applications*, 1:1431–1440, 2007. 31

[107] H. De Battista, P.F. Puleston, R.J. Mantz, and C.F. Christiansen. Sliding mode control of wind energy systems with doig - power efficiency and torsional dynamics. *IEEE Transactions on Power Systems*, 15 (2):728–734, 2000. 31

[108] S. Suryanarayanan, A. Avagliano, and C. Barbu. Vibration damping methods for variable speed wind turbines, September 2008. US 7,423,352B2. 32

[109] M. Laubrock, T. P. Woldmann, and S. Bilges. Method for the active damping of the drive train in a wind energy plant, March 2009. US 7,501,798B2. 32

[110] G. K. Andersen, K. B. Larsen, and F. B. Bendixen. Variable speed wind turbine, a resonant control system, a method for operating a variable speed wind turbine, use of a resonant control system and use of a method in a variable speed wind turbine, March 2011. US7,902,686B2. 32

[111] P. Nielsen. Damping of Drive Train Oscillations by DC-Link Absortion Means, April 2011. WO 2011/045263A1. 32

[112] José Luis Domínguez-García, Oriol Gomis-Bellmunt, Lluís Trilla-Romero, and Adrià Junyent-Ferré. Vector control of squirrel cage induction generator for wind power. In *Proc. of the International Conference on Electrical Machines (ICEM2010)*, 2010. 32

[113] F.M. Hughes, O. Anaya-Lara, N. Jenkins, and G. Strbac. Control of DFIG-based wind generation for power network support. *IEEE Transactions on Power Systems*, 20:1958–1966, 2005. 32, 35, 39, 42

[114] C. Jauch. *Stability and Control of Wind Farms in Power Systems*. PhD thesis, Aalborg University - Risø, 2006. 33, 42

[115] C. Jauch, T. Cronin, P. Sørensen, and B.B. Jensen. Design of a wind turbine pitch angle controller for power system stabilization. *Renewable Energy*, 32:2334–2349, 2007. 33, 42

[116] C. Jauch, T. Cronin, P. Sørensen, and B.B. Jensen. A fuzzy logic pitch angle controller for power system stabilization. *Wind Energy*, 10:19–30, 2007. 33, 42, 45

[117] E. Valsera-Naranjo, A. Sumper, O. Gomis-Bellmunt, A. Junyent-Ferré, and M. Martínez-Rojas. Pitch control system design to improve frequency response capability of fixes-speed wind turbine systems. *European Transactions on Electrical Power*, 21(7):1984–2006, 2011. 34

[118] G. Ramtharan, J.B. Ekanayake, and N. Jenkins. Frequency support from doubly fed induction generator wind turbines. *IET Renewable Power Generation*, 1:1–9, 2007. 34

[119] P. Moutis, E. Loukarakis, S. Papathanasiou, and N.D. Hartziargyriou. Primary load-frequency control from pitch-controlled wind turbines. In *IEEE Power Tech 2009*, pages 1–7, 2009. 34

[120] M.H. Ali and W. Bin. Comparison of Stabilization Methods for Fixed-Speed Wind Generator Systems. *IEEE Transaction on Power Delivery*, 25:323–331, 2010. 34, 42

[121] M. H. Ali, M. Park, I.K. Yu, T. Murata, and J. Tamura. Improvement of Wind-Generator Stability by Fuzzy-Logic-Controlled SMES. *IEEE Transactions on Industry Applications*, 45:1045–1051, 2009. 34, 42

[122] M. J. Hossain, H. R. Pota, V. A. Ugrinovski, and R. A. Ramos. Simultaneous STATCOM and Pitch Angle Control for Improved LVRT Capability of Fixed-Speed Wind Turbines. *IEEE Transactions on Sustainable Energy*, 1:142–151, 2010. 34, 42

[123] J. Morren. *Grid support by power electronic converters of Distributed Generation Units*. PhD thesis, Technische Universiteit Delft, 2006. 35

[124] E.V. Larsen and D.A. Swann. Applying Power System Stabilizers. Part I: Genearl Concepts. *IEEE Transactions on Power Apparatus and Systems*, PAS-100:3017–3024, 1981. 35, 46

[125] O. Anaya-Lara, F. M. Hughes, N. Jenkins, and G. Strbac. Power System Stabilizer for a Generic DFIG-Based Wind Turbine Controller. In *Proc. of the 8th IEE International Conference on AC and DC Power Transmission*, pages 145–149, 2006. 35, 39, 42, 45

[126] F.M. Hughes, O. Anaya-Lara, N. Jenkins, and Strbac G. A Power Sytem Stabilizer for DFIG-Based Wind Generation. *IEEE Transactions on Power Systems*, 21:763–772, 2006. 36, 39, 42, 45

[127] D.P. Ke, C.Y. Chung, and Y. Xue. Controller Design for DFIG-based Wind Power Generation to Damp Interarea Oscillation. In *Proc. of the 5th International Conference on Critical Infrastructure (CRIS)*, pages 1–6, 2010. 36, 39, 42

[128] F.M. Hughes, O. Anaya-Lara, G. Ramatharan, N. Jenkins, and G. Strbac. Influence of Tower Shadow and Wind Trurbulence on the Performance of Power System Stabilizers for DFIG-Based Wind Farms. *IEEE Transactions on Energy Conversion*, 23:519–528, 2008. 36, 39, 42

[129] Y. Mishra, S. Mishra, M. Tripathy, N. Senroy, and Z.Y. Dong. Improving Stability of a DFIG-Based Wind Power System with Tuned Damping Controller. *IEEE Transactions on Energy Conversion*, 24:650–660, 2009. 36, 42

[130] Y. Mishra, S. Mishra, F. Li, Z.Y. Dong, and R.C. Bansal. Small-Signal Stability Analysis of a DFIG-Based Wind Power System Under Different Modes of Operation. *IEEE Transactions on Energy Conversion*, 24:972–982, 2009. 36, 42

[131] N Kshatriya, U.D. Annakkage, F.M. Hughes, and A.M. Gole. Optimized Partial Eigenstructure Assignment-Based Design of a Combined PSS and Active Damping Controller for a DFIG. *IEEE Transactions on Power Systems*, 25:866–876, 2010. 36, 42

[132] N. D. Caliao, G. Ramatharan, J. Ekanayake, and N. Jenkins. Power oscillation damping controller for fully rated converter wind turbines. In *Proc. of the International Universities' Power Engineering Conference (UPEC2010)*, 2010. 36, 39, 42, 46

[133] K. Elkington, M. Ghandhari, and L. Söder. Using power system stabilisers in doubly fed induction generators. In *Proc. of the Australasian Universities Power Engineering Conference (AUPEC'08)*, pages 1–6, 2008. 36, 38, 39, 42, 73, 99, 108

[134] K. Elkington. *Modelling and control of doubly fed induction generators in power systems: Towards understanding the impact of large wind parks on power system stability.* PhD thesis, KTH, 2009. 36, 38, 39, 42

[135] J. L. Domínguez-García, O. Gomis-Bellmunt, F. Bianchi, and A. Sumper. Power system stabilizer control for wind power to enhance power system stability. In *Proc. of 5th International Scientific Conference on Physics and Control*, pages 1–6, 2011. 37, 39, 42

[136] G. Tsourakis and C. Vournas. A controller for wind generators to increase damping of power oscillations. In *Proc. of the IEEE International Symposium on Circuits and Systems*, page 2195, 2010. 37, 39

[137] Z. Miao, L. Fan, D. Osborn, and S. Yuvarajan. Control of DFIG based wind generation to improve inter-area oscillations damping. In *Proc. of the IEEE Power and Energy Society General Meeting - Conversion and Delivery of Electrical Energy in the 21th Century*, pages 1–7, 2008. 37, 42

[138] Z. Miao, L. Fan, D. Osborn, and S. Yuvarajan. Control of DFIG-Based Wind Generation to Improve Interarea Oscillation Damping.

IEEE Transaction on Energy Conversion, 24:415–422, 2009. 37, 39, 42, 45

[139] L. Fan, H. Yin, and Z. Miao. On Active/Reactive Power Modulation of DFIG-Based Wind Generation for Interarea Oscillation Damping. *IEEE Transactions on Energy Conversion*, 26:513–521, 2011. 37, 38, 39, 42

[140] A. Mendonça and J.A. Peças-Lopes. Simultaneous tuning of power system stabilizers installed in DFIG-Based wind generation. In *Power Tech 2007*, pages 219–224, 2007. 37, 42

[141] C. Gallardo and P. Ledesma. Analysis of inter-area mode oscillations using a PSS for Variable Speed Wind Power Converter and Modal decomposition. In *Proc. of the 7th WSEAS International Conference on Application of Electrical Engineering (AEE'08)*, pages 160–168, 2008. 37

[142] C. Gallardo. Design and coordination of wind stabilizers for damping power system oscillations using modal decomposition. In *Proc. of the IEEE International Electric Machines and Drives Conference*, pages 1815–1819, 2009. 37

[143] C. Gallardo and P. Ledesma. Damping of inter-area mode oscillations with high penetration of the power system in wind. In *Proc. of the 34th Annual Conference of the IEEE Industrial Electronics Society*, pages 2066–2071, 2008. 37

[144] P. Ledesma and C. Gallardo. Contribution of variable-speed wind farms to damping of power system oscillations. In *Proc. of the Power Tech 2007*, pages 1698–1702, 2007. 37

[145] G. Tsourakis, B.M. Nomikos, and C.D. Vournas. Contribution of doubly fed wind generators to oscillation damping. *IEEE Transactions on Energy Conversion*, 24:783–791, 2009. 38, 42, 46, 48

[146] C. Jauch. Transient and dynamic control of a variable speed wind turbine with synchronous generator. *Wind Energy*, 10:247–269, 2007. 38

[147] H. Yin, L. Fan, and Z. Miao. Reactive power modulation for inter-area oscillation damping of DFIG-based wind generation. In *Proc. of the IEEE Power and Energy Society General Meeting*, pages 1–9, 2010. 39, 42

[148] B. Gong, D. Xu, and B. Wu. Network damping capability of DFIG-based Wind Farm. In *Proc. of the IEEE Energy Conversion Congress and Exposition*, 2010. 40, 42

[149] C. Martinez, G. Joos, and B.T Ooi. Power system stabilizers in variable speed wind farms. In *Proc. of the Power & Energy Society General Meeting*, pages 1–7, 2009. 40, 41, 42, 45, 46

[150] R. D. Fernández, P. E. Battaiotto, and R. J. Mantz. Wind farm non-linear control for damping electromechanical oscillations of power systems. *Renewable Energy*, 33:2258–2265, 2008. 40, 41, 42

[151] J. L. Domínguez-García, O. Gomis-Bellmunt, F. Bianchi, and A. Sumper. Power oscillation damping supported by wind power: A review. *Renewable and Sustainable Energy Reviews*, 16(7):4994–5006, 2012. 45, 64

[152] J. L. Domínguez-García, O. Gomis-Bellmunt, F. Bianchi, and A. Sumper. Pss controller for wind power generation systems. *International Journal of Modern Physics B*, 26(25):1246012, 2012. 45

[153] J. L. Domínguez-García, O. Gomis-Bellmunt, F. Bianchi, A. Sumper, and A. Sudri-Andreu. Power system stabiliser capability of offshore wind power plants. In *Proceedings of European Wind Energy Conference & Exhibition 2012 (EWEA)*, 2012. 45, 46

[154] M. Klein, G.J. Rogers, and P. Kundur. A fundamental study of inter-area oscillations in power systems. *IEEE Transactions on Power Systems*, 6(3):914–921, 1991. 47

[155] L. Rouco and F.L. Pagola. An eigenvalue sensitivity approach to location and controller design of controllable series capacitors for damping power system oscillations. *IEEE Trans. Power Systems*, 12(4):1660–1666, 1997. 63

[156] A.M.A. Hamdan. An investigation of the significance of singular value decomposition in power system dynamics. *Electrical Power and Energy Systems*, 21:417–424, 1999. 63, 67

[157] M.M. Farsangi, Y.H. Song, and K.Y. Lee. Choice of facts device control inputs for damping interarea oscillations. *IEEE Transactions on Power Systems*, 19(2):1135–1143, 2004. 63, 69, 92

[158] M.M. Farsangi, H. Nezamabadi-pour, Y.H. Song, and K.Y. Lee. Placement of SVCs ans selection of stabilizing signals in power systems. *IEEE Transactions on Power Systems*, 22(3):1061–1071, 2007. 63, 69

[159] A. Heniche and I. Kamwa. Assessment of two methods to select wide-area signals for power system damping control. *IEEE Transactions on Power Systems*, 23(2):572–581, 2008. 63, 68, 91

[160] Y. Zhang and A. Bose. Design of wide-area damping controllers for interarea oscillations. *IEEE Transactions on Power Systems*, 23(3):1136–1143, 2008. 63

[161] Y. Li, C. Rehtanz, S. Rüberg, L. Luo, and Y. Cao. Assessment and choice of input signals for multiple hvdc and facts wide-area damping controllers. *IEEE Transactions on Power Systems*, 2012. 63, 92

[162] J.V. Milanović and A.C. Serrano Duque. Identification of electromechanical modes and placement of PSSs using relative gain array. *IEEE Transactions on Power Systems*, 19(1):410–417, 2004. 63

[163] J. L. Domínguez-García, F.D. Bianchi, and O. Gomis-Bellmunt. Control signal selection for damping oscillations with wind power plants based on fundamental limitations. *IEEE Trans. Power Systems*, (Submitted), 2012. 63, 69

[164] E. Licéaga-Castro, J. Licéaga-Castro, and C. E. Ugalde-Loo. Beyond the exitence of diagonal controllers: from the relative gain array to the multivariable structure function. In *44th IEEE CDC, and ECC*, 2005. 64, 70, 71, 72, 73, 81

[165] C. E. Ugalde-Loo, E. Acha, and E. Licéaga-Castro. Fundamental analysis of the electromechanical oscillation damping control loop of the static var compensator using individual channel analysis and design. *IEEE Transactions on Power Delivery*, 25(4):3053–3069, 2010. 64

[166] C. E. Ugalde-Loo. *Dynamical Modelling of Power Systems with Power Electronic Controllers using Individual Channel Analysis and Design.* PhD thesis, Universisty of Glasgow, 2009. 64

[167] S. Skogestad and I. Postlethwaite. *Multivariable Feedback Control - Analysis and Design.* John Wiley & Sons, Chichester, (UK), 2nd edition, 2007. 64, 66, 67, 69, 70, 83

[168] K. Ogata. *Modern Control Engineering*. Prentice Hall, 1997. 68

[169] F.L. Pagola, I.J. Pérez-Arriaga, and G.C. Verghese. On sensitivities, residues and participations: Applications to oscillatory stability analysis and control. *IEEE Trans. Power Systems*, 4(1):278–285, 1989. 68, 76

[170] A. Heniche and I. Kamwa. Control loops selection to damp inter-area oscillations of electrical networks. *IEEE Transactions on Power Systems*, 17(2):378–384, 2002. 68, 69

[171] J.S. Freudenberg and D.P. Looze. Right half plane poles and zeros and design tradeoffs in feedback systems. *IEEE Transactions on Automatic Control*, 30(6):555–565, 1985. 69, 79

[172] J.S. Freudenberg, C.V. Hollot, R.H. Middleton, and V. Toochinda. Fundamental design limitations of the general control configuration. *IEEE Transactions on Automatic Control*, 48(8):1355–1370, 2003. 69, 92, 93, 95

[173] M. Van der Wal and B. de Jager. A review of methods for input/output selection. *Automatica*, 37:487–510, 2001. 69

[174] W.E. Leithead and J. O'Reilly. m-input m-output feedback by individual channel design. part1. structural issues. *International Journal of Control*, 56(6):1347–1397, 1992. 71, 72

[175] J. O'Reilly and W.E. Leithead. Multivariable control by 'individual channel design'. *Int. Journal of Control*, 54:1–46, 1991. 71, 72

[176] W.E. Leithead and J. O'Reilly. Investigation of the icd structure of systems defined by state-space models. *International Journal of Control*, 60(1):71–89, 1994. 81

[177] J. L. Domínguez-García, F.D. Bianchi, and O. Gomis-Bellmunt. Analysis of the damping contribution of power system stabilisers driving wind power plants. *Wind Energy*, page In Press, 2012. 91

[178] H. Wu, K.S. Tsakalis, and G.T. Heydt. Evaluation of time delay effects to wide-area power system stabilizer design. *IEEE Transactions on Power Systems*, 19(4):1935–1941, 2004. 91

[179] F. Aminifar, M. Fotuhi-Firuzabad, M. Shahidehpour, and A. Safdarian. Impact of WAMS malfunction on power system reliability assessment. *IEEE Transactions on Smart Grid*, 3(3):1302–1309, 2012. 91

[180] V. Wertz, E.I. Silva, G.C. Goodwin, and B. Codrons. Performance limitations arising in the control of power plants. In *17th IFAC World Congress*, 2008. 92

[181] Chi-Tsong Chen. *Linear System Theory and Design*. Oxford University Press, Inc., New York, NY, USA, 3rd edition, 1998. 94

[182] A.M.A. Hamdan and A.M. Elabdalla. Geometric measures of modal controllability and observability of power system models. *Electric Power System Research*, 15(2):147–155, 1988. 95

[183] R.S. Sánchez-Peña and M. Sznaider. *Robust Systems: Theory and Applications*. Wiley, 1998. 95, 96, 114

[184] S. Gordon. SuperGrid to the rescue. *IET Power Engineer*, 20 (5):30–33, 2006. 119

[185] Working Group B4.39. Integration of Large Scale Wind Generation Using HVDC and Power Electronics. Technical report, CIGRE, 2009. 119

[186] Friends of SuperGrid. Position paper on the EC Communication for a European Infrastructure Package: SuperGrid Phase 1. Technical report, Friends of SuperGrid, 2010. 119

[187] Vattenfall Europe, Energitek.dk, and Svenska Kraftnät. An Analysis of Offshore Grid Connection at Kriegers Flak in the Baltic Sea. Technical report, Vattenfall Europe Transmission, Energitek.dk, and Svenska Kraftnät, 2009. 119

[188] P. Breseti, W.L. Kling, R.L. Hendriks, and R. Vailati. HVDC Connection of Offshore Wind Farms to the Transmission System. *IEEE Transactions on Energy Conversion*, 22 (1):37–43, 2007. 119

[189] O. Gomis-Bellmunt, J. Liang, J. Ekanayake, and N. Jenkins. Voltage-current characteristics of multi-terminal HVDC-VSC for offshore wind farms. *Electric Power Systems Research*, 81 (2):440–450, 2011. 119

[190] D. Van Hertem and M. Ghandhari. Multi-terminal VSC HVDC for the european supergrid: Obstacles. *Renewable and Sustainable Energy Reviews*, 14:3156–3163, 2010. 119

[191] V. Lescale, A. Kumar, L. Juhlin, H. Björklund, and K. Nyberg. Challenges with multi-terminal UHVDC transmissions. In *Proceedings of POWERCON2008 & IEEE Power India Conference*, 2008. 119

[192] D. Van Hertem, M. Ghandhari, and M. Delimar. Technical limitations towards a supergrid - a European prospective. In *Proceedings of the IEEE International Energy Conference and Exhibition (EnergyCon)*, 2010. 119

[193] J. Häfner and B. Jacobson. Proactive Hybrid HVDC Breakers - A key innovation for reliable HVDC grids. In *Proceedings of The Electric Power System of the Future, Cigré 2011, Bologna Symposium*, 2011. 119

[194] J. Yang, J. Fletcher, and J. O'Reilly. Multiterminal DC Wind Farm Collection Grid Internal Fault Analysis and Protection Design. *IEEE Transactions on Power Delivery*, 25 (4):2308–2318, 2010. 120

[195] M. Merlin, T. Green, P. Mitcheson, D. Trainer, D. Critchley, and R. Crookes. A new hybrid multi-level voltage-source converter with dc fault blocking capability. In *Proceedings of the 9th IET International Conference on AC and DC Transmission (ACDC)*, 2010. 120

[196] Mainstream Renewable Power. How the supergrid is really going to be built. In *Workshop "Developement of offshore grid in the Baltic/North Sea area" EWEC, Marseille*, 2009. 121

[197] N. Barberis Negra, J. Todorovic, and T. Ackermann. Loss evaluation of HVAC and HVDC transmission solution for large offshore wind farms. *Electric Power Systems Research*, 76:916–927, 2006. 121

[198] D. Lane. Round 3 Offshore Wind Farm Connection Study. Technical report, The Crown State, 2010. 121, 123

[199] National Grid Electricity Transmission. Offshore developement information statement 2010. Technical report, National Grid, 2010. 122, 123, 134, 136

[200] IEC60287: Electric Cables - Calculation of the current rating, 1993. 123

[201] R. King. *Electrical Transmission System for Large Offshore Wind Farms*. PhD thesis, Cardiff University, 2011. 123

[202] G. Moore, editor. *Electric Cables Handbook*. Blackwell, 1997. 123

[203] ABB. XPLE Submarine Cable Systems: Attachment to XLPE Land Cable Systems - Users Guide. 123

[204] P. Nielsen. Offshore Wind Energy Projects: Altener Project, Feasibility Study Guidelines. Technical report, SeaWind, 2003. 123

[205] F. Gatta, A. Geri, S. Lauria, and M. Maccioni. Steady-state operating conditions of very long EHVAC cable lines. *Electric Power Systems Research*, 81:1525–2533, 2011. 123

[206] Working Group B1.19. General guidelines for the integration of a new underground cable system in the network. Technical report, CIGRE, 2004. 123

[207] M. Dicorato, G. Forte, M. Pisani, and M. Trovato. Guidelines for assessment of investment cost for offshore wind generation. *Renewable Energy*, 36 (8):2043–2051, 2011. 127, 131, 132, 133

[208] S. Lundberg. Performance comparison of wind parks. Technical report, Chalmers University of Technology, 2003. 127, 132

[209] M.J. Heathcote. *The J & P Transformer Book: a practical technology of the power transformer*. Newness, 1998. 128

[210] J. Olivares-Galván, F. De León, P. Georgilakis, and R Escarela-Pérez. Selection of cooper against aluminim winding for distribution transformers. *IET Electric Power Applications*, 4 (6):474–485, 2010. 131

[211] I. Martínez de Alegría, J Martín, I. Kortabarria, J. Andreu, and P. Ibañez Ereño. Transmission alternatives for offshore electrical power. *Renewable and Sustainable Energy Reviews*, 13:1027–1038, 2009. 132

[212] Tranche A and Dogger Bank: Project One, October 2010. 136

A

List of Publications

In this chapter, the list of publications both journals and conferences papers, derived from the development of the thesis are presented.

A.1 Journal articles

[**J1**] Domínguez-García, J.L., Gomis-Bellmunt, O., Trilla-Romero, Ll., Junyent-Ferré, A., Indirect Vector Control of Squirrel Cage Induction Generator Wind Turbine, *Computer and Mathematics with Applications, vol 64 (2), pp 102-114 (2012), Elsevier.* DOI: `http://dx.doi.org/10.1016/j.camwa.2012.01.021`

[**J2**] Domínguez-García, J.L., Gomis-Bellmunt, O., Bianchi. F.D., Sumper, A., Power oscillation damping supported by wind power: A review, *Renewable and Sustainable Energy Reviews, vol 16 (7), pp 4994-5006 (2012), Elsevier.* DOI: `http://dx.doi.org/10.1016/j.rser.2012.03.063`

[**J3**] Domínguez-García, J.L., Gomis-Bellmunt, O., Bianchi. F.D., Sumper, A., PSS controller for wind power generation systems, *International Journal of Modern Physics B, vol 26 (25), 1246012 (2012), World Scientific.* DOI: `http://dx.doi.org/10.1142/S0217979212460125`

[**J4**] Domínguez-García, J.L., Rogers, D., Ugalde-Loo, C., Liang, J., Gomis-Bellmunt, O., Effect of non-standard operating frequencies on the economic cost of offshore ac networks, *Renewable Energy, vol 44, pp 267-*

280 (2012), Elsevier. DOI: http://dx.doi.org/10.1016/j.renene.2012.01.093

[**J5**] Domínguez-García, J.L., Bianchi. F.D., Gomis-Bellmunt, O., Analysis of the damping contribution of power system stabilizers driving wind power plants, *Wind Energy, In Press, Wiley.* DOI: http://dx.doi.org/10.1002/we.1574

[**J6**] Domínguez-García, J.L., Bianchi. F.D., Gomis-Bellmunt, O., Control signal selection for damping oscillations with wind power plants based on fundamental limitations, *Accepted for publication in IEEE Transactions on Power Systems*

[**J7**] Domínguez-García, J.L., Ugalde-Loo, C., Bianchi. F.D., Gomis-Bellmunt, O., Input-output signal selection for damping of power system oscillations using wind power plants, *Submitted to International Journal of Electric Power & Energy Systems*

A.2 Conference articles

[**C1**] Domínguez-García, J.L., Gomis-Bellmunt, O., Trilla-Romero, Ll. and Junyent-Ferré, A., Vector Control of Squirrel Cage Induction Generator for Wind Power. *In Proceedings of International Conference on Electrical Machines, (ICEM 2010), 6-8 of September of 2010, Rome (Italy)* DOI: http://dx.doi.org/10.1109/ICELMACH.2010.5608021

[**C2**] Domínguez-García, J.L., Gomis-Bellmunt, O., Bianchi, F., Sumper, A., Power System Stabilizer Control for Wind Power to Enhance Power System Stability. *In Proceedings of Physics and Control Congress (PhysCon 2011), 5-8 of September of 2011, León (Spain)* Online: http://lib.physcon.ru/doc?id=5b6c5ada5411

[**C3**] Domínguez-García, J.L., Gomis-Bellmunt, O., Bianchi, F., Sudrià-Andreu, A. Power Control of Voltage Source Converter for Distributed Generation. *In Proceedings of Physics and Control Congress (PhysCon 2011), 5-8 of September of 2011, León (Spain)* Online: http://lib.physcon.ru/doc?id=e0232adb87e7

[**C4**] Domínguez-García, J.L.,Gomis-Bellmunt, O., Sudrià-Andreu, A., Trilla-Romero, Ll., Indirect Vector Control of an Induction Generator with LVRT Capability *In Proceedings of European Conference on Power*

Electronics and Applications (EPE 2011), 30 of August -1 of September of 2011, Birmingham (UK)

[**C5**] Domínguez-García, J.L., Gomis-Bellmunt, O., Bianchi, F., Sumper, A., Sudrià-Andreu, A., Power System Stabiliser Capability of Offshore Wind Power Plants *Presented as lecture session at EWEA 2012, 16-19 of April of 2012, Copenhagen (Denmark)*

A.3 Other publications

Within this section other relevant publications not directly related to the thesis are introduced.

[**O1**] Marzband, M., Sumper, A., Ruiz-Alvárez, A., Domínguez-García, J.L., Tomoiaga, B., Experimental evaluation of a real time energy management system for stand-alone microgrids in day-ahead markets, *Applied Energy, vol 106, pp 365-376 (2013), Elsevier.* DOI: `http://dx.doi.org/10.1016/j.apenergy.2013.02.018`

[**O2**] García-Planas, M.I., Domínguez-García, J.L., Alternative tests for functional and pointwise output-controllability of linear time-invariant systems, *System & Control letters, vol 62, pp 382-387 (2013), Elsevier.* DOI: `http://dx.doi.org/10.1016/j.sysconle.2013.02.003`

[**O3**] De Prada Gil, M., Mancilla-David, F., Domínguez-García, J.L., Muljadi, E., Singh, M., Gomis-Bellmunt, O., Sumper, A., Contribution of Type–2 Wind Turbines to Sub-Synchronous Resonance Damping, *Submitted to International Journal of Electric Power & Energy Systems*

[**O4**] De Prada Gil, M., Domínguez-García, J.L., Mancilla-David, F., Muljadi, E., Singh, M., Gomis-Bellmunt, O., Sumper, A., Type–2 Wind Turbine with Additional Sub-Synchronous Resonance Damping, *In Proceedings of Fifth Annual Green Technologies Conference (GreenTech 2013), 4-5 of April of 2013, Denver (USA)*

[**O5**] Domínguez-García, J.L., García-Planas, M.I. Output controllability and steady output controllability analysis of fixed wind speed turbine. *In Proceedings of Physics and Control Congress (PhysCon 2011), 5-8 of September of 2011, León (Spain)* Online: `http://lib.physcon.ru/doc?id=ffc6b99b2e5f`

B

Power system linearization of synchronous machine infinite bus power system with wind power generation

The nonlinear synchronous machine infinite bus with wind power plants power system analyzed in Chapters 5 and 6 are governed by the synchronous generator equations [36]

$$\begin{aligned}
\dot{\delta} &= \omega - \omega_s, \\
\dot{\omega} &= \frac{\omega_s}{2H}\left(P_m - \frac{E'V_1}{X'}\sin(\delta - \theta_1) - D\omega\right), \\
\dot{E}' &= \frac{1}{T_0}\left(E_f - \frac{X}{X'}E' + \frac{X - X'}{X'}V_1\cos(\delta - \theta_1)\right),
\end{aligned} \tag{B.1}$$

where δ, ω and E' are the rotor angle, the rotor frequency and the internal electromagnetic field (EMF) of the synchronous generator, respectively. The transient reactance and the rotor reactance of the synchronous generator are given by X' and X, respectively, T_0 is the open-circuit time constant, P_m is the mechanical input power, ω_s denotes the synchronous reference, D is the mechanical damping, H refers to the inertia constant and E_f excitation voltage.

The power flow equations are given by

$$
\begin{aligned}
P_g &= \frac{E'V_1}{X'}\sin(\delta-\theta_1),\\
Q_g &= \frac{E'^2}{X'}-\frac{E'V_1}{X'}\cos(\delta-\theta_1),\\
P_{12} &= \frac{V_1V_2}{X_{12}}\sin(\theta_1-\theta_2),\\
Q_{12} &= \frac{V_1^2}{X_{12}}-\frac{V_1V_2}{X_{12}}\cos(\theta_1-\theta_2),\\
P_{wt2} &= \frac{V_{wt}V_2}{X_{wt2}}\sin(\theta_{wt}-\theta_2),\\
Q_{wt2} &= \frac{V_{wt}^2}{X_{wt2}}-\frac{V_{wt}V_2}{Xwt2}\cos(\theta_{wt}-\theta_2),\\
P_{2\infty} &= \frac{V_2V_\infty}{X_{2\infty}}\sin(\theta_2-\theta_\infty),\\
Q_{2\infty} &= \frac{V_2^2}{X_{2\infty}}-\frac{V_2V_\infty}{X_{2\infty}}\cos(\theta_2-\theta_\infty),
\end{aligned}
\tag{B.2}
$$

where P_i and Q_i ($i \in \{g, 12, wt2, 2\infty\}$) are the active and reactive power transferred through the electrical lines, [V_i and θ_i ($i \in \{g, 12, wt2, 2\infty\}$) represent the voltage magnitude and phase angle of the power system busses, and X_i ($i \in \{g, 12, wt2, 2\infty\}$) are the reactances of the lines.

As disturbance w causing the oscillations is considered the mechanical power reference of the synchronous generator T_m. The signal to be controlled, that is the signals on which the oscillation must be damped, is the angle of the synchronous machine $z = \delta$. As possible control signals u are considered the active power P_{wt} and the reactive power Q_{wt} and as local measure y the voltage magnitude measured at the WPP connection point V_{wt} and the phase angle of the voltage WPP bus θ_{wt}.

B.1 Linearization

After linearizing the nonlinear model compound by (B.1) and (B.2), the following state equations are obtained

$$\begin{aligned} \dot{x} &= Ax + B_w w + B_u u, \\ z &= C_z x, \\ y &= C_y x + D_{yu} u, \end{aligned} \tag{B.3}$$

where

$$\begin{aligned} x &= \begin{bmatrix} \Delta\delta \\ \Delta\omega \\ \Delta E' \end{bmatrix}; \\ u &= \begin{bmatrix} \Delta P_{wt} \\ \Delta Q_{wt} \end{bmatrix}; \\ w &= [\Delta T_m]; \\ y &= \begin{bmatrix} \Delta V_{wt} \\ \Delta\theta_{wt} \end{bmatrix}; \\ z &= [\Delta\delta]. \end{aligned} \tag{B.4}$$

with Δ denotes the incremental values, and the rest of parameters are defined as:

$$\begin{aligned} A &= A_1 + M_1 A_2, \\ B_u &= M_1 N_1 M_5 N_2, \\ B_w &= \begin{bmatrix} 0 & 0 \\ \dfrac{1}{M} & 0 \end{bmatrix}, \\ C_z &= \begin{bmatrix} 1 & 0 & 0 \end{bmatrix}, \\ C_y &= -M_6^{-1} M_7 N_2 (M_2 - M_3 N_1 M_2), \\ D_{yu} &= M_6^{-1} - M_6^{-1} M_7 N_2, \end{aligned} \tag{B.5}$$

The matrices presented in the set of equations (B.5) are described as follows,

$$A_1 = \begin{bmatrix} 0 & 1 & 0 \\ \dfrac{-E_0' V_{10}}{M \cdot X'} \cos(\delta_0 - \theta_{10}) & \dfrac{-D}{M} & \dfrac{-V_{10}}{M \cdot X'} \sin(\delta_0 - \theta_{10}) \\ \dfrac{-X + X'}{T_0 \cdot X'} V_{10} \sin(\delta_0 - \theta_{10}) & 0 & \dfrac{-X}{T_0 \cdot X'} \end{bmatrix}, \quad \text{(B.6)}$$

$$M_1 = \begin{bmatrix} 0 & 0 \\ \dfrac{-E_0'}{M \cdot X'} \sin(\delta_0 - \theta_{10}) & \dfrac{E_0' V_{10}}{M \cdot X'} \cos(\delta_0 - \theta_{10}) \\ \dfrac{X - X'}{T_0 \cdot X'} \cos(\delta_0 - \theta_{10}) & \dfrac{X - X'}{T_0 \cdot X'} V_{10} \sin(\delta_{10} - \theta_{10}) \end{bmatrix}, \quad \text{(B.7)}$$

$$M_2 = \begin{bmatrix} \dfrac{-E_0' V_{10}}{X'} \cos(\delta_0 - \theta_{10}) & 0 & \dfrac{V_{10}}{X'} \sin(\delta_0 - \theta_{10}) \\ \dfrac{E_0' V_{10}}{X'} \sin(\delta_0 - \theta_{10}) & 0 & \dfrac{2E_0'}{X'} - \dfrac{V_{10}}{X'} \cos(\delta_0 - \theta_{10}) \end{bmatrix}, \quad \text{(B.8)}$$

$$M_3 = \begin{bmatrix} \dfrac{E_0'}{X'} \sin(\delta_0 - \theta_{10}) & \dfrac{-E_0' V_{10}}{X'} \cos(\delta_0 - \theta_{10}) \\ \dfrac{E_0'}{X'} \cos(\delta_0 - \theta_{10}) & \dfrac{-E_{10}' V_{10}}{X'} \sin(\delta_0 - \theta_{10}) \end{bmatrix}, \quad \text{(B.9)}$$

$$M_4 = \begin{bmatrix} \dfrac{V_{20}}{X_{12}} \sin(\theta_{10} - \theta_{20}) & \dfrac{V_{10} V_{20}}{X_{12}} \cos(\theta_{10} - \theta_{20}) \\ \dfrac{2V_{10}}{X_{12}} - \dfrac{V_{20}}{X_{12}} \cos(\theta_{10} - \theta_{20}) & \dfrac{V_{10} V_{20}}{X_{12}} \sin(\theta_{10} - \theta_{20}) \end{bmatrix}, \quad \text{(B.10)}$$

$$M_5 = \begin{bmatrix} \dfrac{V_{10}}{X_{12}} \sin(\theta_{10} - \theta_{20}) & \dfrac{-V_{10} V_{20}}{X_{12}} \cos(\theta_{10} - \theta_{20}) \\ -\dfrac{V_{10}}{X_{12}} \cos(\theta_{10} - \theta_{20}) & \dfrac{-V_{10} V_{20}}{X_{12}} \sin(\theta_{10} - \theta_{20}) \end{bmatrix}, \quad \text{(B.11)}$$

$$M_6 = \begin{bmatrix} \dfrac{V_{20}}{X_{wt2}}\sin(\theta_{wt0}-\theta_{20}) & \dfrac{V_{wt0}V_{20}}{X_{wt2}}\cos(\theta_{wt0}-\theta_{20}) \\ \dfrac{2V_{wt0}}{X_{wt2}} - \dfrac{V_{20}}{X_{wt2}}\cos(\theta_{wt0}-\theta_{20}) & \dfrac{V_{wt0}V_{20}}{X_{wt2}}\sin(\theta_{wt0}-\theta_{20}) \end{bmatrix}, \quad \text{(B.12)}$$

$$M_7 = \begin{bmatrix} \dfrac{V_{wt0}}{X_{wt2}}\sin(\theta_{wt0}-\theta_{20}) & \dfrac{-V_{wt0}V_{20}}{X_{wt2}}\cos(\theta_{wt0}-\theta_{20}) \\ -\dfrac{V_{wt0}}{X_{wt2}}\cos(\theta_{wt0}-\theta_{20}) & \dfrac{-V_{wt0}V_{20}}{X_{wt2}}\sin(\theta_{wt0}-\theta_{20}) \end{bmatrix}, \quad \text{(B.13)}$$

$$M_8 = \begin{bmatrix} \dfrac{V_{\infty 0}}{X_{2\infty}}\sin(\theta_{20}) & \dfrac{V_{20}V_{\infty 0}}{X_{2\infty}}\cos(\theta_{20}) \\ \dfrac{2V_{20}}{X_{2\infty}} - \dfrac{V_{\infty 0}}{X_{2\infty}}\cos(\theta_{20}) & \dfrac{V_{20}V_{\infty 0}}{X_{2\infty}}\sin(\theta_{20}) \end{bmatrix}, \quad \text{(B.14)}$$

where the subscript 0 refers to the operating point of linearization which is calculated by means of a power flow.

It is worth to remark that the same linearization procedure has been used for the studies done in Chapters 5 and 6; However, for the case presented in Chapter 5, signals w and z are set 0 since the perturbation signal and the signal to be controlled are the same as the input and output signals used for the control definition.